High Angular Resolution Studies of Late-type Stars by Lunar Occultations in the Near-Infrared

A Thesis submitted to
Gujarat University

for
The degree of
Doctor of Philosophy in Physics

by
SOUMEN MONDAL

Physical Research Laboratory
Ahmedabad-380 009
INDIA

March 2004

Certificate

I hereby declare that the work presented in this thesis is original and has not formed the basis for the award of any degree or diploma by any University or Institution.

Soumen Mondal
(Author)

Certified by:

Prof. T. Chandrasekhar
(Thesis Supervisor)
Astronomy & Astrophysics Division
Physical Research Laboratory
Ahmedabad
INDIA

Dedicated to my parents

Late Sri Kashi Nath Mondal

&

Gita Rani Mondal

Acknowledgements

I would first like to express my utmost sense of gratitude to my thesis supervisor, Prof. T. Chandrasekhar, for his invaluable guidance throughout the duration of my thesis work. Scientific discussions with him have always been fruitful and for this I am greatly indebted to him. He has introduced me to the field of observational astronomy and I have been benefited much from his expertise in observations and instrumentation. I am also thankful for his helpful advices at my personal life. I am also thankful to him for critically reading this thesis.

I would like to express my gratefulness to Prof. B.G. Anandrao for fruitful academic discussion, encouragement and his concern towards my thesis. I am grateful to Prof. N.M. Ashok for his concern towards my work and academic help whenever I needed. I am also thankful to Prof. U.C. Joshi and Drs. H.O. Vats, D.P.K. Banerjee, K.S. Baliyan, A. K. Singal and P. Janardhan for their concern about thesis work and encouragement. I am thankful to Prof. Sandip K. Chakrabarti, S.N. Bose National Centre for Basic Science, Calcutta, for his concern towards my thesis. I would like to express deep dense of gratitude to Prof. B. Chakraborty, Jadavpur University, Calcutta, who gave me first flavor in research.

I express my thanks to PRL for providing me excellent facilities and Dept. of Space, Govt. of India for funding my research. My sincere thanks are due to academic committee of PRL for critically reviewing my work at several times.

I am grateful to Dr. P.G. Tuthill, University of New South Wales, Australia for providing his valuable observed data on Keck 10m telescope used in this thesis (Chapter 3). I would like to thank Dr. Sam Ragland for providing MIA program used in this thesis. I am also thankful to Dr. Anandmayee Tej for her kind co-operation.

I am truly indebted to Mr. P.K. Kikani for accompanying me during frequent observations run at Mt. Abu. It is a memorable experience to conduct observations with him. I am thankful Mr. N.S. Jog for helping me in computer related problems. I am thankful to Mr. N.V. Dalal for assisting me during observations run. I am also thankful to Mt. Abu observatory staffs, especially, Mr. Rajesh Shah, Mr. G.S. Rajpurohit, Mr. Jinesh Jain, Mr. A.K. Mathur, Mr. Pitambar Singh, Mr. Padam Singh, and Mr. Narayan Singh for me helping in conduct smooth observations.

I am grateful to Thaltej Librarian Mrs. Uma Desai, all staff members of Library at PRL main campus and computer center for providing prompt facilities. I am also thankful to all staff members of workshop, particularly, Mr. A.J. Shroff and Mr. Atmaram Panchal during the development of the two channel photometer.

Life at PRL hostel in the conducive atmosphere of the students community is always a memorable experience. Many good moments I have shared with them and I am thankful to all of them. I remember the care of Anirban, Subrata, Jitti, Sudeshna, Krishna, Saikrishna and Dipu-Amrita during my illness in 1999 and thankful to all of them. I am thankful to Tarak, Prasanta, Sarika, Lokesh, Jayendra, Sanjeev, Pathak, Santosh, Harish, Ganguly, Gowda, Jayesh, Manoj, Sanjoy, Nagar, Sataraj, Subhrangshu, Ashoka and other members of community for making life jovial during my stay at PRL hostel. I must remember memorable company of Muthu, Koushik, Rajesh, Aninda, Ghosh, Nanda, Ravi, Ram, Debuda, Anil, Som, Sajesh, Dulichand, Sankar, Vinai, Ashishda, and Supriyoda.

This thesis would not have been possible without the encouragement from my father throughout my career. My heart swells realizing that he can not touch this thesis. I wish his blessings. I remember my uncle late Nemai Ch. Mondal who taught me first lessons of science in school. My mother, brother 'Raju' and other family members keep their patience for my good career and always pray for my well-establishment. Simple thanks are not enough to express my feelings towards them and I love them all.

Finally, and most importantly, my wife 'Jhuma' has patiently waited over last several months (years?) hoping that I will spend more time(?) at home after this thesis. My loving daughter 'Tanisi' knows that when I am coming out from home, is only to roam and she wants to come. Her neural network has not adopted to all frequencies in life. At times, I really miss her moments of joy. They really encourage me and keep me going.

Soumen
PRL, Ahmedabad
17 March 2004

Research Publications

1. Evidence of asymmetric structure in the atmosphere of Mira variable U Orionis from lunar occultation in near-infrared.
   Soumen Mondal and T. Chandrasekhar
   2004, **MNRAS , 348**, 1332

2. Lunar Occultations with Infrared arrays.
   T. Chandrasekhar, Rajesh Shah and **Soumen Mondal**
   2003, **Bull. Astr. Soc. India, 31,** 471

3. Possible photometric evidence of ejection of bullets in the relativistic jet source SS433.
   Sandip K. Chakrabarti, S. Pal, A. Nandi, B.G. Anandrao and **Soumen Mondal**
   2003, **APJL , 595**, 45

4. Dust Structure around Wolf-Rayet star WR104 from Lunar Occultation observations at 2.2μm.
   Soumen Mondal and T. Chandrasekhar
   2002, **MNRAS, 334**, 143

5. A remote controlled fast infrared photometer for simultaneous lunar occultation observations in K and L bands - Successful observations of two M3 giants.
   Soumen Mondal, T. Chandrasekhar and P.K. Kikani
   2002, **Bull. Astr. Soc. India, 30**, 881

6. High angular resolution structures in the dust shell surrounding WR104 from Lunar occultation observations at 2.2 μm.
   Soumen Mondal and T. Chandrasekhar
   2002, **Bull. Astr. Soc. India, 30**, 661

7. Fine structure in the inner dust shell of IRC+10216 from lunar occultation observations at 2.2μm.
   T. Chandrasekhar and **Soumen Mondal**
   2001, **MNRAS, 322**, 356

8. Evidence of clumpy dust shell structure in IRC+10216 from K band Lunar Occultation Observations.
   T. Chandrasekhar and **Soumen Mondal**
   2001, **Proceedings. of IAU symp. No. 205**, ed. R. T.Schilizzi, Manchester, UK, p296

9. Infrared observations of Comet Hale-Bopp(1995 01) at Gurusikhar Observatory.
   T. Chandrasekhar, N.M. Ashok, A. Tej, **S. Mondal** and P.V. Watson
   2000, **Earth Moon and Planets, 81**, 111

10. A Two Channel High Speed Photometer for Lunar Occultations Studies in the Near-IR.
    Soumen Mondal, T. Chandrasekhar, N.M. Ashok and P.K. Kikani
    1999, **Bull. Astr. Soc. India, 27**, 335

Contents

Chapter 1

Introduction

1.1 Introduction

The quest for high angular resolution to resolve the 'distant' stars began in the early years of the 20th century when it was realized these distant point like objects were like our Sun. Historically the first stellar angular diameter had been measured in 1920 in the pioneering work of Michelson & Pease (1921) using an optical astronomical interferometer though the idea was implanted more than 50 years before in the work of Fizeau (1868). Use of separate apertures to achieve increased spatial resolution was first suggested by Fizeau (1868). A landmark paper of Michelson & Pease (1921) reported the angular diameter of Betelgeuse (α Ori) to be 47 milliarcseconds using a 20 ft stellar interferometer on 100 inch Hooker telescope at Mt. Wilson, USA. Later they were able to measure only 6 cool giants and supergiants. However, attempts to extend the work to other stars and longer baselines failed due to mechanical limitations. The next major development in the field of high angular resolution (HAR) had to wait till 1956 when Hanbury Brown & Twiss (1956) discussed a novel approach to HAR called Intensity Interferometer. Hanbury Brown & Twiss (1967) first reported 15 angular diameters measurements of B0 - G2 spectral type stars. Intensity interferometer was operated at Narrabri observatory, Australia consisting of two 6.7m reflectors mounted on circular railway track of 188m diameter. But this method was not used elsewhere because of low sensitivity (B = 2.5 mag).The explosive growth of the field of high angular resolution during 1970s and beyond began when the nature of stellar images degraded by the atmospheric turbulence was first realized by Labeyrie (1970). The first direct interference fringes between separate telescopes by Michelson interferometry method were reported by Labeyrie (1975) using Interfèrométre á Deux Télescopes (I2T) at Observatoire de la Cote d'Azur, France.

1.2 High Angular Resolution Imaging

Detailed direct images which can be viewed by conventional optical and infrared telescopes are limited by turbulence in the earth's atmosphere. In the absence of an atmosphere (like observation from a space platform) the imaging performance of a perfect telescope would be limited by diffraction at the finite telescope aperture. Imaging optically through such an aperture results in natural spread due to diffraction effects of wave nature of light. The point spread function of a perfect telescope is given by an Airy disc pattern. If we consider two distant point sources separated by an angle θ, then according to Lord Rayleigh two sources will be just resolved when the center of the Airy disc of one image is superimposed upon the first minimum of the other image (and vice versa). The Rayleigh criterion usually called *diffraction limit* for a circular aperture is given by,

$$\theta = 1.22\frac{\lambda}{D} \quad \text{rad} \tag{1.1}$$

Where λ is the wavelength and D is the aperture size. Therefore the angular resolution of a diffraction limited 10m telescope in the visible part of spectrum (λ = 0.5 μm) would be 12 milliarcsecond (mas) while in the infrared (λ = 2.2 μm) it is increased by a factor of about 4 (i.e. 50 mas). The diffraction limited performance of a single 10m telescope permits high angular resolution study of only a limited number of extended astrophysical objects like thick circumstellar shells.

Ground based optical and infrared telescopes suffer from image degradation caused by the earth's atmosphere. The image distortions are caused by both spatial and temporal variations of refractive index in the turbulent air above the telescope, called *seeing*. Hence the atmosphere acts as a constantly changing lens to distort the image. The refractive index variations cause variations in optical path which in turn distort the phase of an incoming light wavefront from a stellar source across the telescope aperture. The phase variations are characterized by spatial and temporal scales. The spatial scale is a length r_o, equal to the diameter of a circular aperture over which the rms variation in the phase of a light wavefront is one radian. This spatial scale is called *Fried parameter or coherence length* (Fried 1966).

At visible wavelengths the typical size of r_o is about 10 cm under good seeing conditions (about 0.5 arcsecond). Use of the statistical theory of Kolmogorov atmospheric turbulence model leads to the conclusion that r_o increase with wavelength and is proportional to $\lambda^{6/5}$ (Fried 1966). Hence at infrared wavelength of 2.2 μm the value of r_o would be about 50 cm

(Léna et al. 1998). The timescale of the refractive index variation is derived by assuming that an unchanging screen of turbulence (r_o) is blown across the telescope by the wind. Called *coherence time* of the atmosphere t_o it is given by t_o=r_o/v_{wind}. At visible wavelengths t_o is about 5 ms at good sites (seeing about 0.5 arcsecond) while at 2.2 μm it is about 55 ms by assuming wind velocity of 20 m/s. These atmospheric parameters (r_o and t_o) have restricted the sensitivity of high angular resolution observations by the interferometric method (Busher 1988; Quirrenbach et al. 1994). The effects of *scintillation* on high angular resolution observations is discussed in the next section 1.3.3. The phase and amplitude of a incoming wavefront is perturbed by the atmospheric turbulence. In wavefront perturbation 'phase fluctuation' is related to 'seeing' while 'amplitude fluctuation' is related to 'scintillation'.

In a short exposure image (i.e. $t < t_o$) made with a telescope whose primary mirror is a few times larger than r_o one can obtain speckle pattern. Each speckle is of angular size (λ/D) and contains information upto diffraction limit of the telescope. It is located within a 'seeing' envelope of angular size (λ/r_o). No of speckles in the image $\sim$ $(r_o/D)^2$. Labeyrie (1970) suggested that *speckle interferometry* could be used to retrieve high angular resolution information (upto diffraction limit) from short exposure images. This can perhaps be considered the starting point of modern stellar optical interferometer era. The speckle techniques have since made important contributions for detection of binary stars (McAlister 1985).

For long exposure images to reach diffraction limited resolutions the optical train of the telescope must include *Adaptive Optics* (AO). The advent of AO systems are based on principle suggested by Babcock (1953). AO basically compensates in real time degradation of an image caused by the atmosphere. An AO system basically consists of three main devices, a wave-front corrector, a wave-front sensor and a control system. They operate in a rapid closed feedback loop. The wave-front corrector first compensates for the distortion of the incoming wave fronts. The part of the light is diverted toward the wave-front sensor to eliminate the residual aberrations which remain to be compensated. The control system uses the wave-front sensor signal to update the control signal applied to the wave-front corrector. As the incoming wave-front evolves, these operations are repeated indefinitely. Another key aspect of adaptive optics is the need for a nearby bright 'guide' star to sense the wave-front. Bright stars may be used as wavefront references for this correction, but most astronomical targets lack nearby sufficient bright 'guide' stars within isoplanatic patch. An isoplanatic patch is an angular distance in the sky such that light from two stars within that region will suffer an rms phase error of about 1 radian. At 0.5 μm it is order of 10 arcsecond. AO observations of these targets from the ground can only be accomplished with the use of novel idea artificial laser guide stars (Foy & Labeyrie 1985; Harper et al. 1994). The basic concept is to project a laser beam from the telescope and focus it to a spot, to produce an artificial star along the line of the sight of an astronomical target. The resonance backscatter from mesospheric sodium at approximately 94 km altitude is used for this purpose. Multi mirror telescope (MMT) array telescopes on Mt. Hopkins in Arizona obtained the first image corrected using AO with a sodium laser beacon (Lloyd-Hart et al. 1998).

Diffraction-limited resolution of a large aperture telescope can be also recovered by *aperture masking* experiment. This is done by masking off the primary mirror so that light beam from small sub-apertures, smaller than r_o, are brought together at the focal plane of the telescope. Fringes are formed at focal plane from pairs of sub- aperture like in a Young double slit experiment. Maximum separation (baseline) of a pair of holes is the diameter of the primary mirror. Pupil masks are designed in a non-redundant configuration wherein each separation are unique. Such experiments have been carried out on Keck 10m telescope to get diffraction limited performance (about 50 mas @2.2 μm) and details can be found in Tuthill et al.(2000b). Numerous results have came out from these experiments (Tuthill et al. 2001, 1999a; Monnier 1999).

Atmospheric limit can also be bypassed by space based observations. Presently the biggest operational space telescope in the UV to optical/IR region, *Hubble Space Telescope* (HST) has an aperture size of 2.4 meter. The diffraction limit resolution of HST in the UV (0.25 μm) region is about 20 mas. On board instrument *Fine Guidance Sensors (FGS)* of HST has the main purpose of maintaining pointing stability of the telescope at the millisecond level within its dynamical range upto about 17 mag in visual band (Bradley et al. 1997). As a science instrument, the shearing interferometric mode of FGS has yielded important information on the asymmetric spatial structure of Mira stars (R Leonis and W Hydrae) with an spatial angular resolution of 10 mas in the visual band (Lattanzi et al. 1997). Parallaxes of cataclysmic variable and dwarf novae stars have been also determined by FGS (McArthur et al. 2001; Harrison et al. 2000). White dwarf binary in Mira (O Cet) has been observed by another on board high angular resolution instrument *Faint Object Camera* (FOC) of HST in the UV (Karovkska et al. 1997). Hot spot on the surface of supergiant Betelgeuse has also been revealed by FOC (Gilliland & Dupree 1996). FOC has an FWHM of $\sim$38 mas at 0.255 μm (Gilliland et al. 1996).

1.3 High Angular Resolution beyond the Diffraction Limit

To achieve finer resolution beyond the diffraction limit of a single telescope at the level of milliarcsecond one has to deal with the challenges of long baseline interferometry or contend with the high but one dimensional resolution of the lunar occultation technique. In the following section the long baseline and lunar occultation details are discussed briefly.

1.3.1 Optical/Infrared Long Baseline Interferometry

The basic principle behind stellar interferometry is similar to Young's 'two-slit' experiment which demonstrated the wave properties of light (Thomas Young, 1803). In 'two-slit' experiment slits are illuminated by one coherent monochromatic light source. The coherent beams interfere under certain condition to produce constructive or destructive fringes which can be projected on screen or detector plane. Long baseline Interferometry has developed on such a principle wherein two telescope are separated by a distance (baseline). The angular resolution of such system is determined by the baseline b at which fringe contrast reduces to zero. It is given by

$$Resolution\ \ of\ \ interferometer = \frac{\lambda}{2b}\, rad \tag{1.2}$$

Where λ is the wavelength of observation and b, the baseline. For example, 110 m baseline interferometer (PTI) operating at 2.2 μm has an angular resolution of about 2 mas. Quantitatively one generally measures the fringe contrast which is also called visibility. For simple two slit experiment visibility can be written as,

$$V = \frac{I_{max} - I_{min}}{I_{max} + I_{min}} = \frac{Fringe\ \ amplitude}{Average\ \ intensity} \tag{1.3}$$

Where I_{max} and I_{min} denote the maximum and minimum intensity of the fringes. In practice the observed visibility is a function of spatial frequency (=D/λ), where D is the projected baseline vector onto plane of the sky (=b$\cos\theta$). The observed visibility is generally modeled considering Uniform Diameter (UD) of the stellar source but deviations from UD are also modeled (Tuthill et al. 1999b).

A number of long baseline optical/infrared interferometers have commenced their scientific programs listed in Table 1.1 (Monnier 2003). Details on historical developments and individual projects can be found elsewhere (Quirrenbach 2001; Saha 2002). These instruments will provide accurate measurements of the angular sizes of single stars and the

Table 1.1: Currently Operating Optical/Infrared Interferometers (Monnier 2003)

Acronym	Full Name	Location	Telescope No.	Telescope Size(m)	Max. Baseline (m)	Wavelength	Start
CHARA	Center for High Angular Resolution Astronomy	Mt Wilson, CA, USA	6	1.0	330	Vis.,Near-IR	2000
COAST	Cambridge Optical Aperture Synthesis Telescope	Cambridge, England	5	0.40	47(100)	Vis., near-IR	1992
GI2T	Grand interéromètre á 2 Télescopes	Plateau de Calern, France	2	1.52	65	Vis., near-IR	1985
IOTA	Infrared-Optical Telescope Array	Mt. Hopkins, AZ, USA	3	0.45	38	Vis., near-IR, 4 μm	1993
ISI	Infrared Spatial Interferometer	Mt. Wilson, CA, USA	2 (3)	1.65	80 (100)	Mid-IR	1988
Keck-I	Keck Interferometer	Mauna Kea, HI, USA	2	10.0	85	Near-IR, mid-IR	2001
Mira-I	Mitaka Infrared Array	Mitaka, Tokyo, Japan	2	0.25	30	Vis.	1998
NPOI	Navy Prototype Optical Interferometer	Flagstaff, AZ, USA	6	0.12	64 (250)	Vis.	1994
PTI	Palomar Testbed Interferometer	Mt. Palomar, CA, USA	3	0.40	110	Near-IR	1996
SUSI	Sydney University Stellar Interferometer	Narrabri, Australia	2	0.14	64(640)	Vis.	1992
VLTI	Very Large Telescope Interferometer	Paranal, Chile	4	8.0	130	Near-IR, mid-IR	2001
LBTI	Large Binocular Telescope Interferometer	Mt. Graham, AZ, USA	2	8.4	23	Near-IR,mid-IR	$\sim$2006
MRO	Magdalena Ridge Observatory	Magdalena Ridge, NM, USA	$\sim$10	$\sim$1.5	$\sim$1000	Vis.,Near-IR	$\sim$2007
OHANA	Optical Hawaiian Array for Nanoradian Astron.	Mauna Kea, HI, USA	$\sim$6	3.5-10	$\sim$1000	Near-IR	$\sim$2006

angular separations of binary systems at resolutions impossible with conventional telescopes. The atmospheric coherence scale, r_o and coherence time, t_o always put a limit on the aperture size of the interferometer and the integration time in sampling. Hence sensitivity of the interferometer was limited until recently. Now big aperture interferometers with AO systems (Keck, VLTI) have pushed sensitivity limit upto more than factor of 2 in magnitude.

Recent developments include two giant interferometers at Keck I and VLTI equipped with adaptive optics which have seen first fringes during 2001. Keck interferometers combine beams from two 10m telescopes. In it's future plan it will take advantage of four 1.8m auxiliary telescopes to increase sensitivity and resolution by further extending the baseline. Details of Keck interferometer can be found in Colavita et al. (1998). Very Large Telescope Interferometer (VLTI) has seen first fringes during 2001. The four unit telescopes are operational since at the end of 2002 (Richichi & Paresce 2003; Paresce 2003). Sensitivity and resolution will be further improve with the inclusion of three 1.8m auxiliary telescopes in future plan. Both giants have pushed the magnitude sensitivity upto about 10 mag in K.

Imaging structurally complex sources in a model-independent manner is one of the 'Holy Grails' of optical/IR interferometry. But with two telescopes interferometer it was never possible to extract phase information. With atleast three telescope such phase information can be retrieved by method of *closure phase* measurement. The closure phase is defined as the sum of the observed phases for the three baselines made by three elements of the interferometer. Now image construction is even possible in LBI by knowing both phase and amplitude (Jennison 1958; Monnier 2000).

The fringe visibility measured using a particular baseline gives one component of the object Fourier transform. However, a Fourier transform is a complex quantity, having both an amplitude and phase. While the amplitude is given by the fringe visibility, the phase is given by the position of the fringes. The fringes from an interferometer are continually changing due to atmospheric turbulence. In case of three telescope interferometer one can measure three sets of fringes simultaneously. They are all moving, but they don't move independently. Their movement is due to the atmosphere, but their relative positions contain information of phase about the object. Three optical/infrared interferometers have demonstrated the closure phase measurement and published results on closed binary and asymmetry structure of the sources, COAST-5T (Baldwin et al. 1996; Young et al. 2000), NPOI-6T (Bensen et al. 1997; Hummel et al. 2003; Tycner et al. 2003) and very recently

IOTA-3T (Monnier et al. 2004a; Monnier et al. 2004b).

1.3.2 Historical Perspectives of Lunar Occultations of Stellar Sources

The idea to determine stellar diameter from the study of lunar occultations began after a suggestion by MacMahon (1909) that stellar diameter could be deduced directly by observing lunar occultation with rapidly moving photographic films. MacMahon underestimated the length of time it would take for the stars to disappear because he treated the problem by the methods of geometrical optics and therefore did not take the diffraction effect into account. Eddington (1918) replied to MacMahon's suggestion and indicated that diffraction effect would mask the true diameter for all but the largest stars. Later Williams (1939) and Whitford (1939) included stellar diameter and detector bandwidth in the theoretical treatment of the diffraction pattern and published observations to illustrate the effects. Whitford successfully recorded diffraction fringes of β Cep and ν Aqr in 1938 using high speed sensitivity photocells. The modern era of lunar occultation was started during 1970 by introducing the new technique of high speed digital recording (Nather & Evans 1970). The detailed analysis procedure of light curve by non-linear least squares was also developed during 1970 (Nather & McCant 1970). An exhaustive historical outline on lunar occultation can be found in Warner (1988) and White (1987).

The observations of lunar occultation in the near infrared region using InSb detector was pioneered at Kitt Peak National Observatory (KPNO) during 1974 with numerous measurements of angular diameters by Ridgway and his co-workers (Ridgway, Wells & Carbon 1974, Ridgway 1977, Ridgway et al. 1979, 1982; Schmidtke et al. 1986). Near Infrared lunar occultation methods were further developed by Richichi and his team at TIRGO observatory (Richichi et al. 1992, 1996). The group is continuing to explore the lunar occultation observations. A large number of important results have been published (Richichi & Calamai 2003 and references therein). The Physical Research Laboratory (PRL) in India started lunar occultation program in the near-IR during early 1990s and numerous results have been published (Ragland et al., 1998; Chandrasekhar 1999; Tej 1999). This group is continuing to explore the high angular resolution capability of lunar occultation using a 1.2m telescope (this thesis).

1.3.3 Lunar Occultation Technique

A detailed review of lunar occultation technique can be found in Richichi (1994). The observations of LO is the only available technique by a single telescope that can deliver angular resolution greatly exceeding its diffraction limit. LO has demonstrated its capability to resolve the source of about 2.0 milliarcsecond with a small 1m class telescope. The instrument generally used for recording lunar occultations is an optical/Infrared photometer having fast sampling rate of about 1 milliseconds.

In this process the Fresnel diffraction modulation of the stellar light level occur just prior to the disappearance of the star behind the darklimb of Moon (disappearance) or just after reappearance of the star from behind the darklimb of Moon (reappearance). The diffraction fringes sweeps across the earth and are collected by ground-based telescopes. *The high angular resolution is encoded in the fringe pattern at Moon's distance, which is rapidly scanned by the telescope as the Moon moves across the sky.* Two important facts underlines its success as a high angular resolution technique. Firstly, the diffraction pattern is formed well outside the atmosphere and secondly, the telescope plays only the role of collecting already formed fringes as rapidly as possible. The average distance between Moon and earth is about 3.8×10^5 Km. The practical success of LO is because of the distance between the Moon and earth which makes it possible to sample the event with sampling rate (about 1 millisecond) of present day detectors along with their preamplifier electronics. The observed light curve can be considered to be the resultant of many Fresnel patterns formed by point sources represented by strip integrated stellar disk perpendicular to the direction of occultation and convolved with several instrumental smearing effects (e.g. system time response, optical bandwidth of filter and finite aperture of the telescope). Extended sources (more than 40 mas) do not show any fringe pattern as diffraction gives way to geometrical optics. The simulated light curves are shown in Fig. 1.1.

The intensity pattern from a monochromatic point source occulted by sharp lunar limb is basically equivalent to straight edge diffraction (Born & Wolf 1959) which is given by,

$$I(t) = 0.5 I_o \left[(0.5 + C(\omega))^2 + (0.5 + S(\omega))^2 \right] \quad (1.4)$$

Where I_o is the stellar brightness and $C(\omega)$ and $S(\omega)$ are the classical Fresnel diffraction integral which are defined as,

$$C(\omega) = \int_0^{\omega} \cos(\frac{\pi t^2}{2}) dt \quad (1.5)$$

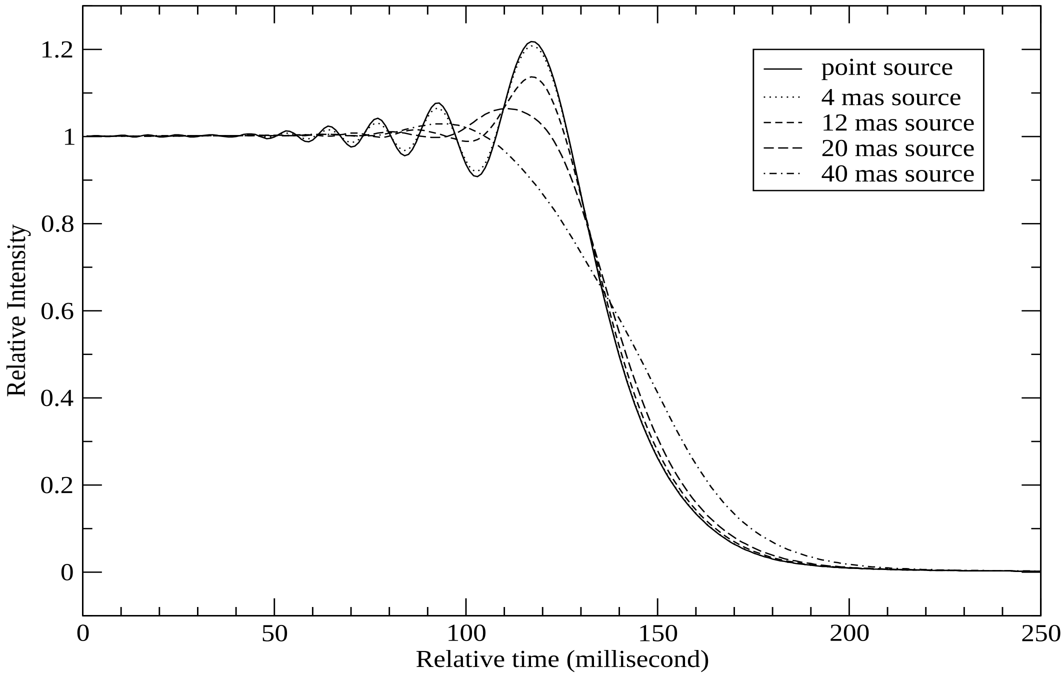

Figure 1.1: *The Simulated light curves in the K-band are generated considering all instrumental effects e.g. time response, filter bandwidth and telescope aperture. The lunar velocity component along the direction of occultation is assumed to be 0.5 km/s.*

$$S(\omega) = \int_0^{\omega} \sin(\frac{\pi t^2}{2})dt \tag{1.6}$$

where the dimensionless Fresnel number ω is written as,

$$\omega = \left(\frac{2}{\lambda D}\right)^{1/2} v(t - t_0) \tag{1.7}$$

Where v is the lunar velocity component in the direction of occultation perpendicular to the lunar limb and (t - t_0) is the relative time from the geometric point of occultation, D is the distance to the moon and λ is the wavelength of observations. The geometric point of occultation is where the stellar intensity reduces to 25% of its value.

In Fresnel pattern the maximum intensities occur at ω =$\sqrt{3/2 + 4N}$ and minimum intensities at ω = $\sqrt{7/2 + 4N}$ for N= 0, 1, 2, 3.....etc. From the above eqn.(1.7) one can find that typical time scale of a event. Considering the average lunar distance of 3.8×10^5 km and typical lunar velocity of 0.5 km/s the timescale to cross the fifth maxima of fringes (means ω = 4.18) in the detector will be about 175 milliseconds from the geometrical point of occultation. In practical observations of even point sources it is difficult to see fringes beyond the fifth because of instrumental effects and scintillation noise. The photometric sequence of about one second is generally adequate to model the lunar occultation light curve. To remove sky gradients additional one second of data would be useful.

In contrast to optical interferometers lunar occultation has not affected by the atmospheric parameters (r_o and τ_o). Scintillation is related to intensity fluctuation in the aperture plane. It generally arises at higher level of the atmosphere while 'seeing' is due to low level turbulence. Scintillation is major problem in observing lunar occultations in the J,H, K bands as bright sources involved. The frequencies involved in scintillation are similar to those of the occultation fringes so that they can not be filtered out completely. But using polynomials low frequency variation can be modeled. The noise level in occultation is therefore largely due to the effect of the scintillation.

1.3.4 Scope of Lunar Occultations

Lunar Occultation is one of most effective techniques in terms of angular resolution and cost in comparison with other HAR techniques. Further in case of lunar occultation it is possible to observe bright IR sources with ground-based 1m class telescopes with simple high speed IR photometers for angular diameter measurements. This technique has yielded important results during the last two decades. However, lunar occultation has certain inherent drawbacks. It provides only a one dimensional occultation scan across the source. Though two telescope interferometry does the same job of one dimensional scan, multiaperture with closure phase (discussed earlier) has been recently implemented to get 2-D information. The 2-D information of the source is in principle possible from lunar occultation if the same source is observed from different sites or repeated lunar occultation on the same source from the same site but at different position angles. In this thesis lunar occultations of U Orionis (Mira variable) observed at different locations on the same day in the K-band show asymmetric nature of the source (details in chapter 4). Another source ν Vir (M1 III) was observed three times from the same site through position angles (57 - 135^o). The source does not show any asymmetry (details in chapter 6). A further limitation of lunar occultation is that it is event based and covers only those sources which lie in the path of the Moon.

The effective temperature is a fundamental parameter which can be estimated by a distance independent manner. *The calibration of effective temperature to the spectral type (K0 - M6) for the stars cooler than Sun was first established exclusively on lunar occultation* *results (Ridgway et al. 1980).* Details about scale of effective temperature are discussed in chapter 6 of this thesis.

Lunar occultation observations of the environments of mass-losing stars have revealed a wealth of information. *Model independent algorithm first introduced by Richichi (1989) is a novel method to retrieve one dimensional brightness profile from lunar occultation light curves*. The algorithm is briefly discussed in chapter 2 of this thesis. The case of WR104 is discussed in chapter 3. On other sources like IRC+10216 too the method has been used (Chandrasekhar & Mondal 2001; Richichi, Chandrasekhar & Leinert 2003).

Binary and multiple stars have been indispensable tool for astronomers to determine stellar masses. Lunar occultation can provide an close detection (about 5 mas) and several measurements are reported from photoelectric observations (Evans et al. 1985 and references therein) as well as from infrared region (Richichi et al. 2000 and references therein). Speckle interferometry is widely used in binary detection with diffraction limited resolution (McAlister 1985; Hartkopf et al. 2001).

1.4 Stellar evolution and AGB stars

Almost all the stars studied in this thesis with one important exception (WR104) are late-type stars of spectral type later than K0. These stars have all evolved beyond the main-sequence stage in their evolutionary history. Those are classified broadly as Red Giant Branch (RGB) stars. More evolved stars in RGB phase are in Asymptotic Giant Branch (AGB) phase. Mira variables and stars in late K to M spectral classes are the candidates in AGB phase. Supergiants are more massive and luminous than giants in similar spectral type. The characteristic of WR stars are described individually in chapter 3 of this thesis. Most of the information of this section pertaining to stellar evolution comes from Iben (1985), Weidemann et al. (1990) and Padmanabhan (2001). One can find detailed review of this subject in Shu (1982)

Stellar structure and evolution are characterized by their masses. Based on this facts, stars are roughly divided into low-mass($\leq$2 $M_{\odot}$), intermediate-mass (2 $\geq$ M $\leq$ 8 $M_{\odot}$) and high-mass ($\geq$9 $M_{\odot}$).

The schematic diagram of the stellar evolution stages in the Hertzsprung-Russel (H-R) diagram for a star of 1, 5, 25 $M_{\odot}$ is shown in the Fig. 1.2 (reproduced from Iben (1985)). The H-R diagram is a plot of surface temperature versus luminosity for a collection of stars. Mostly based on theoretical calculations and observational statistics, it describes the phases a star experiences during its life journey.

Dense clumps of gas and molecules collapse under their own gravity leading to a new star. In continuing process of collapse they generate high density and temperature (about 10^7 K) to ignite hydrogen in the center of star. The first- and longest- phase of stellar evolution occurs in which reactions fusing hydrogen into helium is taking place in the stellar core. The Sun, a typically low-mass star, is expected to spend seven billion years in main-sequence. One solar mass star spends about 75% of its total life on the *main sequence* (MS) .

Further evolution of *low-mass* stars ends the main-sequence phase when after almost all hydrogen is converted to helium. At this time, the core contracts under its own weight. Gravitational released energy lead to hydrogen burning in the shell. This causes the star to bloat up in size and to increase temperature. The star will move up in the H-R diagram. This epoch is called *the red giant branch (RGB) phase*. The fusing process in the core ceases and non-burning core of helium is left which contracts gravitationally and the released energy enhances the hydrogen fusion reaction in the shell. This heats up the outer layers, causing them to expand. The radius of star increase further and decreases the surface temperature.

The main energy source on the RGB is hydrogen shell burning. Convection in the outer layers occurs as a result of the increased opacity caused by the temperature decrease, and this convective zone gradually moves toward the H-burning shell. The processed material is *dredged-up* to the surface of the stars by convective process.

Eventually the core becomes sufficiently hot or trigger helium burning, but this occurs after the electrons in the core have already become degenerate. In such a case, the temperature increase does not affect the pressure significantly and helium burning occurs as runway process, known as *helium flash*. This phase is referred to as the *Horizontal Branch* (HB).

At the end of HB phase (about couple of million years) the central helium will be exhausted and eventually the core of carbon and oxygen materials starts to shrink. Eventually the temperature of the shell increase to ignite He fusion. A phase of thick helium shell burning, during which H-shell is inert and the star increases in luminosity, called early-asymptotic giant branch (E-AGB) because the star approaches this point asymptotically in the luminosity-temperature (L-T_{eff}) relation of H-R diagram. E-AGB is followed by double shell burning phase of *thermally pulsating AGB* (TP-AGB).

Intermediate mass stars are then those which do not produce a degenerate core, do not

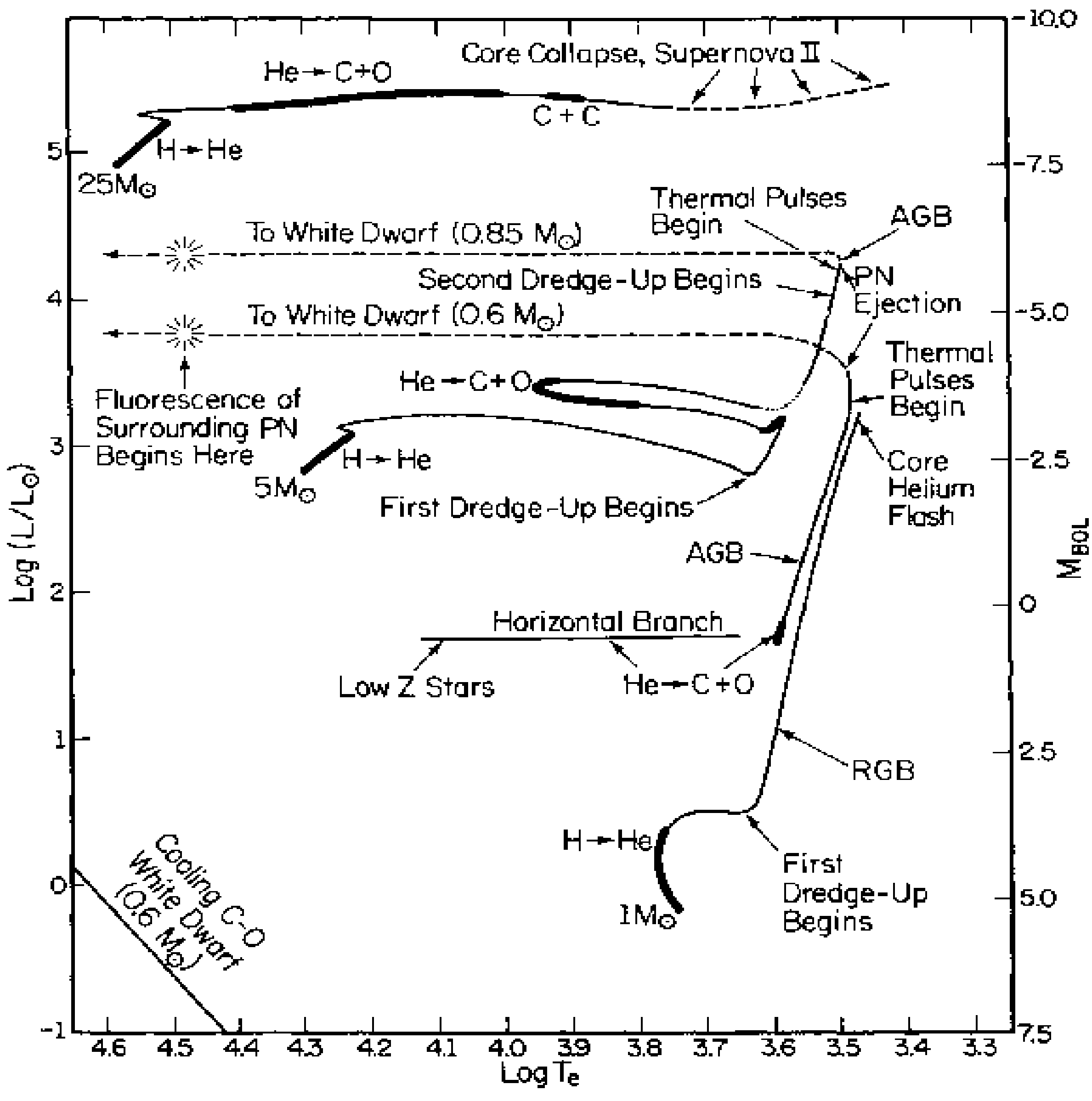

Figure 1.2: *Stellar evolution of 1, 5 and 25 $M_{\odot}$ star in the H-R diagram (reproduction from Iben (1985)). The starting point lies on main-sequence and as the star evolves moves up and to right in the H-R diagram (towards higher luminosity and lower temperature)*

climb a RGB and ignite helium under non-degenerate conditions. In the H-R diagram they evolve nearly horizontally from main sequence to red giant region.

In AGB phase the star reaches its largest radius about 200 $R_\odot$ and effective temperature about 3000 K. The large radius corresponds to a low effective gravity at the surface of the star. Several process, e.g. pulsation and radiation pressure, compete to lift the materials from the stellar surface to several stellar radii. At this distance dust can condense and radiation pressure on dust grains accelerate the materials into interstellar space. The mass-loss can reach values 10^{-6} to 10^{-4} $M_\odot$/yr.

Little is known of further evolution after the AGB phase. The outer region of stars undergo large instabilities (*superwind phase*), leading to an eventual ejection of a significant fraction of materials to form a *planetary nebula*. The core ultimately will becomes a *white dwarf* supported by the degeneracy pressure of electrons.

High-mass stars with masses ≥ 8 $M_\odot$ may proceed further in the nuclear cycle and ignite carbon burning in the core. The ignition of carbon is quite explosive and they may end up with violent *supernova explosion*. Final fate of a star depends on final mass compared to *Chandrasekhar limit*. The Chandrasekhar limit is the mass of core to be 1.4 M$\odot$ which is the maximum allowed mass of electron gas to be stable hydrodynamically. The star of final mass below Chandrasekhar limit will turn to a white dwarf. Stars with a final mass above this limit turns to a *neutron star or black hole*.

The theoretical stellar evolution tracks for initial masses of 1, 2, 3 and 5 $M_\odot$ are plotted in the Fig. 1.3. The model tracks are taken from Girardi et al. (2000). The tracks are presented for the initial solar composition [Z =0.019, Y =0.273]. The model tracks are evolved from the main-sequence at constant mass. The tracks are stopped during TP-AGB phase in the low and intermediate mass stars. A small number of 2 - 5 thermal pulses are considered for masses upto 5 $M_\odot$ in these model tracks.

The theory of stellar evolution has been able to understand the position of the stars in the H-R diagram. Stars observed in this thesis which have distance estimations from *Hipparcos* parallax or Period-Luminosity (in case of Miras) have been plotted in the H-R diagram. The effective temperature are derived from angular diameter measurements by lunar occultations. The uncertainty in the effective temperatures are less than 5% except two stars IRC+20205 and Z Sco wherein the uncertainty is about 11%. Individual sources are discussed in chapter 5 and chapter 6 in this thesis. Luminosity is estimated using the relation L = $4\pi d^2 F_{bol}$, where d is the distance to the source and F_{bol} is the bolometric flux measured by integrating observed flux over all wavelengths. Uncertainty in luminosity is

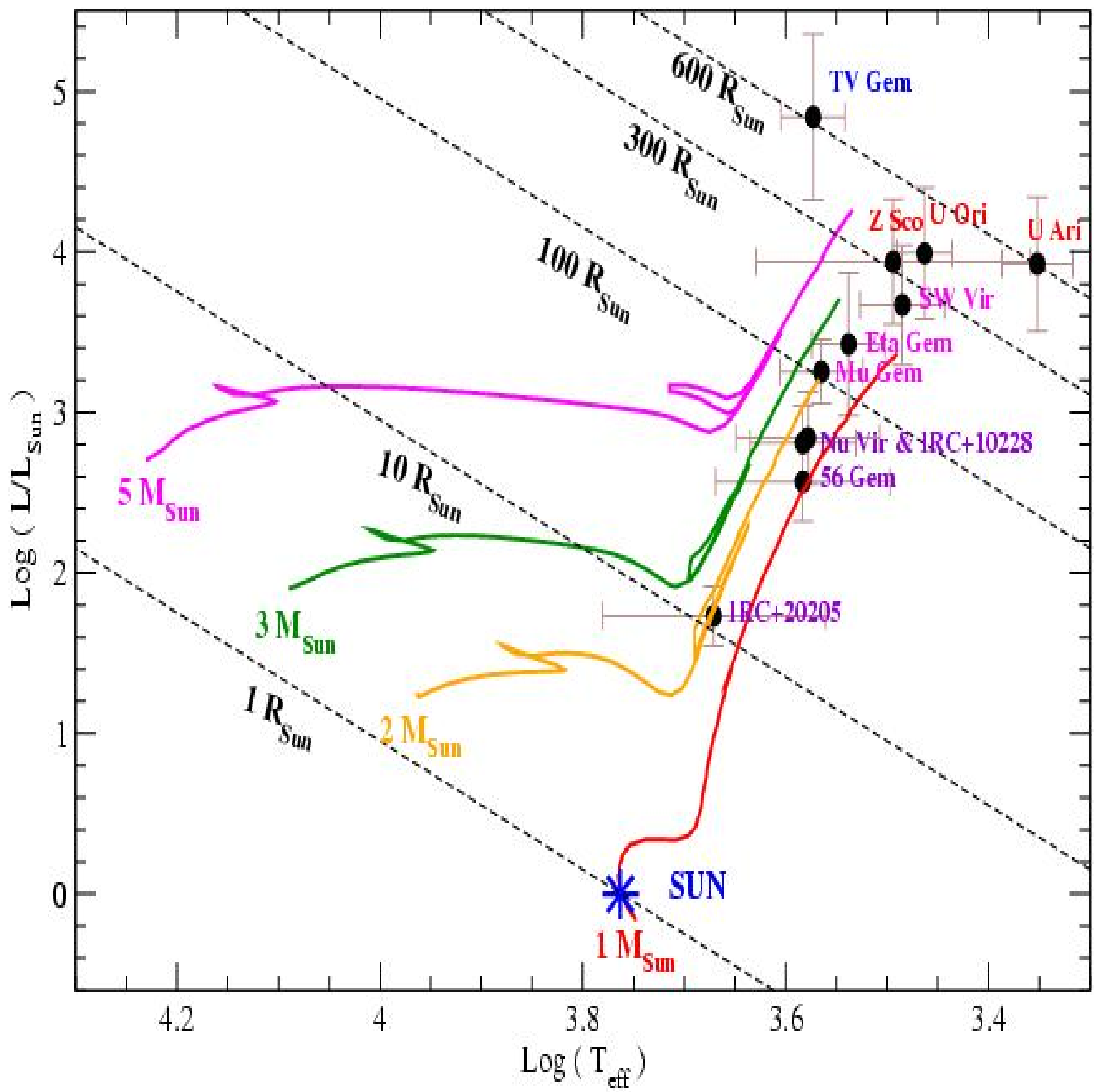

Figure 1.3: *Theoretical model tracks of 1, 2 , 3 and 5 $M_\odot$ stars in the H-R diagram starting from main-sequence to AGB (adopted from Girardi et al. (2000)). Tracks of constant radius for 1, 10, 100, 300 and 600 $R_\odot$ are overplotted. Some observed stars in this thesis are superimposed on the model tracks.*

in the range about 20 - 50% and mostly comes from the distance estimation. The line of constant radius is estimated and plotted in the Fig. 1.3.

Stars observed in this thesis are mostly belong to AGB phase. Three Miras (U Ori, U Ari and Z Sco) are well in the region of TP-AGB phase and SW Vir (SRb) is also close to this region. While η Gem, μ Gem, ν Vir, IRC+10228 and 56 Gem are all apparently in the region of AGB phase of the theoretical tracks. IRC+20205 is apparently in the position of RGB phase or E-AGB phase. TV Gem is isolated from the rest in the diagram as it is a supergiant. Supergiants are high mass stars (more than 8 $M_\odot$) and those tracks are not shown in Fig. 1.3.

1.5 Layout of the Thesis

The thesis consists of seven chapters.

Chapter 1 begins with a brief description of high angular resolution studies with emphasis on the lunar occultation technique, highlighting important results in HAR studies with a brief discussion on studies carried out here.

Chapter 2 is dedicated to instrumentation and data-analysis of lunar occultation light curve. The two channel high speed IR photometer for lunar occultation studies are described.

Chapter 3 describes the study of high angular resolution dust structures around Wolf-Rayet star WR104 at 2.2 μm.

Chapter 4 presents evidence of asymmetric spatial structures in the atmosphere of Mira variable U Orionis from occultation observations at 2.2 μm.

Chapter 5 describes multiwavelength angular diameter measurements of Mira and semi-regular variables in the K and L$'$-bands. Pulsation mode of Mira and semi-regular variables are discussed.

Chapter 6 concerns with the angular diameter measurements of other K - M giants and supergiants. Effective temperatures are derived from angular diameter measurements and compared with existing calibration scale of spectral type vs. effective temperature.

Finally **Chapter 7** presents summary of results and suggestions for future work.

Chapter 2

Instrumentation, Technique and Data Analysis

This chapter discusses the design and performance of a specially built two channel high speed photometer for recording lunar occultation events simultaneously at two wavelengths K-(2.2 μm) and L$'$ (3.8 μm)-band lunar occultations. Data analysis procedures are also discussed.

2.1 Two channel high speed infrared photometer

The basic purpose of a high-speed infrared photometer is to record the radiation flux from a stellar source with a high time resolution in the range of microsecond to millisecond. Real time high speed acquisition system for multichannel mode have wide potential not only for scientific observations but also for development of observational technology. Such high speed photometry in different wavelengths range have several applications in observational astronomy like pulsar, x-ray binary studies (Eikenberry et al. 1996), lunar occultation observations (Chandrasekhar et al. 1992) and fringe detection for infrared and optical interferometry (Mallbet et al. 1999). In the present context the two channel photometer (TCP) is primarily designed for observing simultaneously in two colours, near infrared light curves of stellar sources produced by lunar occultations (Mondal, et al. 1999). Time resolution of 1-2 millisecond (ms) is required to observe occultation light curves as the occultation events are fast with typical event duration of 200 -300 ms.

The infrared lunar occultation technique has the potential to reach high angular resolution at the level of milliarcseconds (mas) even with modest telescope apertures in the 1-meter class. This potential provided the motivation for launching a program of lunar occultation observations at the Physical Research Laboratory (PRL), India. The early efforts in the optical I (0.87μm) band are summarized in Chandrasekhar et al. (1992). Subsequently a near Infrared single channel fast photometer was built for lunar occultation observations mainly in the K-band (Ashok et al. 1994). The lunar occultation in the IR region has distinct advantages compared to the visible region due to reduced scattered lunar background radiation and the fringes being spread out wider by a factor of two resulting in easier sampling. A number of significant results have emerged which are discussed elsewhere (Chandrasekhar 1999). *The two channel high speed IR photometer is a newly built instrument developed at PRL as a part of my thesis work. The scientific importance of simultaneous observations of lunar occultations in two near-IR wavelengths (K (2.2 μm) and L$'$ (3.8 μm)-bands) motivated the development of the new instrument. The K-band angular diameter measurements are essential because the measurements are close to true photospheric diameters of late-type stars (Hofmann et al. 2000) while L$'$-band measurement can probe more efficiently the upper atmospheric layers surrounding these many cool giants and supergiants which result in bigger apparent angular diameters.* In case of cool giants like Mira variables a important consequence of angular diameter measurements, the wavelength-dependent size variations which can be studied from simultaneous measurements. Such observational results are recently reported only for few evolved giants of spectral type later than M5 (Mennesson et al. 2002). Again angular diameter measurements in L$'$ -band are limited in the literature because of observing challenges in the presence of strong terrestrial background.

2.1.1 Basic design of the instrument

Hardware System

The two channel photometer essentially consists of a photometer box and specially designed Cassegrain plate for accommodating two independent detector dewars cooled to liquid nitrogen temperature. The photometer box incorporates a stable 45^o slanted tertiary mirror placed on a vibrator mirror which delivers the telescope beam to the detector aperture. A flip mirror system placed above the tertiary mirror is used for viewing/imaging the extended sky regions. A side looking source can be used for alignment and signal calibration purpose without the telescopic beam. The two channel photometer is shown in Fig. 2.1 mounted at the Cassegrain focus of 1.2m IR telescope at Mount Abu, India operated by PRL.

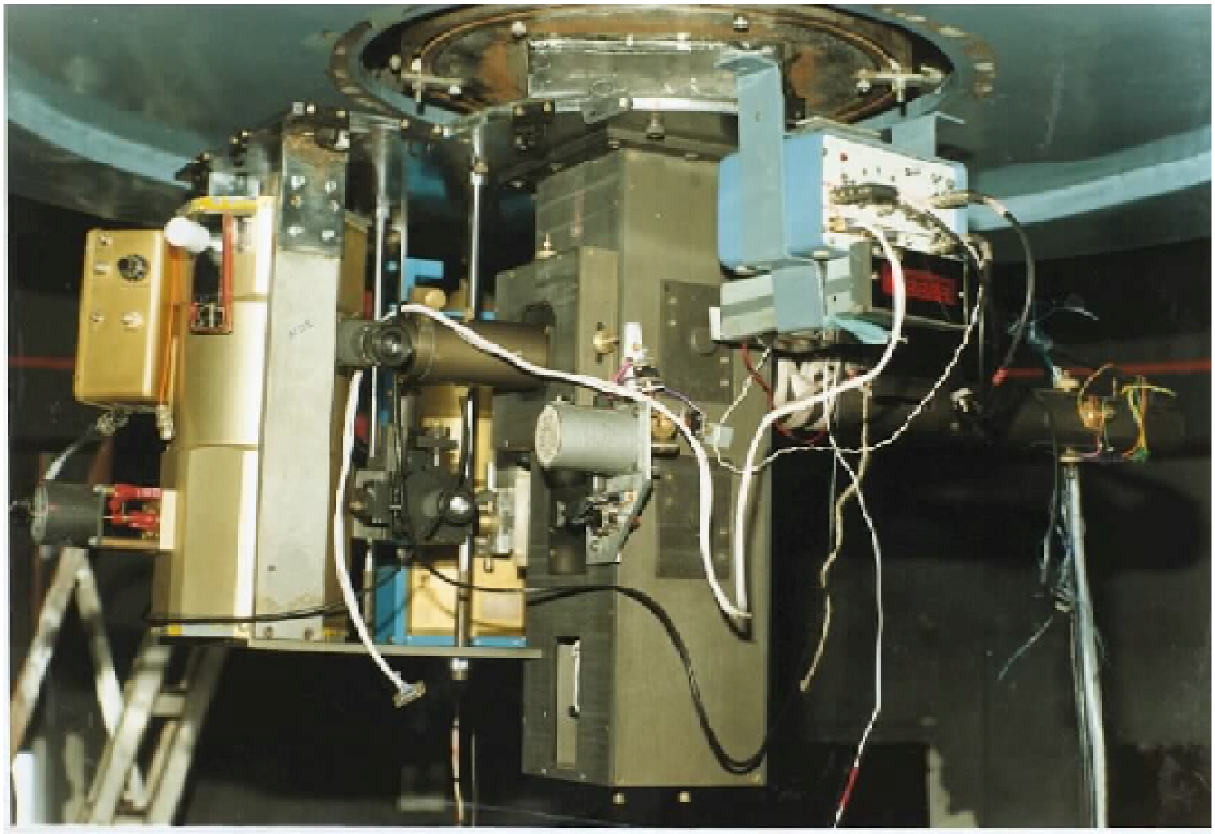

Figure 2.1: *Two channel IR photometer installed at the Cassegrain focus of 1.2m infrared Telescope at Mount Abu, India.*

Optical layout

The optical layout of the instrument with data acquisition electronics setup is shown by schematically Fig. 2.2. The optical/IR beam after right angled reflection from tertiary mirror is subsequently bifurcated into two beams (K transmitted, L′ reflected) by a special dichroic IR beam-splitter, before reaching two separate InSb detectors. The tertiary mirror is attached to the vibrator. In absence of vibrating secondary mirror of the telescope the vibrating tertiary mirror is used for sky subtraction for conventional photometric measurements with a throw in the north-south direction in the sky. The vibrating frequency used for photometric observations is in the range 10-15 Hz.

The characteristic curve of the beam splitter is shown in Fig. 2.3. The shorter wavelength beam (≤ 2.5 μm) covers the filter-bands J, H and K and is transmitted into an aperture of the detector. While the longer wavelength beam (≥ 2.5 μm) covers the filter-bands L and M and is reflected into an aperture of another independent detector. In Table 2.1 parameter of two detectors, pre-amplifier and beam splitter characteristics are mentioned. In

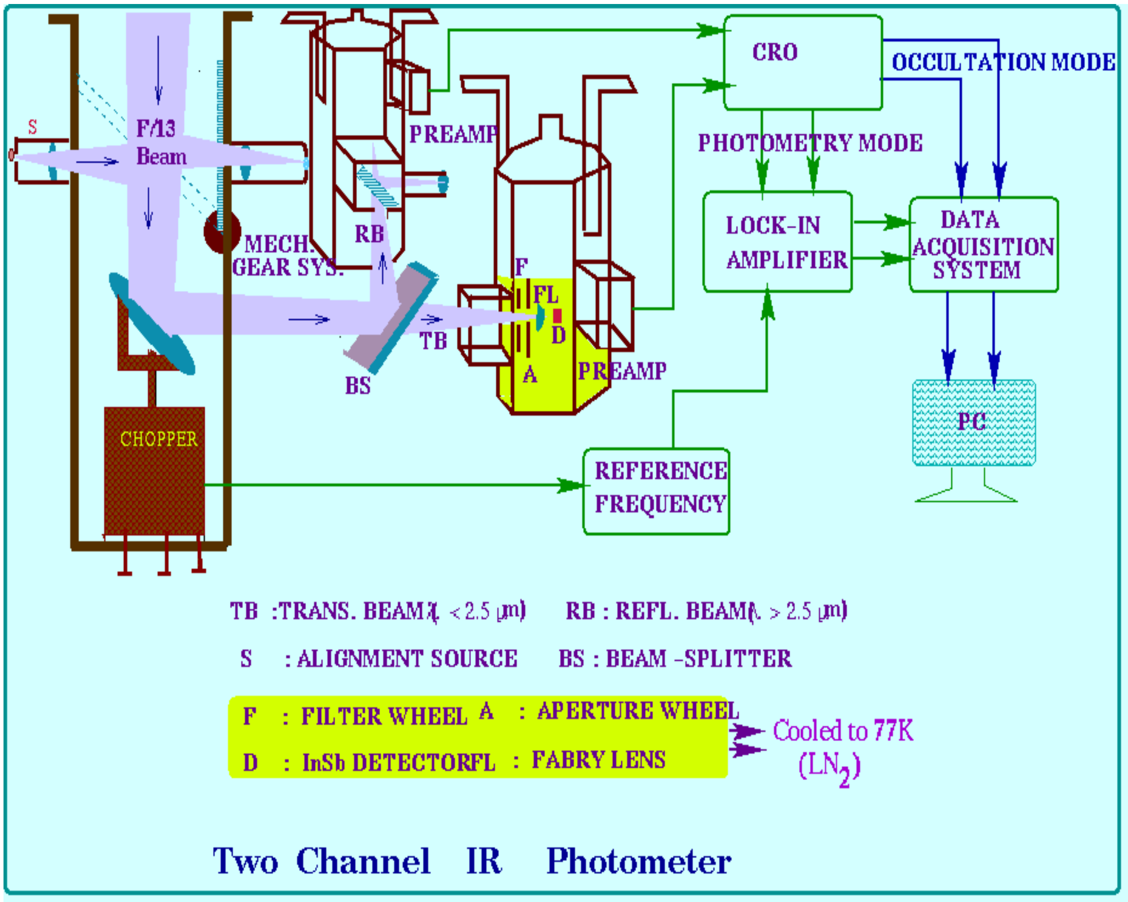

Figure 2.2: *The schematic optical layout from the telescope end to the detectors along with associated electronics.*

Table 2.2 IR filter-band used in this instrument are listed. The filter transmission curves are shown in Fig. 2.4.

Detector System

Two independent single-element InSb detector dewars are used in the transmission and reflection channel. The single-element InSb detector dewars with attached pre-amplifier electronics were acquired from Infrared Laboratories Inc., USA. The detailed specification of the detectors are shown in Table 2.1. The detectors inside dewars have been mounted in side-looking configuration in conjunction with cooled field of view baffling, a filter wheel, aperture wheel slide and a cooled pre-amplifier 1st stage FET. The filter wheels in both dewars are controlled remotely by digital motor drive unit. A cold Fabry lens has been included to reimage the aperture focal plane onto the detector.

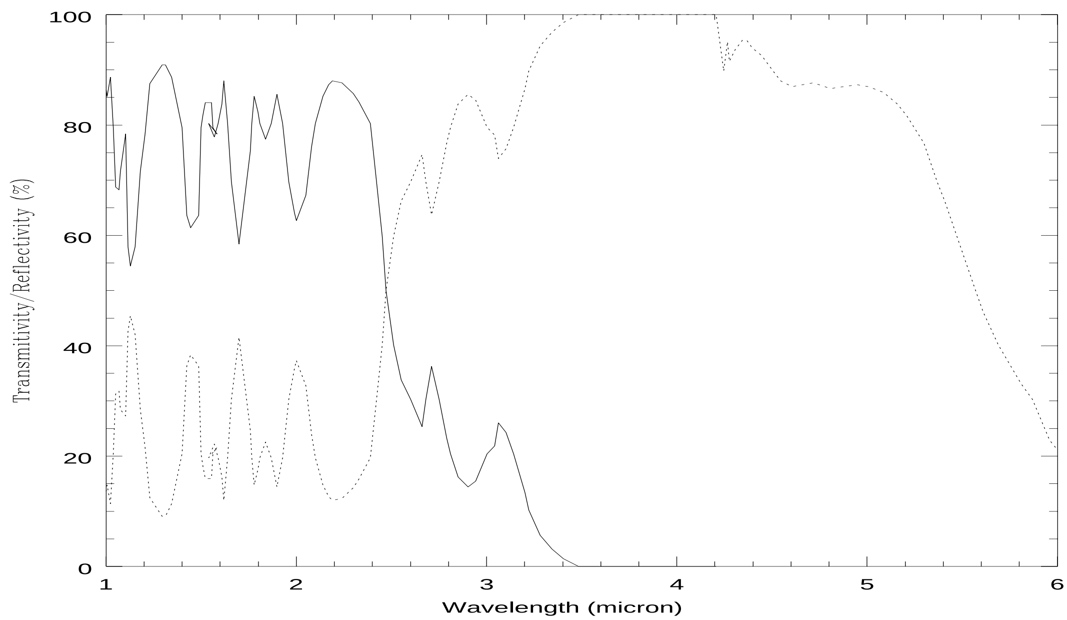

Figure 2.3: *The solid line is the transmittivity and the dotted line is the reflectivity of of the dichroic beam splitter.*

The detector is thermally in good contact with the cold work surface of a liquid nitrogen temperature ($\sim$ 77K) cooled dewar. Briefly, InSb is an intrinsic photovoltaic detector with a band gap, at 77K, of 0.22 eV. Adjacent zones of materials are p and n doped to form a diode. Photon of energy $\geq$ 0.22 eV (i.e. $\lambda \leq 5.5$ μm) are absorbed at the junction to create an electron-hole pair. This is separated by the junction field and appears as charge at the electrodes. The InSb photodetector when operated at 77 K, is sensitive in the wavelength range 1 - 5 μm. The quantum efficiency of InSb detector is about 60% i.e., 60% of incident photons reaching the detectors is converted to electrons.

The pre-amplifier electronics circuit to operate InSb is described by Hall et al. (1975). This low noise matched field effect transistors (FETs) are used as the cooled first stage of the amplifier. The circuit uses feedback to maintain the linearity of detector over a large dynamic range, to improve the frequency response and to control the bias voltage. Hall et

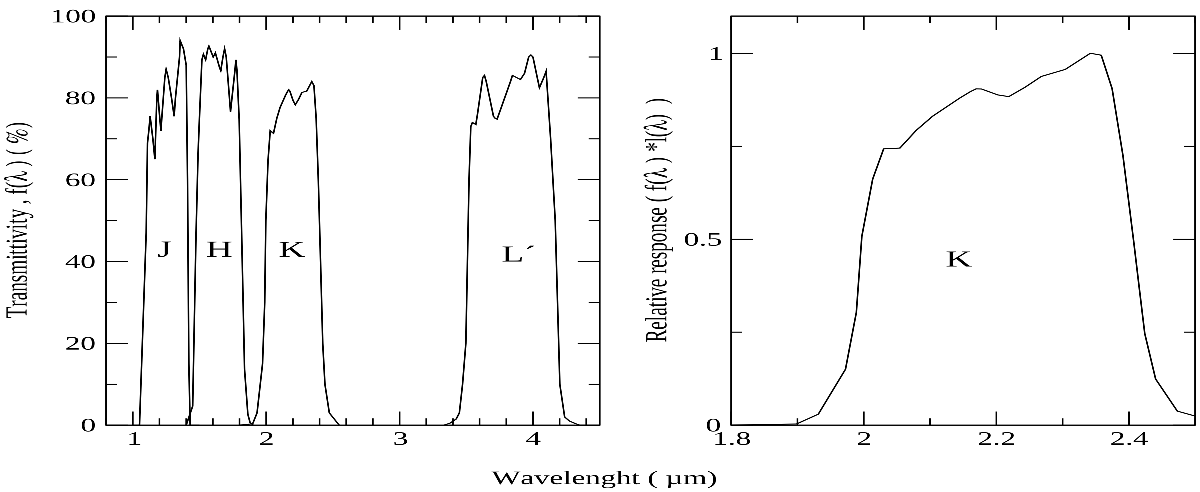

Figure 2.4: **Left:** *The transmittivity of the different standard broad infrared filterbands.* **Right:** *The system wavelength response in K used in data analysis.*

al. (1975) demonstrated the Johnson noise limited operation of InSb detectors with this circuit if the bias voltage across the detector is held close to zero. In practice observations near zero bias voltage becomes problematic for background limited operation in L′. In observations of L′-band we have encountered severe problems of DC drift and noise are much larger than the photon noise or scintillation noise of the source signals. To reduce the stray radiation extra optical baffles have been put inside the dewar. This has improved to some extent the dynamical range of operation.

Field eye-piece cum CCD camera positioning system

Before acquisition of the target object in the detector, the extended region of sky (about 9 arcminutes in size) is first visually inspected or imaged by CCD camera and the object is suitable centered. For this purpose, by the motorized arrangement with help of mechanical gears and remote switching, a 45^o slanted flat mirror is flipped into the telescope beam when it is necessary to divert the beam for viewing/imaging. The telescope beam is reflected into focal reducer by converting f/13 to f/4 beam using an additional lens which enables for viewing/imaging extended region of the sky in the eye-piece/CCD camera. Using this arrangements it is possible to point quickly the target objects into the small aperture of the detector. At the final stage of alignment a dewar eye-piece system is needed to center the star image on the aperture.

Table 2.1: **Detector and Beam-splitter Characteristics**

Components	Specifications	Dewar (CVF) in Transmission	Dewar (Fast) in Reflection
Detector	Material	InSb	InSb
	Diameter	0.5 mm	0.5 mm
	Spectral range	1-5 μm	1 -5 μm
	NEP	4×10^{-15} W/$\sqrt{Hz}$ (20 Hz, K)	5.6×10^{-15} W/$\sqrt{Hz}$ (40 Hz, K)
Pre Amp	Feedback resistor (R_f @77K)	5.7×10^{10} Ω	2.12×10^{10} Ω
	Voltage Responsivity	5×10^{10} V/W	-
	Current Responsivity	-	0.54 A/W
	Noise with R_f	2×10^{-4} V/$\sqrt{Hz}$ @20 Hz	0.31×10^{-6} V/$\sqrt{Hz}$ @40 Hz
Focal Plane Apertures	Size (mm)	0.5, 1, 2	0.5, 1, 2, 3
	corresponding on the sky (for f/13 beam)	6.5″, 13″, 26″	6.5″, 13″, 26″, 39″
Beam Splitter	Material	BK7 Glass	
	Spectral coverage	1 - 2.5 μm (Transmission)	3 - 5 μm (Reflection)
	Transmittivity/ Reflectivity	$\geq$ 80%	$\geq$ 90%
		(Fig. 2.3)	

Table 2.2: **Filter characteristics**

IR Filter	Dewar (CVF) in Transmission λ_{eff} (μm)	$\Delta\lambda$	Dewar (Fast) in Reflection λ_{eff} (μm)	$\Delta\lambda$
J	1.25	0.30	1.25	0.32
H	1.65	0.30	1.65	0.34
K	2.20	0.40	2.20	0.40
L	-		3.80	0.60
M	-		4.70	0.64
CVF_{min}	1.70	0.03	-	
CVF_{max}	3.40	0.03	-	

Auxiliary Electronics System (Fig. 2.2)

With a co-axial cable the pre-amplifier output signal is carried to the data acquisition system (DAS) and parallely the output is monitored on the oscilloscope. In high speed (sampling rate about 1-2 millisecond) occultation mode the lock-in amplifier and chopping the beam are bypassed. And the output signals from the two detectors are directly fed to DAS. Conventional photometry(sampling rate about one to several seconds) the output signal from the detectors is fed to lock-in amplifier followed by the DAS. A lock-in-amplifier is used for phase sensitive detection at reference frequency of the chopper. A Keithley unit (model no. KDC 500/1) is used to digitize simultaneously both channel and receiving the 16 bit analog signal. The DAS incorporates a graphics program which enables any portion of the sampling data to be displayed immediately after the event.

2.1.2 Instrument Performance

The instrument till date is in use as a regular backend instrument for observing lunar occultation observations from 1.2m Telescope at Mount Abu, India. During the period of the thesis the total number of lunar occultation events successfully recorded were thirty six. Out of these number two channel events successfully recorded were only five (Mondal, Chandrasekhar & Kikani 2002a). Due to the large background noise in L′-band only a limited number events were suitable for two channel operation and all are listed in table 2.3. **All L′-band light curves are first time LO observations.** The simultaneous light curves of μ Gem in the K- and L′-band in are shown in Fig. 2.5. The results are discussed in chapter5.

Table 2.3: **Successful two channel observations simultaneously in K- and L′-bands**

Star	Spectral type	Date of observation	m_k	m_L	event type	SNR K	SNR L′
η Gem	M2.5 III	08 Jan 2001	-1.49	-1.59	D	20	10
μ Gem	M3 III	04 Mar 2001	-1.89	-2.01	D	31	09
η Gem	M2.5 III	04 Mar 2001	-1.49	-1.59	D	20	05
U Ari	M4-9.5 IIIe	19 Feb 2002	1.59	0.28	D	30	03
ν Vir	M1 III	27 Mar 2002	0.00	-0.05	D	38	05

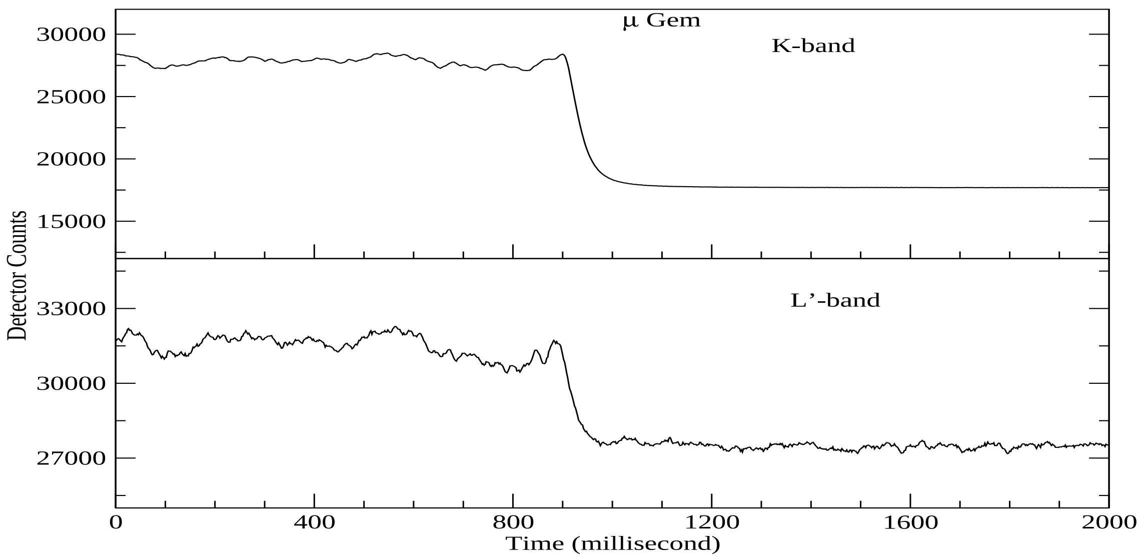

Figure 2.5: *Lunar Occultations of μ Gem observed simultaneously in the K- (2.2 μm) and L′ (3.8 μm)-band on 4 Mar 2001. Results are discussed in chapter 5.*

Limiting angular resolution of the system

The instrumental effects of finite time response of the detector, finite optical bandwidth and finite telescope aperture have to be carefully modeled in the analysis so that their combined effect does not distort the true angular diameter of the source observed. Towards this end lunar occultation observations of a point source is important.

The lunar occultation of IRC+20071 has been recorded in the K-band under clear sky conditions. The trace is good quality which has recorded well upto fifth fringe. The signal to noise ratio of the light curve is $\sim$ 50. The UD model is fitted with five parameters and a 5th order Legendre polynomial is used to fit varying background. The source is unresolved in our analysis of UD model fit, evidenced by the convergence parameter χ^2 of the fit (shown inset of fig.2.6). For resolved sources, the model converges towards an angular diameter which gives a minimum χ^2 value. For unresolved sources χ^2 remains flat upto the resolution limit then increases monotonically with angular diameter. Fig.2.6 shows model best-fit light curve with observed data points.

The spectral type of the source is K5 III (SIMBAD database). Previous reported value of angular diameter is 2.71$\pm$0.15 mas by LO in K (Richichi et al. 1998a). We put an upper limit of a uniform disk (UD) angular diameter to be $\sim$2 mas. The limiting angular resolution of the instrument , when observed in Fast dewar, is $\sim$ 2.0 mas which has also been established earlier (Chandrasekhar 1999).

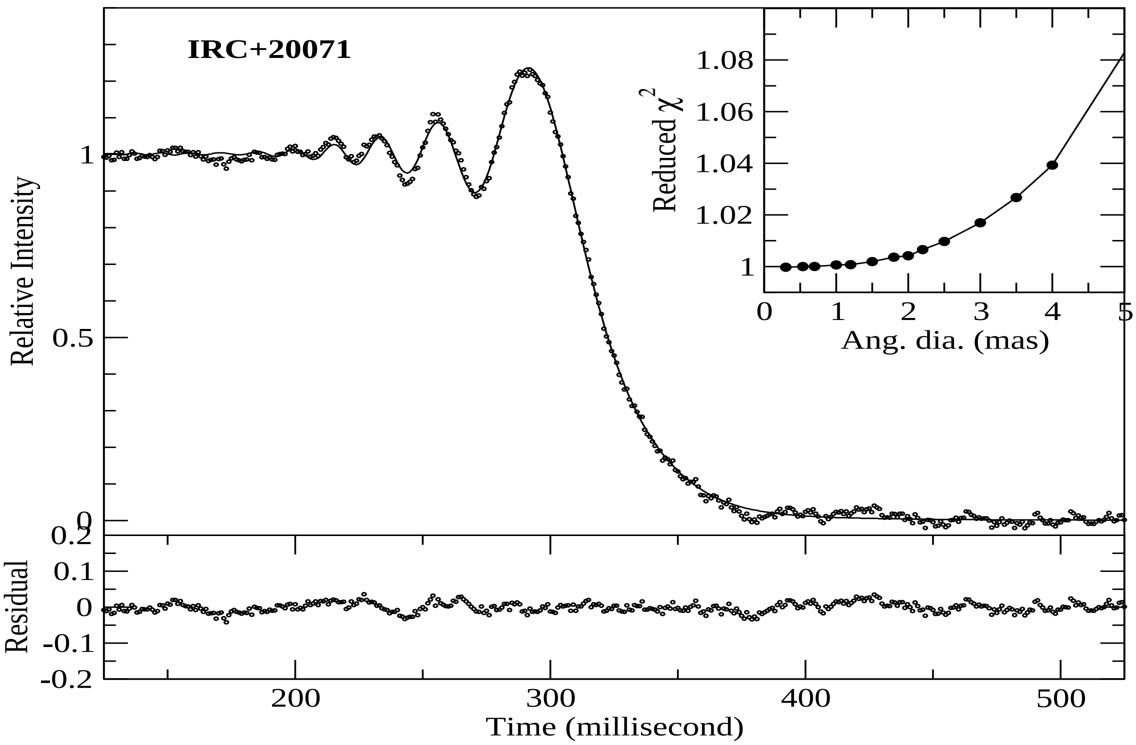

Figure 2.6: **Pointsource:** *The best-fit model curve is superposed on the observed points. The lower panel shows the residual of fit.Inset shows the convergence parameter which does not show a minimum as the source is unresolvable (< 2 mas).*

2.2 Lunar occultation theory and Data Analysis

The lunar occultation light curve is basically a Fresnel diffraction pattern produced transiently during disappearance (or reappearance) of stellar sources behind the sharp limb of the Moon . The light curve can be analyzed by treating it as a combined pattern formed by a series of point sources along the direction of occultation separated in time across stellar disk. The resultant intensity of each point source is the area of the strip of the uniform disk that it represents. The resulting pattern is convolved with smearing effects of various instrumental parameters. The mathematical form of the light curve can be written as,

$$I(t)=\int_{-\infty}^{+\infty}d\phi\int_{-A/2}^{+A/2}d\alpha\int_{\lambda_2}^{\lambda_1}d\lambda\int_{-\Delta\tau}^{0}d\tau S(\phi)O(\alpha)\Lambda(\lambda)T(\tau)F(\omega)+\beta(t) \tag{2.1}$$

Where S(ϕ) is the stellar brightness profile, O(α) is the parameter due to averaging effects of telescopes, T(τ) is the electronics time response of detector and preamplifier, $\Lambda(\lambda)$ is spectral response of the source, F(ω) is the Fresnel expression of diffraction by the straight edge for a monochromatic point source and β(t) is the temporal variation of the background level.

$$F(\omega)=\frac{1}{2}\left[\left(\frac{1}{2}+C(\omega)\right)^2+\left(\frac{1}{2}+S(\omega)\right)^2\right] \tag{2.2}$$

Where C(ω) and S(ω) are the Fresnel integrals and ω is the dimensionless Fresnel number. The Fresnel number can be written as,

$$\omega=\left(\frac{2}{\lambda d}\right)^{\frac{1}{2}}\left[v(t-t_o)+d\tan\phi+\alpha\right] \tag{2.3}$$

Where d is the distance to the Moon, λ is the wavelength of the observation, t_o is the time of geometrical point of occultation which means the time when the star intensity drops down to one fourth of its initial value (I_o), v is the velocity component of lunar shadow in the direction perpendicular to the limb at the point of occultation and α is the linear displacement term due to averaging effect of the telescope aperture. The different averaging effects of the fringes due to finite source size, S(ϕ); finite filter bandwidth and spectral response of detector system $\Lambda(\lambda)$; telescope aperture effect, O(α); detector electronics time response, T(τ) and temporal variation of the background level, β(t) will be discussed individually.

2.2.1 Data Analysis: Nonlinear Least Square Technique

Nather & McCants (1970) introduced a Non-linear Least Squares (NLS) method for analyzing optical lunar occultation light curves. This method has been widely used in both optical and near infrared region. The conventional method of analysis of the lunar occultation light curve involves the assumption of a uniformly illuminated disk whose one dimensional profile along direction of occultation is the quantity obtainable. χ^2 minimization technique is used to obtain best statistical estimation of the multiple parameters. These multiple parameters are (i) geometric time of occultation; (ii) stellar signal counts; (iii) sky-background counts; (iv) velocity component of the Moon in the direction of occultation in km/s (predicted parameter); and (v) the uniform disk angular diameter in milliarcsecond (initial guess parameter). Several instrumental parameters like filter transmission, detector electronics time response and telescopes averaging effects are considered in the analysis produces.

Source brightness profile

The one dimensional brightness profile of source in the direction of occultation can be modelled using by a simple circular disk model. The brightness profile as given by Diercks & Hunger (1952) is,

$$S(\phi) = I_o \frac{\frac{2}{\pi}\left[1 - \left(\frac{\phi}{\Omega}\right)^2\right]^{\frac{1}{2}} + \frac{1}{2}\kappa\left[1 - \left(\frac{\phi}{\Omega}\right)^2\right]}{\left(1 + \frac{2}{3}\kappa\right)} \tag{2.4}$$

Where Ω is angular radius of the star, I_o is the intensity of the unocculted stellar source, κ is the limb-darkening co-efficient and ϕ is the resolution of the model. For uniform disk (UD) model without limb-darkening case κ = 0.0 while for fully darkened disk (FDD) model κ = 1.0. The finite signal to noise ratio in the occultation light curve does not generally allow the limb darkening coefficient to be treated as a free parameter in the model.

The limb-darkening co-efficients are estimated usually from stellar models by considering atomic and molecular opacity data. Menduca (1979) has given the infrared limb-darkening co-efficients of M-type giants and supergiants considering the model of Gustafsson et al. (1975) but it was limited upto the effective temperature of 3750 K. Later Scholz & Takeda (1987) have given estimations based on model of Bessell et al. (1989) for all spectral class of M-type giants and supergiants. Recently more systematic studies of the limb-darkening correction factors of M-type non-Mira and Mira stars for different filter-bands frequently used in observations have been reported (Hofmann et al. 1998a, 1998b). These are based on non-Mira M-giant models of Bessell et al. (1989) and Mira models of Bessell et al. (1996). The potential drawback in these models is poor agreement between angular sizes derived at different wavelength bands (Dyck et al. 2002). For example, the limb-darkening corrections on a set of angular diameter measurements of η Gem are studied in chapter 5 of this thesis. The limb-darkening corrections in the range of 1.04 - 3.8 μm region are considered here. The UD values in that regions underestimate the true size by about 3-5% considering all series of models for non-Mira M-type giants (Hofmann et al. 1998a). Mira models of Hofmann et al. (1998b) list several limb-darkening corrections for measured UD diameters which are dependent on phase, luminosity of the star and mode of pulsations. For example in Z-series models for fundamental mode at maximum phase the

UD value approximately overestimate the true size by 5% in the 1.04 - 3.8 μm. van Belle et al. (2002) found that in all Mira models of Hofmann et al. (1998b) the rms ratio of uniform disk diameter to 'true' photospheric diameter is 1.0$\pm$0.04 (van Belle et al. 2002). The near-infrared continuum radii in most of the model series are close to the true photospheric size and hence uniform disk (UD) profile may be better representative of the true photosphere.

Previously several authors have scaled their measured UD diameters to limb-darkening (LD) diameters to compute effective temperature. For example, to establish the empirical relation between the spectral types and effective temperatures, Dyck et al. (1996) converted measured K-band UD diameter to LD diameter by using the scaling factor of 1.022 (ϕ_{LD} = 1.022ϕ_{UD}) based on model of Scholz & Takeda (1987). To measure effective temperature of extremely cool giant Mira variables from K-band interferometric diameters, van Belle et al. (1996) used the scaling factor of 1.11 at minimum of photometric variability phase and of 0.98 at maximum again based on model of Scholz & Takeda (1987). Perrin et al. (1998) suggested the scaling factor of 1.035 for K-band interferometric measurements. To calibrate the spectral types to effective temperatures Richichi et al. (1999) considered the scaling factor in the range of 1.02 to 1.04 for non-Mira giants spectral types of M2 - M10. The largest scaling factor in K used earlier 1.11, results in only a 5% change in the resultant value of effective temperature. Considering the minimal effects of scaling factor on measured UD value in the infrared and our signal to noise ratio in the occultation curves we have used measured UD to compute T$_{eff}$. The UD profile used in the analysis is given as,

$$S(\phi) = I_o \frac{2}{\pi} \left[1 - \left(\frac{\phi}{\Omega} \right)^2 \right]^{\frac{1}{2}} \tag{2.5}$$

In the numerical modelling the finite source size is sliced into several strips along the direction of occultation and schematic diagram of sliced source is shown in Fig. 2.7. Each slice can be assumed as a point source having the intensity proportional to area of the slice.

In practice, the numerical integration in eqn. 2.1 can be written as,

$$S'(\phi) = \int_{\phi_i - \delta\phi}^{\phi_i + \delta\phi} S(\phi) d\phi \tag{2.6}$$

$$S(\phi) = \frac{S'(\phi)}{\sum_i S'(\phi)} \tag{2.7}$$

Where S(ϕ) is the source function given in eqn. (2.4). The step size, $\delta\phi$, we choose initially 0.02 mas and final run it set to 0.05 mas.

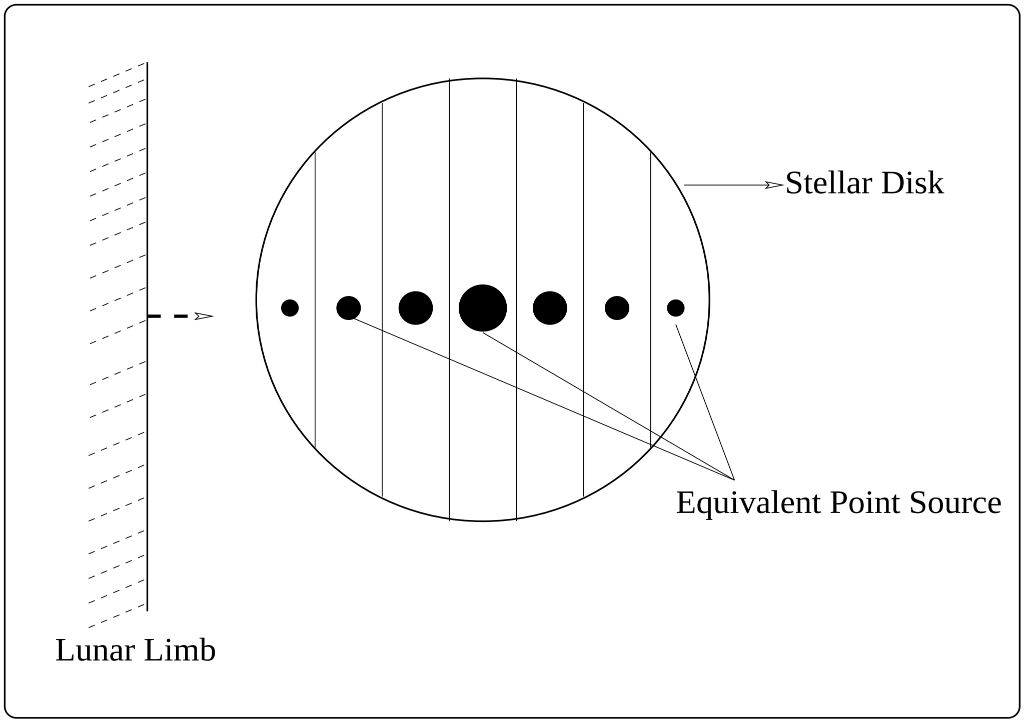

Figure 2.7: *The finite source is sliced into different point sources. The intensity of each point source is equivalent to the area of the strip. Each point source will produce the Fresnel pattern at a different time on the limb and the observed pattern is resultant of all such point sources.*

Optical bandwidth and wavelength response

The wavelength response of the system is defined by the optical filter characteristics curve f(λ) (Fig. 2.4) and wavelength response of the detector l(λ) used. In addition, the spectral energy distribution of the star b(λ) also needs to to be considered when broad band filters are used. The resultant system wavelength response can be written mathematically,

$$\Lambda(\lambda) = f(\lambda)l(\lambda)b(\lambda) \tag{2.8}$$

The function f(λ) can be obtained from filter calibration curve which is plotted in Fig. 2.4 (left). The function l(λ) for InSb detector can be approximated in the K-band as, l(λ) $\propto \lambda$. Fig. 2.5 (right) shows the system wavelength response when K-filter is used (filter transmission curve is multiplied by the detector wavelength response).

The function b(λ) is assumed as a blackbody spectrum, can be written as,

$$b(\lambda) = C_1 \times \frac{\lambda^{-5}}{e^{C_2/\lambda T} - 1} \tag{2.9}$$

where $C_1 = 2\pi hc^2 = 3.742 \times 10^{-16}$ W m^2 s^{-1}, $C_2 = ch/k = 1.4388 \times 10^{-2}$ m K and T is the temperature of the star in degrees Kelvin. The integration of Λ dλ in eqn. 2.1 is numerically is evaluated as,

$$\Lambda_i'(\lambda_i) = \int_{\lambda_i - \delta\lambda}^{\lambda_i + \delta\lambda} \Lambda(\lambda) d\lambda \tag{2.10}$$

$$\Lambda_i(\lambda_i) = \frac{\Lambda_i'(\lambda_i)}{\sum_i \Lambda_i'(\lambda_i)} \tag{2.11}$$

In the analysis $\delta\lambda$ is initially set equal to 0.05 μm and in the final run it is set to 0.025 μm.

Finite Telescope Aperture

The lunar occultation diffraction pattern of the star sweeping over the Earth surface is averaged by the finite telescope aperture. The effect is small in case of 1m class apertures but for large aperture telescope this effect has to be taken into account. In case of Cassegrain telescopes, the secondary obscuration has also to be taken into account. The telescope aperture along the direction of fringe motion is sliced into small pieces as shown in Fig. 2.8. The function can be written mathematically as,

$$\begin{aligned} O(\alpha) &= \left[1 - \left(\frac{\alpha}{T_p}\right)^2\right]^{1/2} - \left[1 - \left(\frac{\alpha}{T_s}\right)^2\right]^{1/2} \text{ when } \alpha \leq T_s \\ &= \left[1 - \left(\frac{\alpha}{T_p}\right)^2\right]^{1/2} \text{ when } T_s < \alpha \leq T_p \end{aligned} \tag{2.12}$$

where T_p (T_s) is the radius of the telescope primary (secondary) mirrors.

Similarly like others numerically the integration is treated in the eqn. 2.1 as,

$$O_i'(\alpha_i) = \int_{\alpha_i - \delta\alpha}^{\alpha_i + \delta\alpha} O(\alpha) d\alpha \tag{2.13}$$

$$O_i(\alpha_i) = \frac{O_i'(\alpha_i)}{\sum_i O_i'(\alpha_i)} \tag{2.14}$$

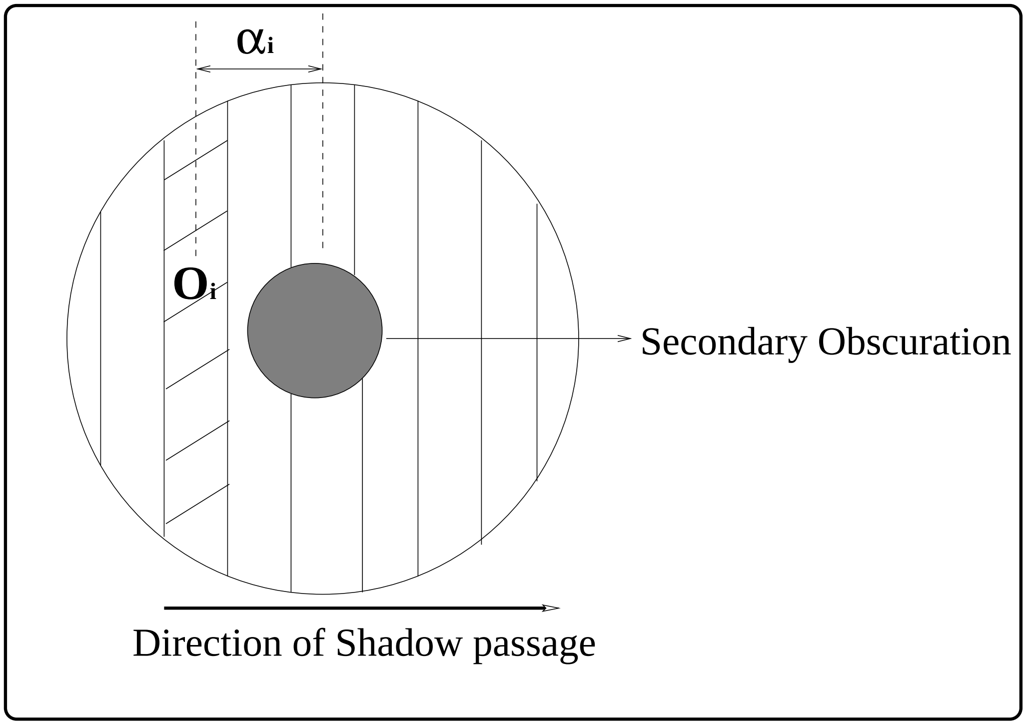

Figure 2.8: *The modelling approach of the telescope aperture.*

Varying Background Light

The background light level, β(t) in eqn.2.1 is often found to vary during the event. In the case of disappearance events, the varying background light shows generally positive gradient, as the Moon approaches the detector aperture field. Such gradient is event dependent and it depends on many factors like lunar phase, atmospheric conditions, air mass and wavelength of observations. In particular events where the varying background can be not accounted by a single gradient, the background light level has been modelled by a polynomial, which has form

$$\beta(t) = \sum_{i=0}^{n} a_i t^i \tag{2.15}$$

The degree of polynomial, n is chosen depending on quality of observed light curve.

Scintillation noise

Fresnel fringe in lunar occultation light curve is formed well outside Earth's turbulent atmosphere but the light curve is collected at telescope aperture after passing through the Earth atmosphere. Lunar occultation being a fast event (sampling time $\sim$ 1 - 2 ms), the effect of atmospheric seeing on the light curve may not be severe though the total event duration is generally above the atmospheric coherence time of $\sim$60 ms. However, scintillation effects are more prominently present in the observations of bright sources.

Knoechel & von der Heide (1978) have shown numerically the presence of scintillation noise in light curve can bias the angular diameter estimation to a large extent. In order to get a statistically correct estimate of the angular diameter, this effect has to be taken into account in the data analysis. The scintillation effect on the occultation light curve can be modelled by a normalized Legendre polynomial of the form,

$$L'(t) = \left[1 + \sum_{i=1}^{m} b_i L_i(t)\right] \tag{2.16}$$

which is multiplied with the theoretical Fresnel diffraction pattern expected for the source in the absence of any background light. m is the order of Legendre polynomial and b_is are treated as free parameters in the model along with other free parameters. Richichi et al. (1992) suggested to damp the portion of the term L(t) after geometrical occultation because the scintillation effects vanishes after the star disappears from aperture. Such cases are actually observed in data. The damping function has the form,

$$\begin{aligned} \rho(t) &= 1 \quad \text{when } t \leq t_o \\ &= I(t) - \beta(t) \quad \text{when } t > t_o \end{aligned} \tag{2.17}$$

Care should be taken in choosing the order of the polynomial because by increasing the order of the polynomial, arbitrarily can lead to spurious fits. During analysis the order of polynomial is considered upto the level where model fringes are completely unaffected and the velocity component has not deviated significantly from the predicted value.

Detector Time Response

Among the instrumental averaging effects, the time response of detector/electronics system is of crucial importance. The time constant of the detector system is defined as the time taken for the signal to drop 1/e (i.e. 36%) of its initial value. The time constant for dewar generally used for transmission channel (called CVF dewar) is $\sim$ 12 millisecond (ms) while other used in transmission channel (called Fast dewar) has a better time constant of $\sim$ 7 ms. Duration of the LO event is typically 200 -300 ms and the light curve is observed with sampling time of 1 - 2 ms. The detectors used here do not have the flat response upto the sampling frequency which results in smearing of the fringes. So, the time response is taken into account in the analysis. The system time response depends upon the pre-amplifier level and after every event the experimental time constant is measured by fast infrared light emitting diode and square wave frequency generator. Extensive experiments on time response of our system can be found in Tej (1999). Typical detectors time response curves for the two dewar used are shown in Fig. 2.9.

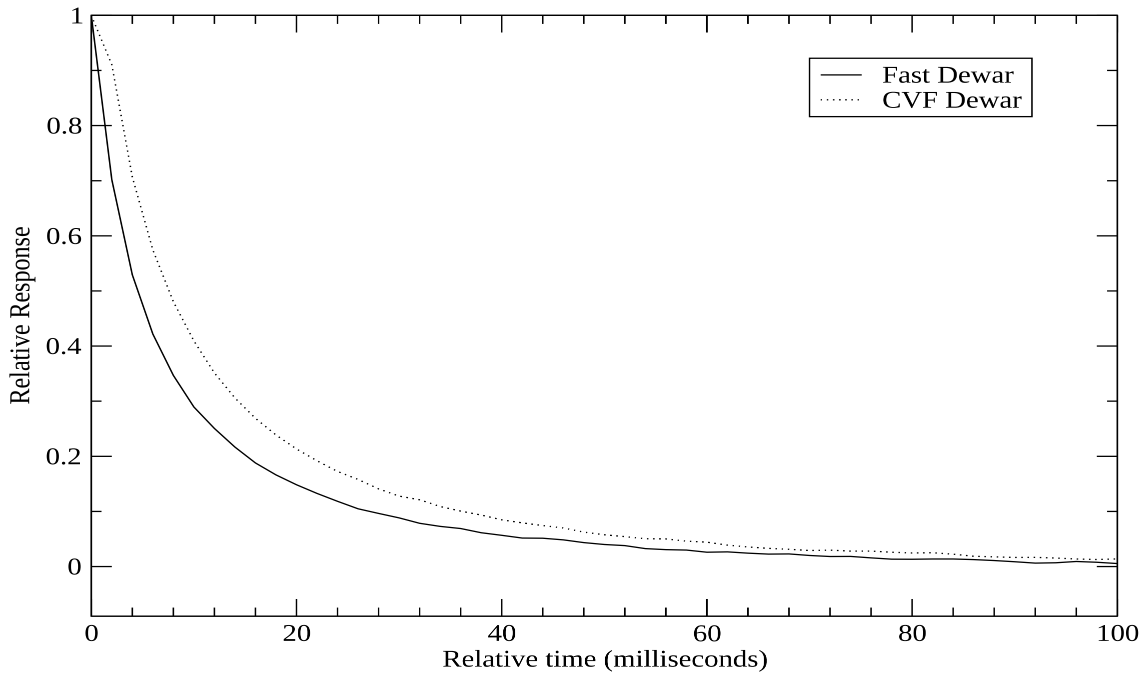

Figure 2.9: *The typical time response of two detectors in Fast and CVF Dewar is shown.*

2.2.2 Model Independent Approach (MIA)

In case of conventional lunar occultation analysis the brightness profile of the source is considered to be a generally simple uniform disk (UD) profile. The UD profiles is more appropriate for compact objects where the source does not have geometric extension. But in case of low surface gravity objects like shell stars which have significant contribution from extended regions in the light curve such simple UD profile fits to the observed data may not produce always satisfactory results. Such examples of deviation from UD fits have been found in two objects, WR 104 (dusty Wolf-Rayet stars) (Mondal & Chandrasekhar

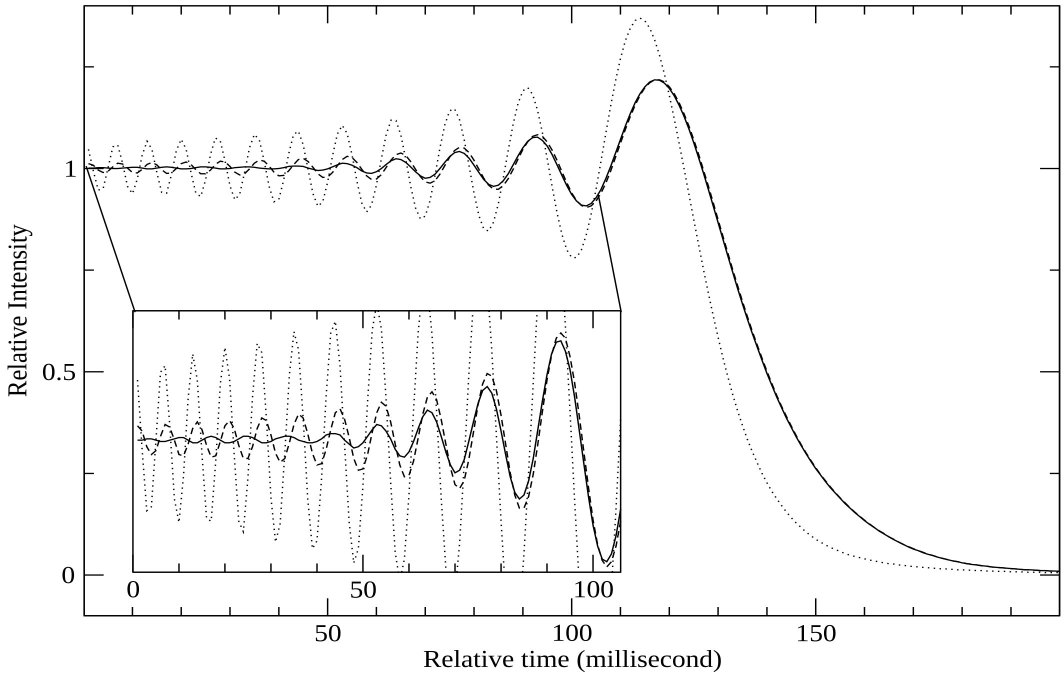

Figure 2.10: *The Simulated light curves of a point source are shown. The different instrumental effects are shown here. The dotted line is generated without time response effect. The dashed line is generated considering time response effect only. The solid line is generated considering all instrumental effects e.g. time response, filter bandwidth and telescope aperture. Inset shows expanded form of the region marked.*

2002b) and U Ori (Mira star) (Mondal & Chandrasekhar 2004) in this thesis. The details are discussed in chapter 3 and chapter 4. Several other examples can be found like highly evolved carbon Mira IRC+10216 and TX Psc (Carbon star) (Chandrasekhar & Mondal 2001; Richichi et al. 1995).

Lunar occultation analysis normally provides one-dimensional high angular resolution ($\sim$ 1 mas) assuming a uniformly illuminated disk. Departures from uniform disk can not be directly retrieved (atleast in optical and near infrared wavelength) from the observed light curve, unless some prior knowledge of the shape of the source is given. In order to overcome this difficulty, Richichi (1989) introduced a deconvolution algorithm (Lucy 1974) which provides iteratively the *most-likely* brightness profile in a statistical sense from starting point of UD profile with several free parameters mentioned earlier.

The technique is essentially a composite algorithm which uses non-linear squares fitting described earlier and Lucy deconvolution algorithm (Lucy 1970), wherein usually the uniform disk profile is assumed as a initial guess profile and is modified iteratively to obtain the best fit of the observed data points. Lucy deconvolution algorithm is developed for rectifications and deconvolution problems in statistical astronomy. First, one has to provide several initial guesses for signal level (I), velocity component along the direction of occultation (v), geometric time of occultation (t_o), background signal (β) and the bigger UD profiles (S(ϕ). The system time response and filterband width effects are also considered in this scheme.

In every iteration the new profile found from the knowledge of instrumental effects and the observed data is fitted using the below mathematical form until satisfactory convergence on S(ϕ). The new profiles after rth iteration is given as,

$$S^{r+1}(\phi) = S(\phi) \int \frac{I(t)}{I^r(t)} \Pi(t, \phi) dt \tag{2.18}$$

where the eqn. (2.1) can be rewritten as,

$$I(t) = \int S(\phi) \Pi(t, \phi) d\phi + \beta \tag{2.19}$$

and the matrix Π describes all the instrumental effects, can be written as,

$$\Pi(t, \phi) = \int_{-A/2}^{+A/2} d\alpha \int_{\lambda_2}^{\lambda_1} d\lambda \int_{-\Delta\tau}^{0} d\tau O(\alpha) \Lambda(\lambda) T(\tau) F(\omega) \tag{2.20}$$

The iterative scheme of the MIA algorithm is shown in the Fig. 2.11.

It is important to perform a sufficiently high number of iterations in order to exploit all the information present in the data, but care has to be taken to avoid contamination by noise. In fact, if too many iterations are performed the restored profile tends to develop a structure with fine details which are fictitious and due to noise in the original data. Therefore limit of the fit should be constrained by computing the standard deviation of observed data and residual of fit.

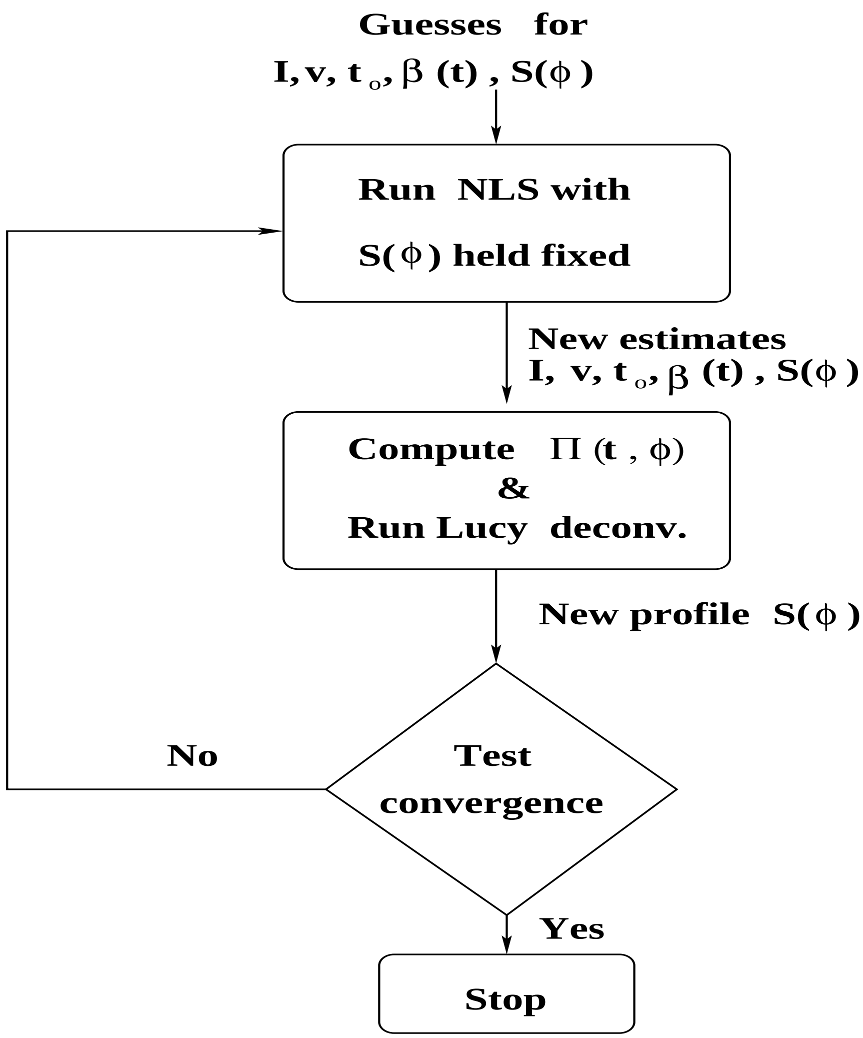

Figure 2.11: *Block diagram of the iterative scheme for brightness profile retrieval from occultation light curves, taken from Richichi (1989).*

2.3 Effective Temperature and Errors

Lunar occultation analysis yields the uniform disk angular diameter of the stellar source. The most direct way to determine the effective temperature of a star is through measurement of its angular diameter, ϕ , and its apparent bolometric flux, F_{bol}. The stellar effective temperature T_{eff} is defined in terms of the stellar luminosity(L) and radius(R_*) by $L = 4\pi\sigma R_*^2 T_{eff}^4$ where σ (= 5.67×10^{-5} erg cm^{-2} K^{-4} s^{-1}), the Stefan-Boltzmann constant. In terms of angular diameter and bolometric flux, the effective temperature can be written as,

$$T_{eff} = 2341 \times \left(\frac{F_{bol}}{\phi^2}\right)^{1/4} \tag{2.21}$$

Where the units of F_{bol} is in 10^{-8} erg cm^2 sec^{-1}, ϕ in mas and T_{eff} in K.

The error in effective temperature is calculated from the relation,

$$\sigma_{T_{eff}} = T_{eff}\left(\frac{1}{16}(\frac{\sigma_{F_{bol}}}{F_{bol}})^2 + \frac{1}{4}(\frac{\sigma_\phi}{\phi})^2\right)^{1/2} \tag{2.22}$$

Bolometric flux is related to fourth power of the effective temperature in the above equation, hence the error introduced due to F_{bol} in estimation of T_{eff} will be less sensitive compared to angular diameter which is proportional to square of T_{eff}. For example, 20% error in F_{bol} (with fixed angular diameter (ϕ)) results 5% error in T_{eff} while 20% error in ϕ (fixed F_{bol}) leads to 10% error. The typical error in F_{bol} is less than 15% and in diameter about 10%, the error in estimation of T_{eff} is about 7%.

As discussed in earlier section of this chapter the K-band angular diameter is close to 'true' photospheric diameter of the stellar source and hence no limb-darkening correction is applied to our measured angular to compute T_{eff}. The limb-darkening corrections for M-type stars in K may bias the results of T_{eff} by only $\sim$2-5% depending on spectral type.

In summary, a two channel high speed infrared photometer has been developed successfully for simultaneous lunar occultation observations in two infrared wavelengths K and L$'$ bands. The instrument can also be used in single channel mode for observations. In later chapters the results from one channel and two channel measurements are discussed.

Chapter 3

Dust shell structure around Wolf-Rayet star WR104

In this chapter a rare lunar occultation observation of a Wolf-Rayet star is discussed and compared with high angular resolution images obtained by aperture masking at the Keck 10m telescope.

3.1 Introduction

The Wolf-Rayet(WR) stars were discovered by C.J.E. Wolf and G. Rayet in 1867. WR stars are massive and highly luminous blue stars at the end of their nuclear burning phase and are thought to be immediate precursors to supernova which would terminate their lives. WR stars are characterized by strong He, N, C and O emission lines, originating in their hot stellar winds with terminal velocities in the range $v_\infty \approx 400$ - 5000 km/s. The intense stellar winds leads to high mass loss rates of the order of 10^{-5} $M_\odot$/yr (van der Hucht 1992). The 7th catalogue of WR stars in our Galaxy, compiled by van der Hucht (2001), lists 227. The WR star census is very much incomplete due to interstellar extinction in the Milky way. The total number 227 comprises 127 WN stars, 87 WC stars, 10 WN/WC stars and 3 WO stars. In case of WR stars, one is dealing primarily with an emission-line spectrum, formed in an optically thick stellar wind . The first steps in understanding these stars could only come with the identification of their lines, which led to the separation of WR stars into two groups WN and WC according to their different chemical composition (Smith et al. 1990; van der Hucht 2001). The WC or WN stars were further classified according to the relative strength of lines of different ionization potentials. This was meant to give an ionization sequence in analogy with the MK classification. But MK classification was based on stellar fundamental quantities (temperature and indirectly, mass), WC (WN) classifications are not directly related to the stellar temperature or other physical parameters. In case of WN stars, higher order of ionized state of nitrogen emission lines are used to classify subtype in the range WN2 - WN11 (Conti 1999). WC stars are classified based on strong carbon ionized emission lines (Crowther et al. 1998).

It has been known since the early days of infrared astronomy that a small fraction of WR stars belonging to the latest WC evolutionary stage show strong infrared emission signifying the presence of a heated dust shell mainly made up of hot carbon grains (Allen, Harvey & Swings 1972; Gehrz & Hackwell 1974; Cohen, Barlow & Kuhi 1975; Williams, van der Hucht & Thé 1987). The dust shell is the result of heavy mass loss from the star(van der Hucht 1992). These WC stars are further classified as variable or persistent dust producers depending upon the variability of infrared emission (Williams & van der Hucht 1992). The existence and survival of the dust shells in the intense radiation field encountered in the vicinity of the Wolf-Rayet stars has however been difficult to explain by the conventional spherically symmetric outflow scheme (Williams et al. 1987). The episodic formation of dust in a long period WR binary system like WR140 appears to coincide with periastron passage with colliding stellar winds at close binary separation of a few AU inducing dust formation (Williams et al. 1990). However the brightest infrared WR stars like WR104 and WR98a are generally non variable and are classified as persistent dust makers (van der Hucht et al. 1996). The nature of the dust formation in these system is still not fully understood. It has been suggested that short period binaries lie buried in these systems with wind-wind collisions again catalyzing dust formation (Usov 1991). On the other hand it has been argued that dust can form in the spherically symmetric wind of a single WR via novel dust formation processes (Zubko 1998). Apart from persistent and episodic dust makers, eclipse like variation of IR emission attributed to episodic obscuration of clumps of dust in the line of sight had been reported from three WC9 spectra by Veen et al. (1998). These variation are similar to R Coronae Borealis (RCB) type of variations but have a small amplitude of ~ 1 mag . High angular resolution observations of the dust envelopes are clearly needed to understand the phenomena of dust production, survival and dissipation around persistent dust makers among the WR stars.

3.2 WR104

3.2.1 Circumstellar Dust Shell around WR104

WR104 (Ve 2-45) is the brightest WR star in the mid-infrared ($\sim 20\ \mu$m). It is surrounded by huge circumstellar dust shell. WR104 is classified as spectral subtype WC9 star by Smith (1968). Its visual magnitude is 13.54 (Smith 1968; Torres & Massey 1987). Allen et al. (1972) estimated that the observed flux corresponded to that of a 900 K blackbody with an angular diameter of 400 mas using 1.6 μm and 2.2 μm photometry. Based on 2.3 - 23 μm photometry, Hackwell, Gehrz & Smith (1974) found that the spectrum of WR104 can be fitted by two-temperature blackbody one of which corresponds to a hot stellar continuum at $\sim$ 35000 K and another one to a cool circumstellar component at $\sim$ 1080 K. Cohen, Barlow & Kuhi (1975) estimated a shell size of 121 mas and a corresponding dust shell temperature of $\sim$ 920 K. They suggested WR104 is viewed edge on with appreciable circumstellar extinction ($A_v \sim 3.6$ mag). Williams et al. (1987) from their extensive infrared photometric study of a large number of Wolf-Rayet stars find that WR104 to be one of the few WR stars in which a substantial fraction ($\sim$ 60%) of the luminosity of the star is reradiated in the infrared by the dust shell. They derive from modeling of the ground based infrared measurements and extinction data, for WR104, an inner edge radius of the dust shell of 48 AU adopting a distance of 1.58 kpc and a shell temperature of 1110 K. In deriving the inner edge radius Williams et al. (1987) assume the binary equivalent of a WC9 star, with a radius 1.5 times that of a single WC9 star or $22R_\odot$. They also estimate the extent of the dust shell in their best fit model to be 4800 AU.

WR104 is suggested to be a binary by Cohen & Kuhi (1977) as the optical emission lines from WR104 are weaker compared to those from other WC9 stars due to dilution by a companion. A RCB type visual fading by $\sim$ 1.1 mag with the disappearance of high ionization spectral features has been recently reported by Crowther (1997). The fading has been attributed to dust cloud condensation with measured dimensions $\geq 20R_*$ taking place beyond $300R_\odot$ or $100R_*$ with the permanent dust shell at a radius of (3000 - 300,000R_*). This behaviour is interpreted in terms of an obscuration of the inner Wolf-Rayet wind by dust cloud condensations. It is also noted that Crowther (1997) derives a stellar radius R_* = $3R_\odot$ which is smaller by a factor of 5 compared to the model dependent value for a single WC9 star used by Williams et al. (1987).

3.2.2 High Angular Resolution measurements of WR104

High angular resolution observations for WR104 are summarized in Table 3.1. One dimensional speckle interferometry (Allen, Burton & Wallace 1981) with 3.9m Anglo-Australian Telescope at 2.2 μm yielded a uniform disc (UD) diameter of 130 $\pm$ 15 milliarcsecond (mas). Multi-band one dimensional speckle observations (Dyck, Simon & Wolstencroft 1984) using the 2.2m telescope of the Mauna Kea Observatory yielded the UD diameter of 130, 250

$\pm$ 70 and 310 $\pm$ 50 mas at 2.2 μm, 3.8 μm and 4.8 μm respectively. The UD value of 3.8 μm and 4.8 μm is larger than 2.2 μm by a factor $\sim$ 2. It may be noted that no asymmetric structures in the dust shell were resolvable by the early efforts.

Table 3.1: **Previous high angular resolution measurement**

Date of Obs.	Method	λ ($\Delta\lambda$) in μm	UD (mas)	References.
1980	speckle interferometry	2.2 (0.4)	130 $\pm$ 15	1
Aug 1981	speckle interferometry	2.2 (0.4)	130	2
Oct 1981	speckle interferometry	3.8 (0.7)	250 $\pm$ 70	2
Jun 1982	speckle interferometry	4.8 (0.5)	310 $\pm$ 50	2
Apr 1998 to Jun 2000	Keck I aperture masking	1.67 (0.33) & 2.27 (0.16)	130	3, 4
May 2001	Lunar occultation	2.2 (0.4)	86 $\pm$ 5	5

Table References : 1. Allen et al. 1981; 2. Dyck et al. 1984; 3. Tuthill et al. 1999a; 4. Tuthill et al. 2002; 5. This work.

Recently by aperture masking interferometry at the Keck I 10m telescope, it has been possible to resolve structures in the dust shell around WR104 (Tuthill, Monnier & Danchi 1999a). The dust emission was observed to be distributed in a rotating 'pinwheel' structure, which can be explained by wind interactions between the WR and OB type companion in a short period binary system. Subsequently another stellar 'pinwheel' system was also observed in Wolf-Rayet star WR98a by the aperture masking method at the Keck I telescope (Monnier, Tuthill & Danchi 1999a) . The aperture masking technique can retrieve spatial information up to the diffraction limit of the Keck I telescope which at 2.2 μm is 50 mas. The two epoch images of Tuthill et al. (1999a) separated by about 3 months taken at 1.65 μm and 2.27 μm clearly show that the pinwheel structure is rotating with a period of 220 $\pm$ 30 days. The size of the pinwheel dust envelope is 130 mas. More recently using four K-band images of WR104 spread over a period of more than 2 years (Tuthill, Monnier & Danchi 2002) the parameters of the system have been refined. The period is better determined to be 243.5 $\pm$ 3.0 days, the viewing angle $11^o \pm 7^o$ and angular velocity of dust outflow 111 $\pm$ 9 mas/yr. Using the angular velocity and the estimated terminal velocity of 1220 $\pm$ 300 kms^{-1} (Howrath & Schmutz 1992) from spectral linewidths, the distance to WR104 can be placed at 2.3 $\pm$ 0.7 kpc. This value is higher than earlier estimates of 1.58 $\pm$ 0.4 kpc (Lundstrom & Stenholm 1984) or 1.91 kpc (Cohen et al. 1975).

In this chapter we present high angular resolution observations obtained in the K-band centered at 2.2 μm by the method of lunar occultations. The occultation observation provided an opportunity of comparing the one dimensional high angular resolution results obtained by relatively simple means with those obtained by a sophisticated aperture masking technique at a large telescope. Lunar occultation (LO) observations provide high spatial resolution (typically $\sim$ 2 mas) one dimensional scan of the source in the direction of occultation. An earlier LO observation of a Wolf-Rayet star WR 112, has been reported by Ragland and Richichi (1998). Recently Lunar occultation of thick dusty shell surrounding the carbon-rich Mira IRC+10216 (CW Leo) has been observed at 2.2 μm by Chandrasekhar & Mondal 2001. Analysis of occultation light curve has shown asymmetric and extremely clumpy dust structure in the dust shell. In this chapter a similar method of analysis is followed for deriving the brightness profile (BP) of the dusty nebula surrounding WR104 observed at 2.2 μm (Mondal & Chandrasekhar 2002b).

3.2.3 Observations and Data Analysis

A unique of opportunity to observe the lunar occultation of the Wolf-Rayet star WR104 occurred in May 2001 at the 1.2m Infrared Telescope of Gurushikhar Observatory, Mt. Abu, India (latitude: 24^o $39'$ $8.8''$ N, longitude: 72^o $46'$ $47.47''$ E, altitude: 1680m). Circumstances of the occultation event are listed in the Table 3.2. The event was a reappearance under excellent sky conditions. Fig. 3.1 shows the schematic geometry of the reappearance event. The telescope was made to track a nearby (within 3^o) an unocculted star till $\sim$ 5 minutes before the event time and then it was precisely switched to the position of the occulted star. The event occurred 10 second after the predicted time. The occultation light curve is shown in Fig. 3.2.

In the case of WR104, the source is embedded in a thick dust shell which is so extended that the usual diffraction effects are negligible. The conventional non-linear least-square

Table 3.2: **Circumstances of the occultation event**

Date	10 May 2001
Event Type	Reappearance
Event time (UT)	$23^h\ 2^m\ 17^s$
Position angle (NESW)	252^o
Contact angle	159^o
Altitude	39^o
Predicted velocity component of Moon in direction of occultation (km s^{-1})	-0.5534
Predicted angular velocity component in direction of occultation (arcsec/sec)	-0.2922
Lunar Phase (days after new Moon)	17.25
Data sampling rate	1 ms
Photometer diaphragm on the sky (arcsec)	26
Wavelength of observation (λ)	2.2 μm
Bandwidth,$\Delta\lambda$ (FWHM)	0.4 μm
K magnitude (Williams et al. 1987)	2.37

analysis for this occultation light curve yields a uniform disc size of 86 $\pm$ 5 mas. However there are clear departures of light curve from a uniform disc which merit further investigation. For this purpose we have used a model-independent algorithm (MIA) introduced by Richichi (1989).

For a proper comparison of Keck images with our LO data we have reduced the 2.27 μm Keck images to one dimension along the direction of our occultation. To achieve this reduction we need to know the orientation of the dust envelope at the epoch of our observation. The rotation period of the dust envelope as deduced by Tuthill et al. (1999a) from their two images is 220 $\pm$ 30 days. We have generated one dimensional scans of the recent Keck images observed on 25 Jun 2000 along the direction of our occultation for various rotation rates ranging from 200 days to 250 days covering the error zone of Tuthill et al.'s estimation of WR104's period. These are shown in Fig. 3.4. To achieve this reduction each of the Keck images are rotated appropriately to match the epoch of our observation and then integrated perpendicular to the direction of occultation to produce one dimensional profile. It can be noted from Fig. 3.4 that the resulting one dimensional scans are quite sensitive to the rotation rate. In comparison with the results of our MIA program we find that rotation period between 240 and 250 days provides the best fitting one dimensional reduction of

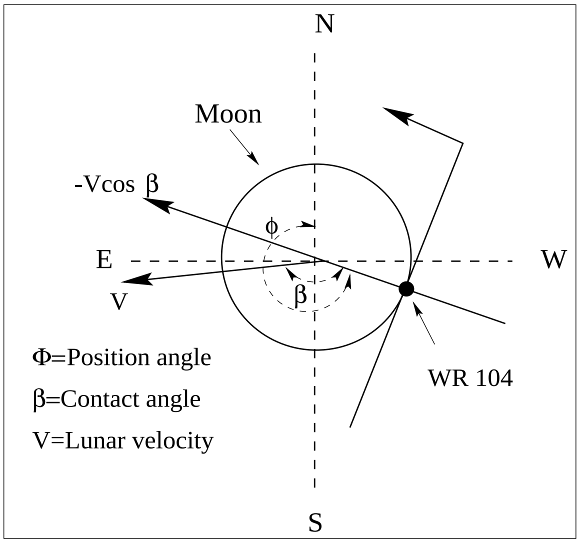

Figure 3.1: *The schematic geometry of Lunar Occultation event of WR104 observed on 10 May 2001 from Gurushikar Observatory.*

Keck images. This results is in good agreement with the recent refined measurement of the rotation rate of 243.5 ± 3 days reported by Tuthill et al. (2002).

The 1D brightness profile derived from the MIA program as well as the corresponding best fit to the occultation light curve are shown in Fig. 3.3 and Fig. 3.2 respectively. Several uniform disc starting profiles from 100 to 200 mas were tried out during the MIA analysis. The best convergence was reached for a starting UD of 170 mas which resulted in the final profile (Fig. 3.3).

The reduced one dimensional six epoch Keck profiles along the direction of our occultation along with our derived brightness profile from LO analysis is shown in Fig. 3.5. Over all a remarkable similarity between the two profiles is apparent. Many structures are not seen in the Keck profiles as their spatial resolution is 50 mas. The LO profile exhibits a lot of fine structure consistent with its higher angular resolution along the direction of occultation. For instance we observe two secondary peaks B and C while the reduced Keck profile in the region shows only one peak attributed to B. The separation between B and C is only 17 mas which would not be resolved by Keck. In order to compare the LO profile with 1-D Keck profiles at the same resolution we have systematically degraded our brightness profile by taking running averages of 70, 80, 90 and 100 points (corresponding resolutions are 70, 80, 90 and 100 mas). We find that with running average of 90 points, our smoothed profile corresponds reasonably well with the 1-D Keck profiles. There are however some differences which could be real resulting from temporal changes taking place in the dust

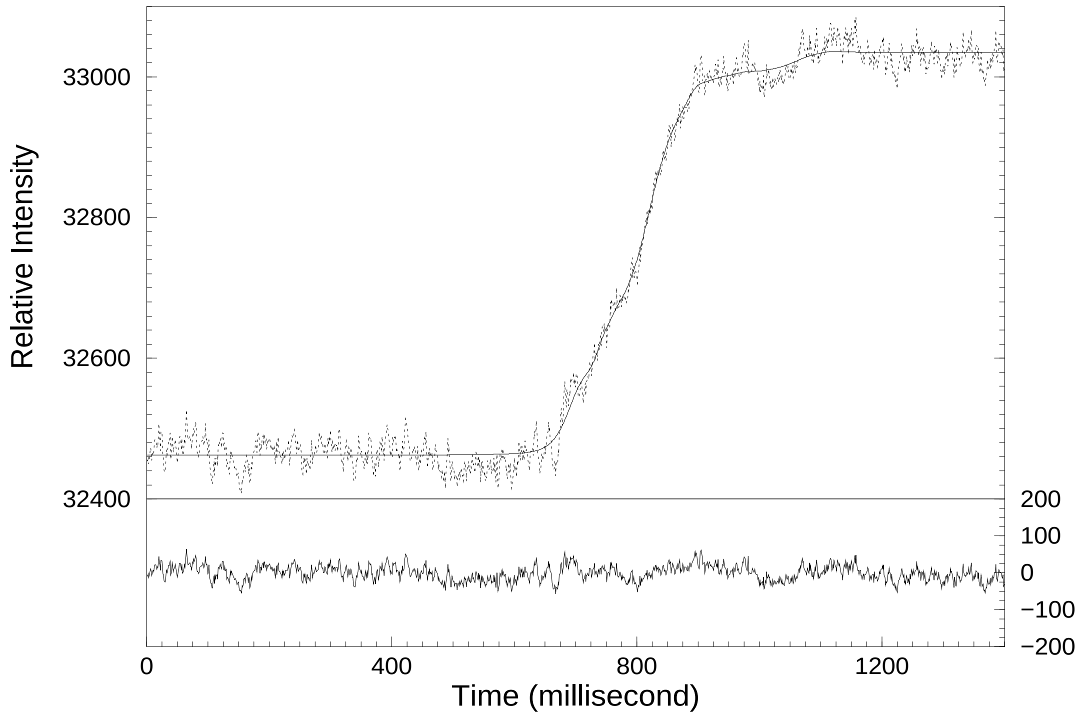

Figure 3.2: *The dotted line is the observed lunar occultation light curve of WR104 in the K-band and the Solid Line is the best fit obtained by the MIA analysis. Lower panel of lower graph shows residuals (data-model) of the best fit.*

shell in one or two rotations.

3.2.4 Results and discussion

Fig. 3.5 shows the one dimensional six epoch Keck profiles plotted along the direction of occultation. It can be seen that both the Keck profiles have similar features - two large peaks and a distinctly smaller one. Further fine structures are not seen in the reduced Keck profiles as the angular resolution achievable is the diffraction limit of the Keck telescope ($\sim$ 50 mas). In comparison the brightness profile generated by the MIA program which provides the best fit to the occultation data has a similarity with the 1-D Keck profiles but exhibits a lot of fine structure. There is a smaller peak (F) at - 70 mas followed by three large peaks A, B, C. There are also a lot more fine structures in the profile which can be identified as

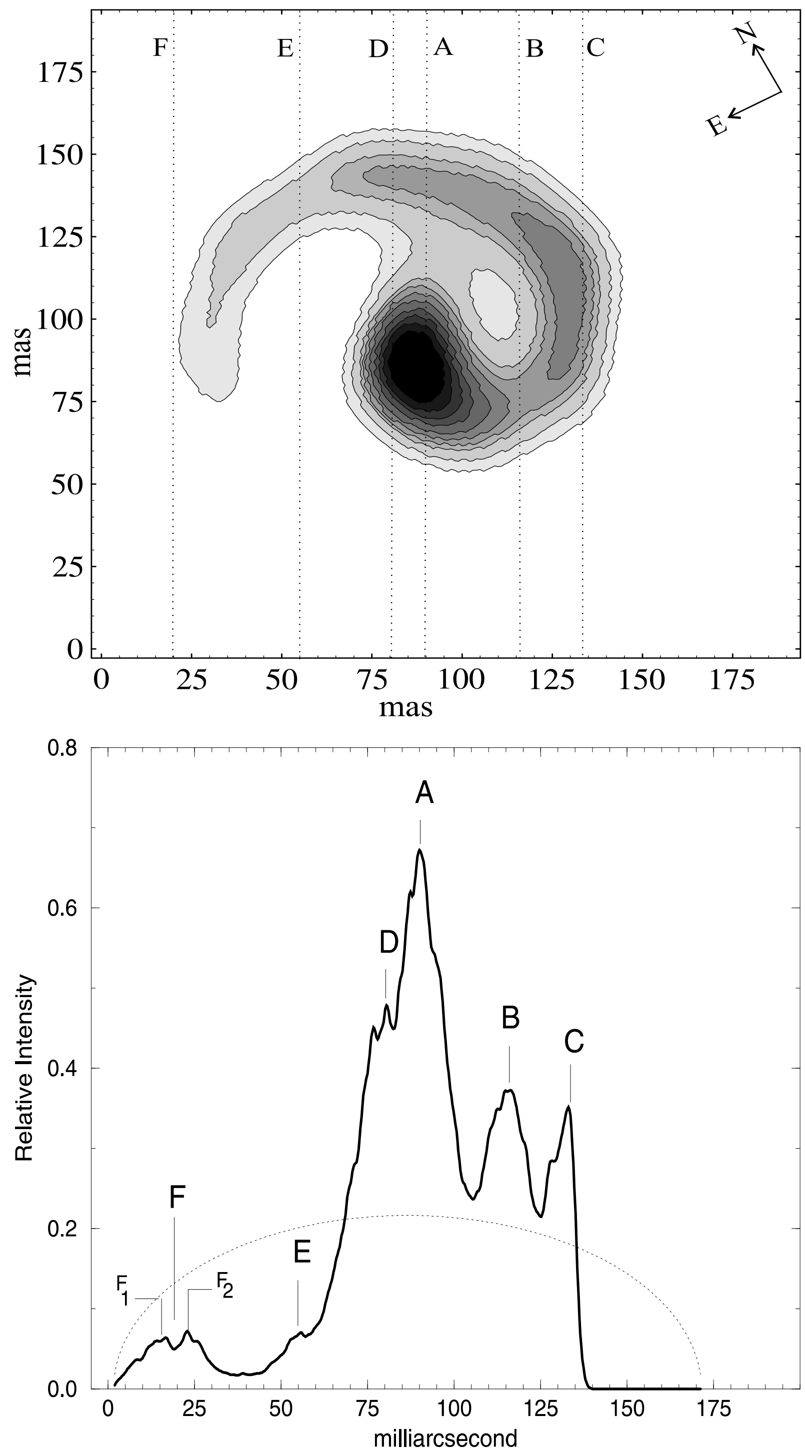

Figure 3.3: **Lower Panel :** *The solid line is the brightness profile of WR104 recovered from model independent algorithm (MIA) program and the dotted line is the uniform disc (UD) profile with a diameter of 170 mas given as a input to MIA.* **Upper Panel :** *Keck I image of WR104 was taken in April 1998. The direction of occultation is along X-axis.*

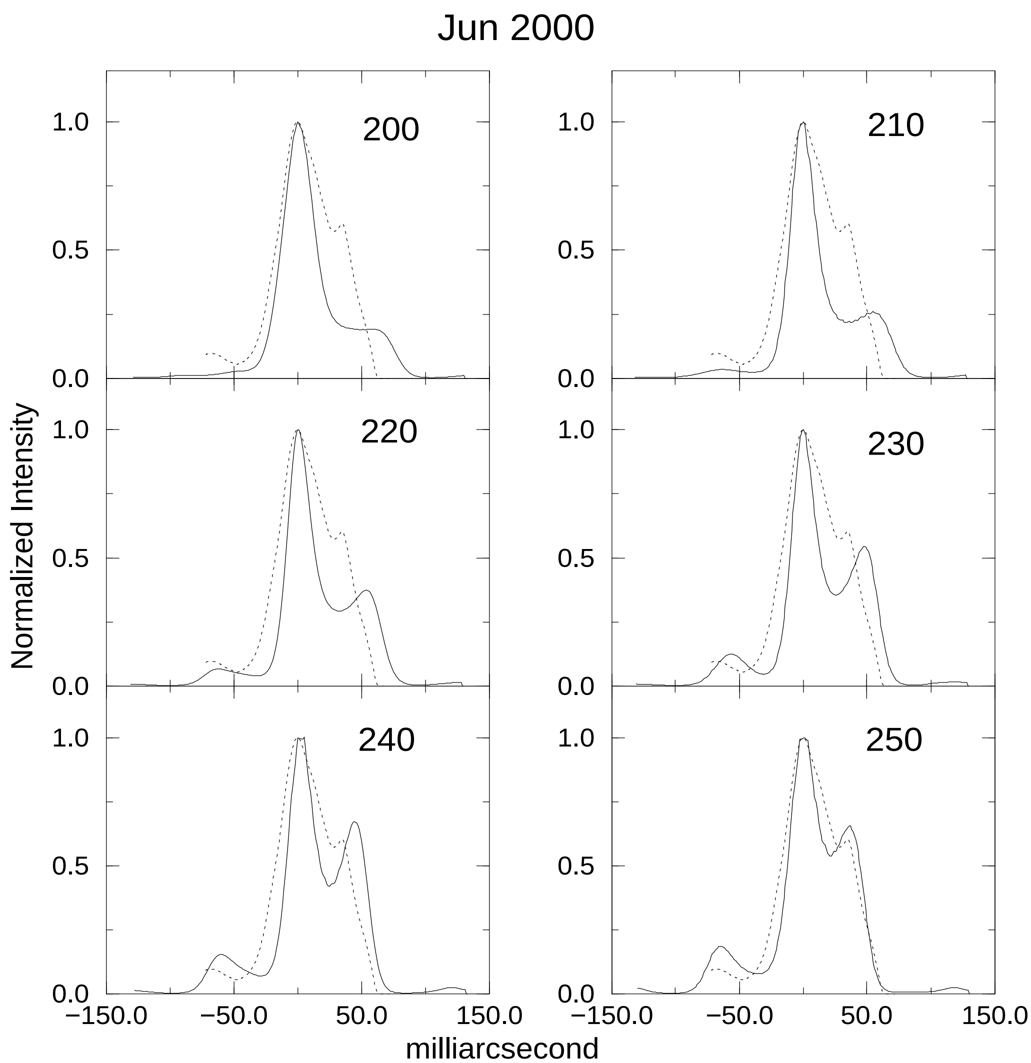

Figure 3.4: *Comparison of Keck I image of WR104 taken on 25 June 2000 reduced to one dimension along the direction of occultation (solid line) with the 90 point running average of the brightness profile obtained from Lunar occultation (dotted line). Different periods of rotation from 200 to 250 days are considered. It can seen that the best fit rotation period lies between 240 and 250 days.*

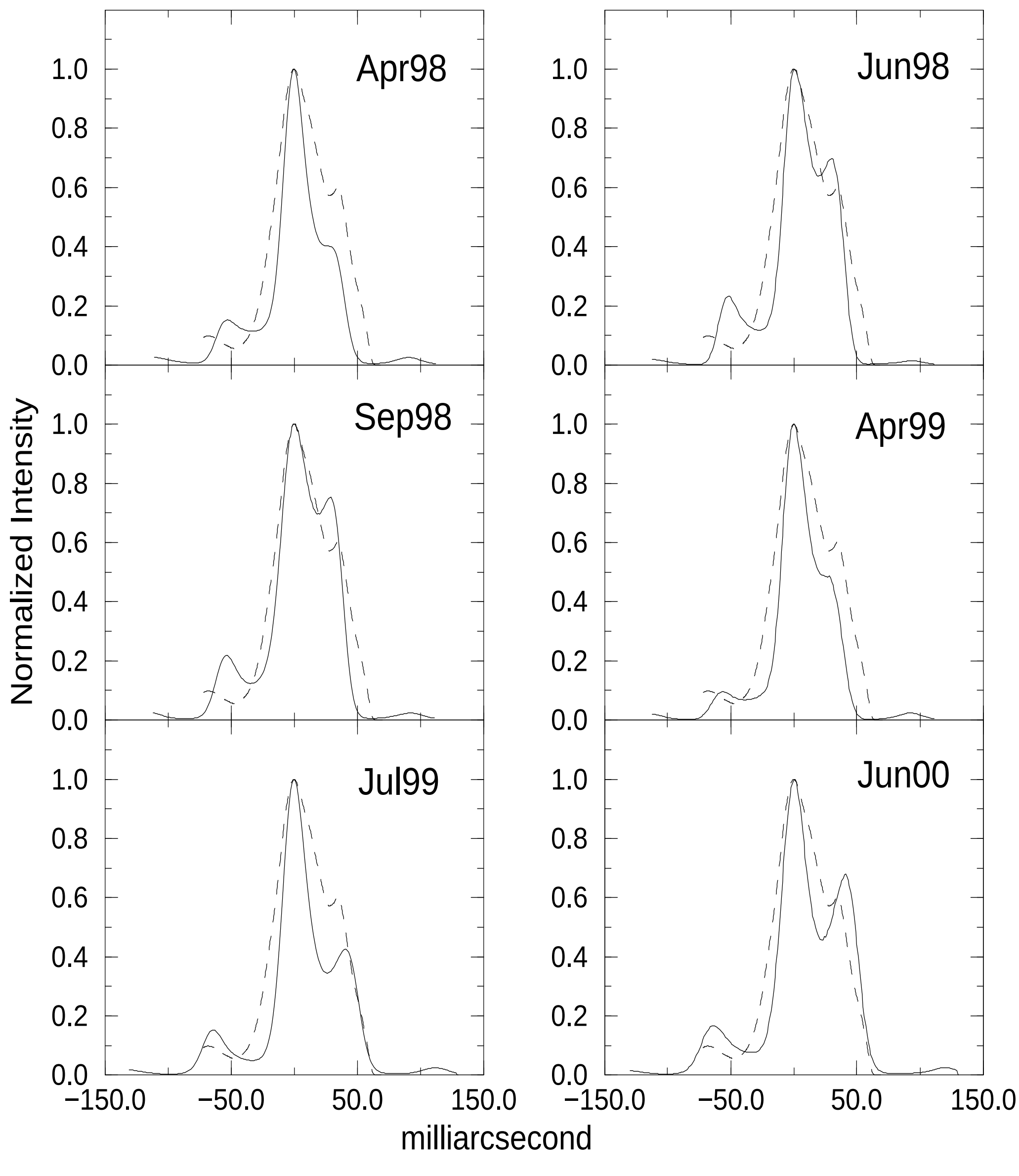

Figure 3.5: *One dimensional brightness profile (BP) along the direction of our occultation obtained for each of the six epoch Keck I images of WR104 (solid line). A rotation period of 243.5 days has been assumed. Superposed on each figure is the smoothed (90 point running average) brightness profile of WR104 obtained from Lunar occultation (dashed line).*

Table 3.3: **Relative positions of features observed by LO and Keck I profiles**

Features	Unit	A	B	C	D	E	F
BP from LO	mas	0.0	26.3	43.07	-9.5	-34.6	-70.0
May 2001	AU	0.0	60.0	99.0	- 22.0	-79.0	-160.0
Nor. Intensity		1.0	0.554	0.523	0.712	0.104	0.107
90 mas avg. LO	mas	0.0	34.0	-	-	-	-68.0
May 2001	AU	0.0	78.0	-	-	-	-156.0
Nor. Intensity		1.0	0.603	-	-	-	0.098
Keck I 1D	mas	0.0	27.0	-	-	-	-53.0
Apr 1998	AU	0.0	62.0	-	-	-	-122.0
Nor. Intensity		1.0	0.401	-	-	-	0.15
Keck I 1D	mas	0.0	30.0	-	-	-	-52.0
Jun 1998	AU	0.0	68.0	-	-	-	-119.0
Nor. Intensity		1.0	0.675	-	-	-	0.233
Keck I 1D	mas	0.0	29.0	-	-	-	-54.0
Sep 1998	AU	0.0	66.0	-	-	-	-124.0
Nor. Intensity		1.0	0.753	-	-	-	0.218
Keck I 1D	mas	0.0	28.0	-	-	-	-56.0
Apr 1999	AU	0.0	64.0	-	-	-	-129.0
Nor. Intensity		1.0	0.486	-	-	-	0.095
Keck I 1D	mas	0.0	40.0	-	-	-	-64.0
Jul 1999	AU	0.0	92.0	-	-	-	-147.0
Nor. Intensity		1.0	0.425	-	-	-	0.153
Keck I 1D	mas	0.0	41.0	-	-	-	-63.0
Jun 2000	AU	0.0	94.0	-	-	-	-145.0
Nor. Intensity		1.0	0.679	-	-	-	0.166

E, D, F_1, F_2 (in Fig. 3.3). The position of the dominant peak (A) coincides with the center of the dust nebula. Relative to A the position of other peaks B, C, and F and also the fine structures D and E are given in Table 3.3. The 90 mas averaged LO profile does not show the features C, D and E and is similar to the 1-D Keck profiles. The corresponding Keck positions are also given in the Table 3.3. Considering the distance to WR104 of 2.3 ± 0.7 kpc adopted by Tuthill et al. (1999a) our 1-D resolution of 2 mas corresponds to $\sim$ 4.6 AU. The separation between the features in linear units (AU) is also given in Table 3.3.

If we identify the rotation period of the pinwheel with the orbital period of the binary system then assuming a combined mass in the range 20 - 50$M_\odot$ (Moffat A.F., Niemela & Marraco 1990) results in a binary separation of $\sim$ 2 AU which at this distance is only $\sim$ 1 mas. This is at the limit of our achievable angular resolution but as emission of the circumstellar dust predominates over the stellar component at near-IR wavelengths the binary signature does not show in the brightness profile. The fine structure that we see in this profile are all attributable to the circumstellar dust shell surrounding WR104.

In Fig. 3.3 we have marked also the positions corresponding to our structures A, B, C, D, E and F by appropriate lines in the Keck images of April 1998 appropriately rotated to epoch of our observations. Unfortunately due to the one dimensional nature of the resolution derived by lunar occultation and also lower resolution of the Keck images ($\sim$ 50 mas at 2.2 μm) it is not possible to pinpoint a specific location in the nebula corresponding to a feature.

The spatial distribution of dust in WR104 provides us a clue about clumpy dust formation and distribution by comparing the restored brightness profile in Fig. 3.3. The flux observed in the K-band is mostly from dust shell surrounding the source. The flux observed from each spatial location of the shell depends on dust. Origin of clumps may be due to instabilities in the WR stellar wind and/or instabilities in the wind-wind compression zone, where one may expect large density enhancements (Moffat & Robert 1994; Le'pine & Moffat 1999). The instabilities are closely related to shocks and, as a consequence,to strong temperature fluctuations. Clumpy spatial distribution also found in episodic dust-forming, long period ($\sim$ 13 yr) WC7 + OB binary WR 137, obtained by high spatial resolution infrared (1.65 and 2.37 μm) images of *HST* (Marchchenko et al. 1999).

The timescale of the dust formation and its features is another aspect to be considered. The pinwheel structure clearly indicates that dust ejected one rotation earlier does not contribute to the observed geometry. The old dust is eclipsed in the orbital plane by the newly formed dust and cools rapidly. It may however be seen at far infrared wavelengths.

For an outflow velocity of 1220 kms^{-1} the distance covered by dust in one rotation is $\sim$ 170 AU. So in comparing our observations with Keck observations taken one to three years earlier we may be actually comparing different generations of dust. This time evolution of the dust could explain the additional peak C and features D and E not seen in the reduced Keck profiles. The difference between the Keck profiles and our smoothed profiles could also be due to minor differences in the pinwheel structure from one rotation to the next. However the overall picture is not greatly altered suggesting that time evolution of the dust shell with different orbits is not a strong effect. Continued high angular resolution observations of WR104 would be invaluable in studying finer details of dust production and dissipation in a WR system.

3.2.5 Conclusion

In conclusion our lunar occultation observations of WR104 trace out remarkably well, in one dimension the pinwheel dust structure surrounding the star seen earlier by the aperture masking techniques at the Keck telescope. Additional fine structures not seen in Keck data are also noted in the one dimensional high angular resolution lunar occultation profiles which could be due to real but small temporal changes in the dust structure.

Chapter 4

Asymmetric spatial structure in the atmosphere of Mira variable U Ori

---

This chapter deals with the studies of spatial asymmetry in the atmosphere of U Ori. The results, obtained from lunar occultation observations in the infrared K-band (2.2 μm), are compared with other high angular resolution observational measurements in near Infrared wavelengths and related data on the star. Several corollary evidences for the spatial asymmetry of the source are also presented.

4.1 Introduction

Due to their relatively large sizes, resolvable angular diameters and high infrared brightnesses, the photosphere and neighborhood of many Mira variables have been well studied over a wide wavelength range by high angular resolution techniques like lunar occultations (LO), single telescope aperture masking (AM) and direct long baseline interferometry (LBI). The picture that emerges is of a complex and very extended Mira atmosphere with generally spherical symmetry but departures from this symmetry have been reported. These departures could be due to stellar rotation, non-radial pulsation or due to hot spots produced by large scale convection processes in outer layers of the atmosphere. Repeated occurrences of asymmetries, large chromatic size variations near deep absorptions due to TiO or VO, evidence of clumps and hot spots are all known aspects of the Mira atmospheres (Tuthill, Haniff & Baldwin 1999b; Young et al. 2000).

The wavelength-dependent size variations are understandable features evidenced from several high angular resolution measurements (detailed discussion in chapter 5). Comparison between continuum and molecular lines in narrow filterbands showed the spatial extent of these type of stars. It is due to wavelength dependent optical depths in a spherically symmetric environment. Many such observations have been reported using aperture masking method (Haniff et al. 1992; Haniff, Scholz & Tuthill 1995; Tuthill et al. 1999a, 1999c) and also by direct LBI method (Thompson, Creech-Eakman & van Belle 2002a and references therein). The angular size variation in the continuum bands are normally attributed to bulk motion of the stellar photosphere while size changes in molecular bands are attributed to opacity variations possibly due to stellar pulsational effects on the extended atmosphere. Chromatic size variations of 7-10% within the K-band at the same phase of Mira star S Lac (M4-8IIIe) has been reported by LBI measurements (Thompson et al. 2002a).

4.2 Asymmetric spatial structures in Miras

Asymmetric spatial structures in Mira variables have been noted earlier and studied by high angular resolution techniques. A few examples of asymmetric structures in Miras can be listed. LBI observations of Mira variable R Tri in the K band (Thompson, Creech-Eakman & Akeson 2002b) show phase dependent significant departures from the spherically symmetric uniform disk (UD) model. An elliptical UD of axial ratio (2b/2a) $\sim$ 0.75 or a spherical UD overlaid with a smaller ellipsoidal disk is found to fit better to the data than a spherical UD. Further the position angle of asymmetry is approximately perpendicular to intrinsic polarization position angles which were observed earlier in visible region (McLean 1979). Apart from this model of an overlaid elliptical thin disk, the asymmetric structure in R Tri could also occur due to a grouping of large star spots about the photospheric equator. In case of O Cet (Mira) a much greater degree of asymmetry compared to R Tri has been reported. Ground based direct imaging by aperture masking method showed asymmetric structures in the atmosphere of Mira in the optical continuum as well as molecular/atomic line bands (Haniff et al. 1992). These authors have estimated the axial ratios of 0.78-0.85 at PA 105 -158^o from the elliptical disk model. HST imaging using Faint Object Camera (FOC) in the UV and optical wavelengths (Karovska et al. 1997) also detected significant asymmetry in this Mira A atmosphere. The de-convolved image of Mira A shows a strong asymmetry at position angle of 175^o prominently at 0.501 μm. Karovska et al. (1997) attribute the asymmetry in Mira A due to bright spots on the surface of the star or in its extended atmosphere. They also suggest that the asymmetry could be an indication of non-radial pulsation in the Mira A atmosphere. Yet another example of the spatial asymmetry in Mira variables is R Cas, determined by the speckle imaging techniques in the optical bands using the Russian 6m Special Astrophysical Observatory telescope (Hofmann et al.

2000). The observed data is again better fitted with a elliptical uniform disk distribution function having axial ratio $\sim$ 0.70 - 0.87 at different position angles.

4.3 Polarization Correlation to Asymmetries

It is now a well-established observational fact that radiation from cool, luminous variable stars is often linear polarized intrinsically and that polarization varies with time in a quasi-periodic manner. Nevertheless, the source of the polarization is still debated. As polarimetry of cool stars progressed, initially from broadband to narrowband measurements and then to fully detailed spectropolarimetry, a complex picture has emerged. In case of Mira variables, a sharp rise in polarization just before maximum brightness argues a grain-growth model (Shawl 1975), whereas the enhanced polarization of the neutral calcium line at λ 0.4226 μm (Tomaszewski et al. 1980) is strongly suggestive of a photospheric origin. The significance of detailed polarimetry studies in continuum and atomic/molecular line bands of Mira variables lies in its ability to probe gross departure from spherical symmetry which allows a net polarization to appear in the integrated starlight. Boyle et al. (1986) discussed the variety of sources where such asymmetries have been proposed by several authors. These are including flattened circumstellar dust shells (Shawl 1975), clouds of aligned grains (Svato$\check{s}$ & $\check{S}$olc 1981), equator-to-pole temperature gradients (Harrington 1969), giant convective cells (Schwarzchild 1975), localized hot-spots (Schwarz & Clarke 1984) and non-radial pulsations of the star (Serkowski 1970). Continuum polarization might be dominated by one of mechanisms associated with different atmospheric layers: Rayleigh scattering (p $\propto \lambda^{-4}$) by H_2 at the photospheric layers; molecular coherent scattering by titanium oxide (in case of O-rich M-variables) in an intermediate layer; or scattering by dust grains (roughly about p $\propto \lambda^{-1}$) in an asymmetric dust shell (Boyle et al. 1986). Enhancements and decreases in polarization relative to continuum values across atomic/molecular bands are not readily explained by dust scattering rather can be explainable due to molecular scattering (Boyle et al. 1986).

From multiple observations one to one correspondence between the direction of polarization and asymmetry has been noted. For example, Vy CMa (spectral type M5Ib) is an irregular variable which shows high polarization (10 -15 %) in optical bands at position angle between 150^o - 180^o. Recent Keck high angular resolution images in the IR bands revealed the asymmetric structures of the source at position angle $\sim 170^o$ (Monnier et al. 1999b). In case of Mira variable R Tri as discussed earlier, the position angle of asymmetry is nearly perpendicular to the intrinsic polarization position angle.

4.4 Studies on U Orionis

U Ori is a Galactic oxygen-rich Mira variable with pulsation period 371 days. The spectral type ranges from M6-M9.5 IIIe (Keenan & McNeil 1989), corresponding to the effective temperature changes of approximately 850K (Richichi et al. 1999). The interstellar visual extinction towards U Ori is $A_v \sim 0.25$ mag (Neckel & Klare 1980), corresponding to $A_K \sim 0.02$ mag. The total (circumstellar + interstellar) extinction in K towards U Ori is $\sim$0.07 mag (Knapp et al. 2003). The distance to U Ori ranges from 250 to 310 pc (Wyatt & Kahn 1983 ; van Belle, Thompson & Creech-Eakman 2002). The photometric light curve is asymmetric with a steep rise and gradual fall during the cycle [Association Francaise des Observateurs d'Etoiles Variables (AFOEV) database]. The visual amplitude (maximum to minimum) of U Ori is 6.5 mag (Mennesson et al. 2002). At 2.2 μm we measure the photometric variability of U Ori to be 0.3 mag. The reported linear radius of U Ori is 370$\pm$96 $R_\odot$ (van Belle et al. 2002). Using the bolometric flux and distance quoted by these authors, the luminosity was calculated to be $\sim$ 7000 $L_\odot$. In the case of U Ori, the phase variation of stellar radius may be better represented by the E-series (first overtone) models of Bessell, Scholz & Wood (1996). Because Z-series models used luminosity and temperature are close to U Ori. It has been noted that in this model the predicted variations of radius with phase in the infrared continuum band are $\sim$ 5-6%.

4.4.1 High Angular Resolution measurements of U Ori Optical to Radio regions

Angular diameter measurements of U Ori (Fig. 4.4) span the range from optical to thermal infrared. Using the aperture masking method on the 4.2m William Herschel Telescope Haniff et al. (1995) derive the photospheric diameter (referring to the layer of unit Rosseland optical depth) of U Ori in the range of 18.5 mas (0.833 μm) to 22.2 mas (0.700 μm) corresponding to their E-series models. In the near-IR one of the earliest measurements of the angular diameter was due to an lunar occultation observed by Ridgway, Wells & Joyce (1977) who obtained a value of 15.45$\pm$0.33 mas at 2.07 μm with a narrow band filter ($\Delta\lambda$=0.03 μm) inside the stellar H_2O absorption band. The measurements in the near-IR are summarized in Table 3 and discussed in section 4.4.5 later. In the thermal IR region U Ori shows substantially larger size. Mennesson et al. (2002) measured the angular diameter of 25.66$\pm$ 0.69 mas in the L$'$-band. Earlier heterodyne Interferometry at 11.4 μm by Danchi et al. (1994) measured the inner dust shell size of 80 mas in U Ori.

At radio wavelengths, interferometric observations of OH maser have been carried out on several occasions since early 1970. The source flared up in the OH maser line at 1612 MHz in 1973 (Pataki & Kolena 1974). The maser shell shows asymmetric geometry and clumpy distribution (Chapman, Cohen & Saikia 1991) which are inconsistent with spherically symmetric mass-loss. The angular extension of OH masers are distributed within a region of 500$\times$700 mas^2 in north-south by east-west, measured by these authors. Maser velocity map shows a gradient in the southeast to northwest direction orthogonal to the maser elongation. Recently Bains et al. (2003), from their subarcsec imaging of U Ori in the H_20 maser line , report an elongation in the direction northeast - southwest at position angle of 30^o while Bower & Johnson (1994) found similar elongation at position angle $\sim$60^o. Interpolating from their VLBI observations of 1612 MHz OH maser emission, Reid et al. (1979) infer a surface magnetic field in U Ori of about 10 Gauss assuming an angular radius of 8 mas. Chapman & Cohen (1985) suggest that the rotation axis of the source is along PA $\sim$ 60^o and which may be bipolar axis of the stellar magnetic field. If this is true, the velocity gradient which is almost orthogonal to the axis may be due to the equatorial density enhancement.

4.4.2 Polarization in U Ori

There is a also evidence of moderate level maximum intrinsic polarization of $\sim$ 1-2% in V and B bands respectively at PA $\approx$ 20^o - 40^o (Dyck & Sandford 1971; Coyne & Magalhaes 1977). However it has been noted that the PA of maximum polarization angle shows variation over phase in case of long period variables (Dyck et al. 1971) and the PA of maximum polarization cannot be used indiscriminately as the direction of the asymmetry. But as in the case of R Tri or Vy CMa some correlation or anticorrelation of the axis of symmetry with polarization can be expected.

4.4.3 Observations and Data Analysis

Circumstances of the lunar occultation event of U Ori are given in Table 4.1. Limited JHK photometry was also carried out on the source (Table 4.2). The observed light curve and best model fit is shown in Fig. 4.1.

In one sense multiple lunar occultation observations are well suited for the determina-

Table 4.1: **Circumstances of the Lunar occultation event**

Star	U Ori
IRC No.	20127
Date	13 Mar 2000
Julian date(0 UT)	2451616.50
Event Type	Disappearance
Event time (UT)	$18^h\ 19^m\ 25.94^s$
Position angle (NESW)	136^o
Contact angle	43.5^o
Pred. V_{comp} (km s^{-1})	0.66
Data sampling rate	2 ms
Filter(FWHM) in μm	2.2 (0.4)

Table 4.2: **JHK Photometry**

J	H	K	Vis. phase
-	-	- 0.75 ± 0.10	0.28
-	-	- 0.66 ± 0.08	0.45
0.44 ± 0.08	-0.22 ± 0.07	- 0.95 ± 0.07	0.08

tion of asymmetry in a source as LO provides a very good angular resolution of $\sim$1 mas in one dimension only. If the position angle of occultation coincides with the asymmetry zone then this could clearly reflect in the determination of UD diameter. Lunar occultations of the same source from different observatories produce different high angular resolution chords across the the source. Earlier studies on the the carbon star TX Psc by Lunar occultation observers had shown the advantage of sampling different chords across a resolvable source (Richichi et al. 1995). Near simultaneous lunar occultation observations separated by only a few hours in the same wavelength band are particularly valuable as they sample different position angles across the source and can pinpoint existence of spatial asymmetries which are independent of phase variations.

In the case of U Ori we have first carried out the NLS analysis. We obtain a UD value of 11.9$\pm$0.3 mas which is different from the value of 15.14$\pm$0.05 mas reported by Richichi & Calamai (2003). Due to the recently reported asymmetry in the source by these authors we have also carried out MIA analysis of our data. Scholz & Takeda (1987) in their limb darkening study of simple Mira model noticed that extended wing like features occur in the outer portions of various monochromatic center to limb variations (CLV). More elaborate models have confirmed the phenomenon. Recent interferometric and lunar occultation observations indicate that a Gaussian type CLV yields a better fit to the data than the conventional CLV curves having a steep decline near the 'edge' of the monochromatic disk (Hofmann, Scholz & Wood 1998b). Hence a uniform disk model would normally not be expected to provide a good fit to LO or interferometric data for Miras.

In Fig. 4.1 we show the best-fit to the data by MIA analysis. For comparison the residual of a fit to the data by a fixed UD source of 15 mas, close to the value reported by Richichi & Calamai (2003) is also shown. It can be clearly seen (in the residuals of fits) that our data fits to a much smaller source size.

Fig. 4.2 shows our brightness profile derived from MIA analysis. The UD values of 11.9 mas and 15 mas are also marked for comparison. It can be seen that our profile is more asymmetric in both near central and outer regions compared to the profile of Richichi et al. (2003). It may be noted that these authors have also mentioned the presence of fainter wings in their brightness profile extending to 20-30 mas or 1-3 stellar radii which they attribute to extended circumstellar emission. In our case the signal to noise in the wings is inadequate to confirm these fainter structures though there are indications as in the bump at $\sim$ 12 mas in Fig. 4.2.

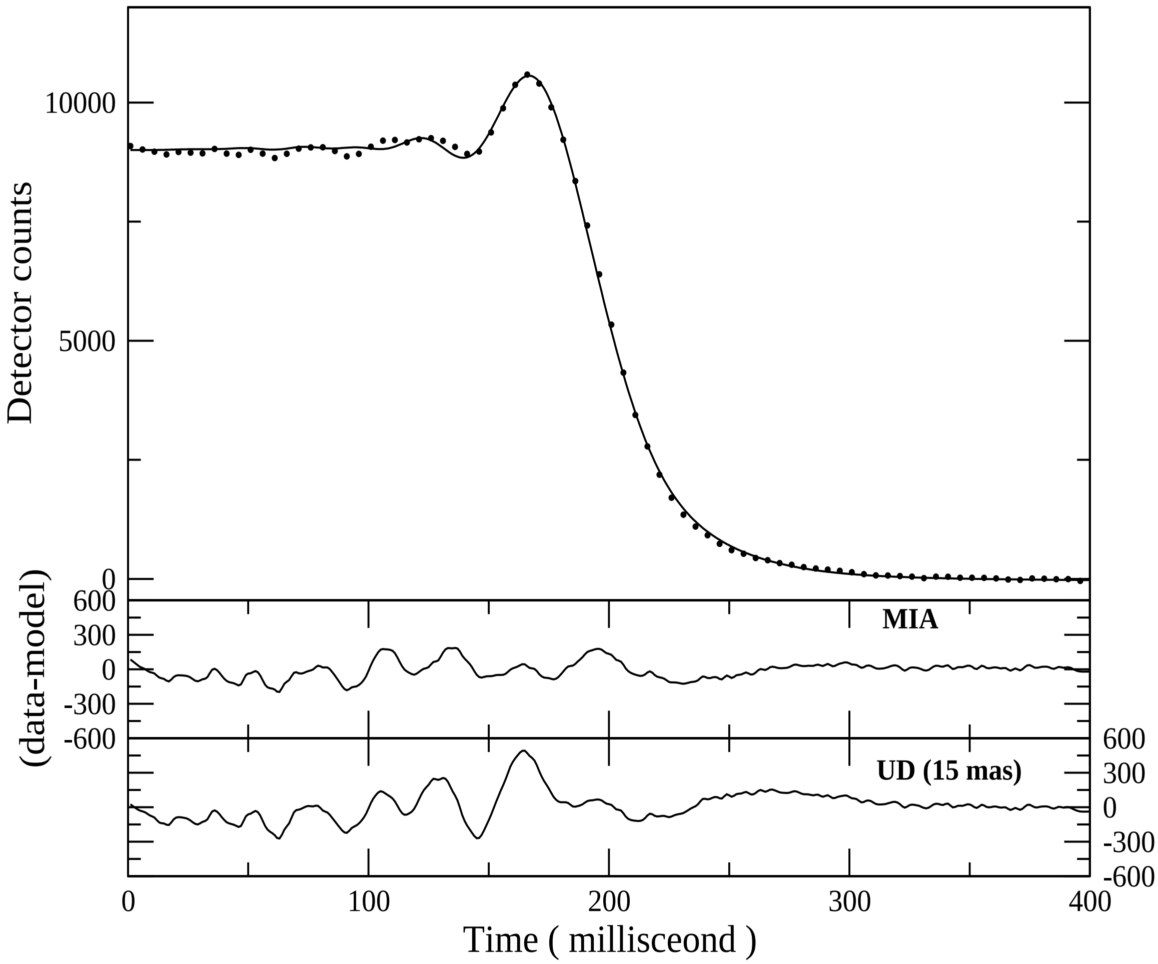

Figure 4.1: *The filled circles are the observed data-points of lunar occultation light curve of U Ori in the K-band (For clarity every fifth point is plotted). The solid line is best fit obtained by the MIA analysis. The residual (data - model) of the fits are shown in expanded form at the bottom panels for MIA and UD for a fixed angular size of 15 mas.*

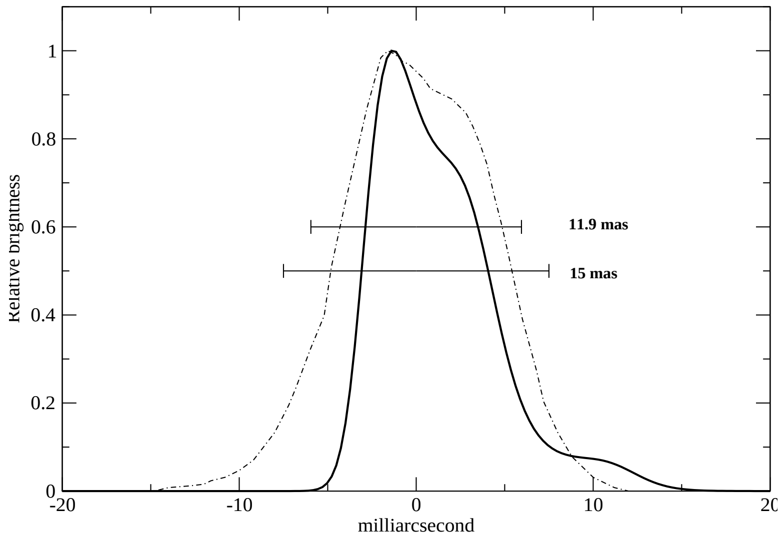

Figure 4.2: *The brightness profile of U Orionis derived from our lunar occultation light curve using model-independent algorithm (MIA) is shown by the solid line and is compared to that of Richichi & Calamai (2003) (dot-dashed line). The two horizontal lines indicate equivalent UD diameter of 11.9 mas (this work) and 15 mas.*

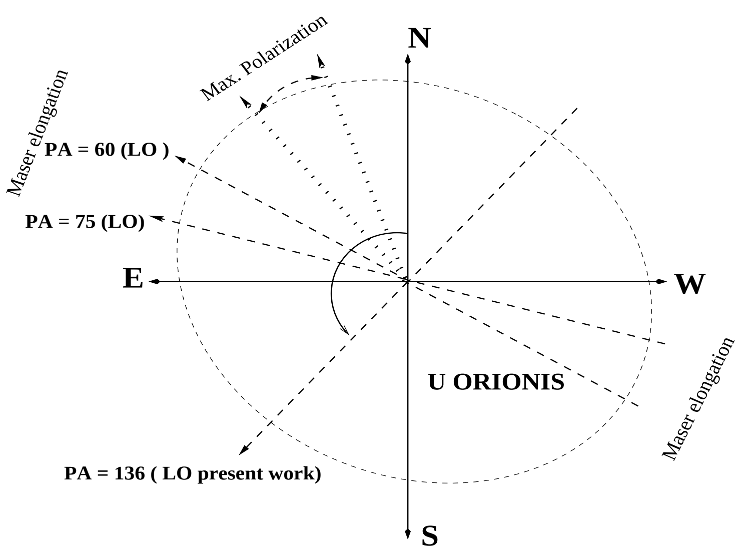

Figure 4.3: *Schematic diagram of asymmetric size of U Orionis is shown and several corollary evidences are depicted. The position angle (PA) of all lunar occultations on U Ori are shown by dashed lines. The direction of OH maser elongation observed at 1665 MHz (Chapman & Cohen 1985) is depicted. Regions of observed PA of maximum intrinsic polarization (Dyck & Standford 1971; Coyne & Magalhaes 1977) are also shown.*

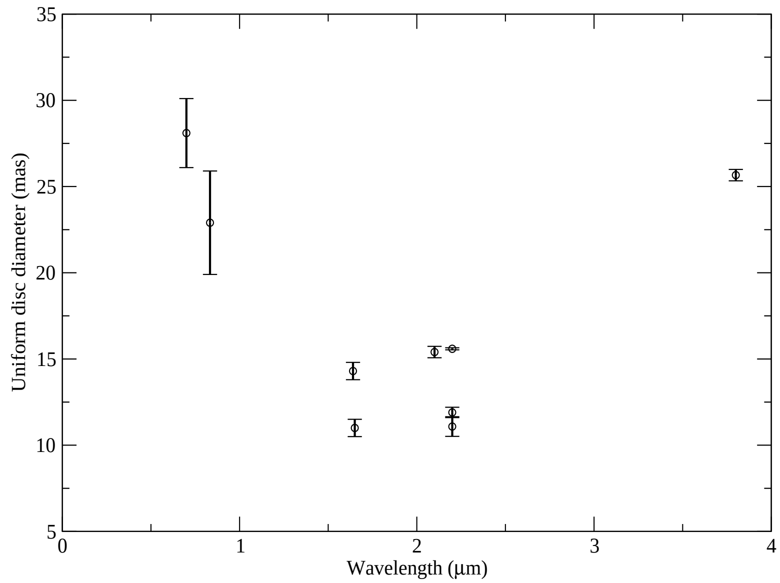

Figure 4.4: *The uniform disc diameter measurements of U Ori from optical to thermal IR are plotted as function of wavelength including the result of present work at 2.2μm. Reference of the other measurements are given in the text.*

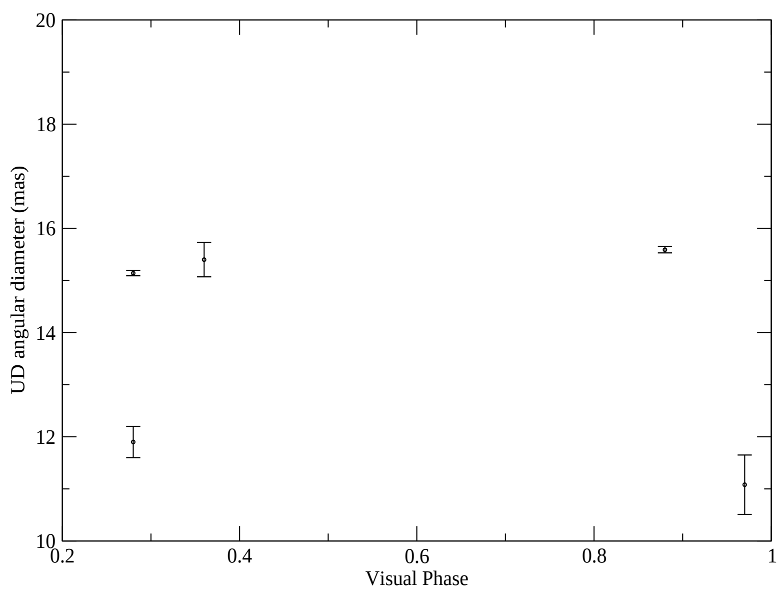

Figure 4.5: *Uniform disc diameters of U Ori at K-band are plotted as function of visual phase including the result of present work. Reference of the other measurements are given in the text.*

Table 4.3: **Angular diameter measurements of U Ori in Infrared bands**

Method[a]	Date	Phase	PA[b] (deg)	$\lambda/\Delta\lambda$ (μm)	Ang. Dia.(UD) (mas)	Ref.
LO	13 Mar 2000	0.28	136	2.20/0.40	11.9 $\pm$0.30	1
LO	13 Mar 2000	0.28	75	2.20/0.40	15.14$\pm$0.05	2
LO	15 Jan 1976	0.36	60	2.07/0.03	15.40$\pm$0.33	3
LBI	08 Oct 1995	0.97	-	2.20/0.40	11.08$\pm$0.57	4
LBI	26 Nov 2000	0.04	-	1.60/0.34	11.00$\pm$0.50	5
LBI	16 Oct 2000	0.88	-	2.16/0.32	15.59$\pm$0.06	6
LBI	20 Nov 2000	0.96	-	3.79/0.54	25.66$\pm$0.69	6

[a] LO : Lunar Occultation; LBI : Long Baseline Interferometry
[b]PA is defined as the angle of the event measured from N through E

Table References : 1. Present work; 2. Richichi et al. (2003); 3. Ridgway et al. (1977); 4. van Belle et al. (1996); 5. Berger et al. (2001); 6. Mennesson et al. (2002).

4.4.4 Results and Discussions

In Table 4.3 all angular diameter measurements of U Ori in the H and K bands are listed. It can be seen that the angular diameter of U Ori in these bands shows a large variation from about 11 to 15.6 mas. The variation is much larger ($\sim$ 25%) than the observational errors involved. We also note that the observed angular diameter variations do not appear to show any phase dependency though data is sparse (Fig. 4.5). Our derived UD value is in good agreement with earlier LBI measurements in the K-band (van Belle et al. 1996) and H-band (Berger et al. 2001) though the phases are different. The interferometric measurements were made close to maximum light while our observation was about midway between maximum and minimum. Interestingly our observations and contemporaneous LO measurement of Richichi et al. (2003) show two well determined but different values of angular diameter. Richichi et al.(2003) obtained a value of 15.14$\pm$0.05 mas at a position angle of 75^o. The authors attribute the asymmetry in the brightness profile and difference among existing angular diameter measurements of U Ori to the pulsational effects in the atmosphere. We derive a value of 11.9±0.3 mas at a position angle 136^o. An earlier LO measurement in 1976 by Ridgway et al.(1977) gave a value of 15.45±0.33 mas. Their position angle of 60^o is close to that of Richichi et al. (2003). It may be noted from Table 3 that all three LO measurements are nearly at the same phase. The difference between them is only in the position angles of the measurement. Our PA of 136^o is separated by 60-75^o from PA of the other two measurements. The LBI measurements of Mennesson et al. (2002), Berger et al. (2001) and van Belle et al. (1996) also show a similar dispersion in angular diameter though the position angle is not quoted (Table 3). Though these observations were done at different epochs, they are nearly at the same photometric phase of U Ori, near its maximum (Fig. 4.5). We note that there are no high angular resolution observations of U Ori near its minimum phase. Possible explanations for the dispersion in the IR angular diameter measurements could be variation in apparent diameter with position angle, wavelength dependent size variation (bandwidth effects), time dependent variation due to stellar pulsation. Out of these possibilities the two well determined lunar occultation angular diameters at the same wavelength on the same day rule out phase effects and bring out the asymmetric spatial structure in the source.

Based on our observations and other available data on U Ori we have developed a schematic picture of U Ori shown in Fig. 4.3. The position angles of occultation observations are marked as also the direction of OH maser elongation (NE-SW) and the maximum polarization position angle (Dyck & Standford 1971).

The picture that emerges is that the IR continuum diameter of U Ori shows large excursion in several measurements much beyond the expected variation with photometric phase. It is possible that that earlier two LOs (Richichi & Ridgway) had shown a bigger value of angular diameter because of these occultation directions were along the asymmetry direction (roughly about PA of $\sim 70^o$) of the source as depicted in the schematic diagram of Fig. 4.3. The equatorial density enhancement has been reported approximately along this position angle in radio observations of OH maser. Further the maximum of intrinsic polarization has also been also been observed nearby (Dyck et al.1971). It is therefore deduced the source has a asymmetric structure with an ellipsoidal elongation at PA $\sim 70^o$. If we consider earlier larger estimation was due to occultation scan along the semi-major axis and lesser value due to scan along the semi-minor axis then the ratio of semi-minor to semi-major axis would be 0.77. The OH maser angular extension also showed such a ratio (Chapman et al. 1991) though the emission is more spatially extended. That the of asymmetric components in the stellar brightness distribution could lead to systematic differences in angular diameter estimations, has been commented upon by Tuthill et al. (1995) while studying diameter variation of O Cet.

Another possibility is that the moderate and even weak magnetic field forms cool spots on surface of U Ori like in AGB stars (Soker 1998). The cool spots facilitate the formation of dust closer to the stellar surface. Such spots can be as big as ≈ 20-30% of the total surface area found in cool red giants (Neff, O'Neal & Saar 1995, Young et al. 2000). Further star spots tend to occur near the photospheric equator. The presence of such large spots in the direction of occultation can affect angular diameter measurements. In LO large spots can cause also fringe distortions. However distortions of the LO profile are not been noticed in our data. It appears less likely that the dispersion in angular diameter measurements of U Ori is due to starspots (Mondal & Chandrasekhar 2004).

4.4.5 Conclusion

From our lunar occultation observations we derive a source brightness profile of U Ori which is markedly more asymmetric than the earlier reports. We attribute the asymmetry and dispersion in angular diameter measurements to an extension or asymmetry of the Mira atmosphere approximately in the direction northeast - southwest at position angle of 50 - 70^o. The reason for this spatial asymmetry could be pulsational mass loss in a preferred direction.

Chapter 5

Miras and Semi-Regular Variables

This chapter deals with the angular diameter measurements of two Mira variables (U Ari and Z Sco), three semi-regular and irregular variables (SW Vir, η Gem and μ Gem) and a supergiant semi-regular variable TV Gem (SRc). U Ari, η Gem and μ Gem were observed simultaneously in the K-band (2.2 μm) and L$'$-band (3.8 μm). All L$'$ measurements are the first reported values for these sources while earlier K-band measurements by other observers exist. Z Sco, SW Vir and TV Gem have been observed only in the K-band. Another Mira variable U Ori, discussed earlier in chapter 3 is considered here only for pulsation mode analysis.

5.1 Introduction

Asymptotic giant branch (AGB) stars are in the last stage of stellar evolution before becoming planetary nebulae and are generally surrounded by a circumstellar dust shell. They have typically mass-loss rates between $10^{-8} - 10^{-4}$ $M_{\odot}$/yr (Knapp & Morris 1985), sometimes losing more than half of their mass while on the AGB. These stars return large quantities of carbon-, oxygen-, and nitrogen-enriched gas to the interstellar medium, contributing significantly to the chemical evolution of the Galaxy (Sedlmayr 1994). Rapid and extensive mass loss via generally spherically symmetric outflowing winds is common during late stellar evolution. Dust is formed in the outflowing winds surrounding the star. The location of dust condensation radius in the circumstellar envelope depends on several conditions like density, chemical composition and stellar temperature. Radiation pressure on the grains causes them to accelerate further outwards and makes a dusty environment around these objects which depends on adequate mass-loss and stellar temperature.

AGB stars include classical Mira variables (visual amplitudes $\geq$ 2.5 mag ; period $\geq$ 100 days), semi-regular SRa variables (visual amplitude $\leq$ 2.5 mag ; periods 35 -1200 days), semi-regular SRb variables (amplitude ≤ 2.5 mag ; with poorly defined periods), and irregular variables Lb type (amplitude is small, no definite periods), as well as supergiant semi-regular variables SRc type. For example, the visual light curves of U Ari (Mira variable) and η Gem (SRb) found in archives of Association Francaise des Observateurs d'Etoiles Variables (AFOEV) are shown in Fig. 5.1. AGB stars can be divided into two main groups depending upon their chemistry, oxygen-rich and carbon-rich. Stars begin their lives on the AGB as oxygen-rich and some, but not all, later become carbon-rich because of carbon dredge-up from their core (Iben & Renzini 1983; Chan & Kwok 1988).

5.2 Observed diversity in multi-wavelength angular size measurements

Measurements of the angular diameters of Mira and semiregular variables provide a direct way to understand their dynamical atmosphere. In particular, simultaneous measurements at multiple wavelengths are valuable as they probe different layers of the stellar atmosphere because of the varying opacity therein. Owing to relatively low surface temperature of late-type giants several molecules (TiO, VO, H_2O & CO etc.) form in the extended atmosphere of these stars. Among them H_2O is most abundant. Due to large opacity effects in some molecular absorption bands, the diameters of these stars change remarkably in those particular passbands. In addition to standard limb-darkening effects in angular diameter measurements one has to be concerned about the effects of molecular lines formed close to the photospheres (particularly in late M-type giants and in Mira variables). Optical depth of unity is reached much higher up in the atmosphere within the absorption band, compared to adjacent continuum. Hence star appears larger at the center of absorption band like TiO than in the nearby continuum. This phenomenon was first realized from speckle measurements of Mira variables O Cet and R Leo in the narrow spectral channel inside deep TiO bands (Labeyrie et al. 1977). The diameters of stars are much larger in these bands than nearby continuum (for e.g. O Cet shows size increase in TiO-band by a factor of ~ 1.4 compared to in the adjacent continuum while for R Leo the factor is 1.8). Subsequently a systematic studies covering a wide spectral range of late-type giants (Quirrenbach et al. 1993) and large sample of Mira variables (Haniff et al. 1995) had found similar extensions.

In infrared J (1.25 μm), H (1.65 μm) and K (2.2 μm)-bands, strong bands of the molecular lines are comparatively less intense than optical bands and the angular diameter measurements in these bands may be close to continuum measurements (Hofmann et al.

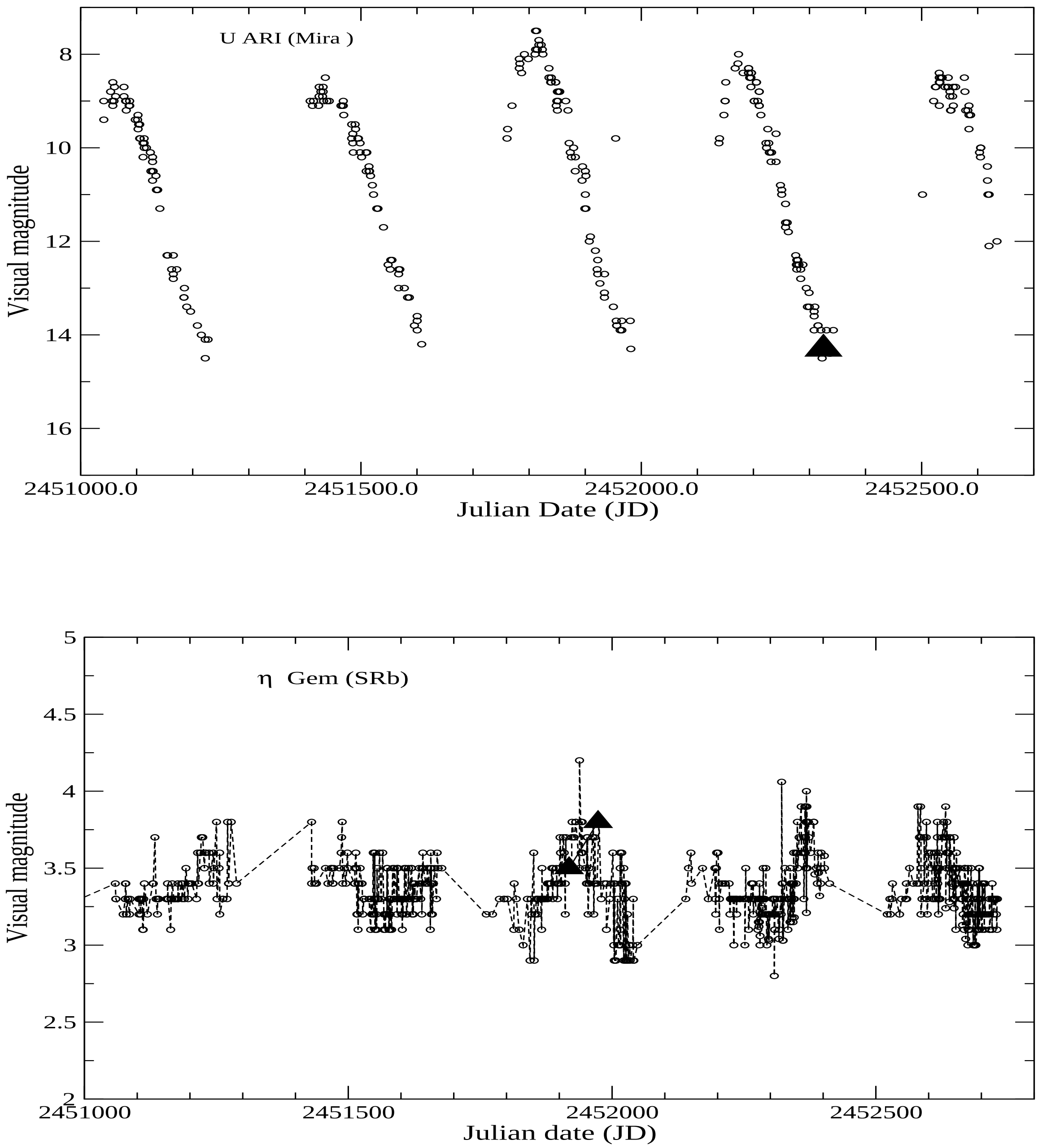

Figure 5.1: *The visual light curves of U Ari and η Gem are shown . Data are downloaded from the archives of Association Francaise des Observateurs d'Etoiles Variables (AFOEV) database. The period of variables are 371 days (U Ari) and 233 days (η Gem). The filled triangles are our observed date of lunar occultation.*

1998b). However this is not always the case. The angular diameter of O Cet was measured by aperture masking method on Keck 10 telescope in narrow filterband centered at 1.25, 1.65, 2.2 & 3.08 μm and an apparent size increase was noted from 1.25 to 3.08 μm ($\phi_{1.24}$ = 23.3 mas, $\phi_{1.65}$ = 28.3 mas, $\phi_{2.26}$ = 31.6 mas, $\phi_{3.08}$ = 59.9 mas) (Tuthill et al. 1999c). Spectral angular diameter measurements of Mira star S Lac in the K-band ($\lambda \sim 2.0$ - 2.4 μm) shows the variation of $\sim$ 7% between blue (~ 2 μm) and red (~ 2.4 μm) wings. Such behavior is attributed due to the opacity effects of molecules like H_2O and CO (Thompson et al. 2002a). Bedding et al.(2001) suggested that large wavelength-dependent variation of continuum radius in M-type Mira stars are unlikely to be caused by atmospheric dust, expect possibly near 1 μm due to scattering effects and but radius measurements may be significantly affected by molecular band contaminations. Recently Jacob & Scholz (2002) in their models showed the strong effects of molecular band contaminations in continuum diameters of M-type Mira stars in contrast to earlier predicted M-type Mira models (Bessell et al. 1996; Hofmann et al. 1998b).

High angular resolution observations in the thermal infrared are particularly interesting because in these bands, contributions from the upper colder atmospheric layers (molecules and dust) close to photosphere (within 2-3 stellar radii) may be more prominent. Tuthill et al. (2000a) from aperture masking experiments on Keck found that R Aqr (Symbiotic Mira) had a marked enlargement (factor of $\sim$ 2) at 3.1 μm compared to shorter IR-bands (1.25 -2.2 μm). These authors (Tuthill et al. 2000a) suggested that such apparent enlargement may be due to molecular opacity effects at 3.1 μm. In more than dozen sample of O-rich Mira and semi-regular variables (spectral type later than M5) Mennesson et al. (2002) found that the apparent sizes in broad L$'$-band ($\sim$3.8 μm) showed an enlargement compared to K, by a factor in the range 1.2- 2.0. Mennesson et al. (2002) has mentioned that such apparent enlargement was not seen in non-Mira giants below spectral type of M5.

At larger wavelength beyond 10 μm, measurements by Infrared Spatial Interferometer (ISI) resolved the dust shells around thirteen evolved giants and supergiants (Danchi et al. 1994). Dust shell within 3-5 stellar radii have been reported in several Miras (like O Cet, R Leo, R Aqr, VX Sgr, IK Tau) while in some other variable giants (including Miras) and supergiants (like U Ori, χ Cyg, W Aql, α Her, α Ori, α Sco) dust shell was found far from the stellar surface ($>$ 8 stellar radii).

5.3 Mode of Pulsation

The mode of pulsation in Miras and semi-regular variables has been uncertain for a long time (Wilson 2000). The unstable mode of pulsation is probably due to the partial hydrogen and helium ionization zone inside stellar convective zone (Gautschy & Saio 1996). Recently several observational attempts have been made in the visible and infrared bands (Haniff et al. 1995; van Belle et al. 1996, 2002) to study the pulsation mode of Mira variables but the evidence has not been conclusive either in favour of fundamental or the first overtone. Theoretical models are also divergent. Some models support fundamental mode (Wilson & Hill 1979; Wood et al. 1999) while others favour the first overtone mode (Perl & Tuchman 1990). The correct understanding of pulsation mode of long period variables is hampered by large uncertainties in distance estimation and measurement of the true photospheric angular diameters due to variable opacities effects. Most of observational studies (Haniff et al. 1995; van belle et al. 2002) show the Miras of period less than 400 days have linear radii larger than $350R_{\odot}$, which for mass of ~ 1 $M_{\odot}$ implies overtone pulsation. In contrast high resolution infrared spectroscopy of Miras shows radial velocity variations in the range of 20 - 30 km/s (Hinkle et al. 1997) and such variations can not be achieved by theoretical dynamical overtone model (Bessell et al. 1996). The optical size measurements of Mira R Leo showed more than 30% variations over phase (Burns et al. 1998). Size measurements in narrow ($\Delta\lambda \sim 0.03$ μm) filterbands centered at 2.2 μm of Mira star S Lac showed the variations of 22% (Thompson et al. 2002a). Still there is no clear cut picture that such variations especially in the infrared region are from the stellar continuum layer or due to modulating effects of the upper layers of Mira atmospheres. The optical continuum diameters of Miras have always showed a larger size compared to the infrared continuum diameter at the same phase. In case of R Leo it has been seen that it has an angular size of 33.1 ± 1.3 mas in 2.16 μm at phase 0.16 and 44.9 ± 2.0 mas in 0.83 μm at nearby phase 0.21 (Tej et al. 1999). In case of semi-regular variables the true size variation will be further less owing to their observed lesser radial velocity change ($\sim$ 4 km/s) (Hinkle et al. 1997).

The SR variables are separated from Miras by shorter period and smaller amplitude. The mode of pulsation of Mira variables are well studied while little attention has been given to pulsation studies of SR variables mode. Studies in globular clusters (Feast 1996) indicate that SR variables to be pulsating in first overtone. Wood et al. (1999) found that most of SR variables in LMC are first or higher overtone pulsators, although some pulsate in fundamental mode with low amplitude. Many SR variables are a member of the double

Table 5.1: **Log of Observations**

Star (var.)	IRC	Date of obser.	Filter(μm) ($\lambda/\Delta\lambda$)	PA (deg.)	v_{comp} (km/s)	event type[a]
U Ari (Mira)	+10040	19 Feb 2002	2.2/0.4	18	0.475	D
			3.8/0.6			
Z Sco (Mira)	-20306	22 Mar 2003	2.2/0.4	155	0.651	R
η Gem (SRa)	+20139	08 Jan 2001	2.2/0.4	21	0.330	D
			3.8/0.6			
		04 Mar 2001	2.2/0.4	68	0.645	D
			3.8/0.6			
μ Gem (Lb)	+20144	04 Mar 2001	2.2/0.4	77	0.767	D
			3.8/0.6			
SW Vir (SRb)	+00230	01 Jun 2001	2.2/0.4	74	0.504	D
TV Gem (SRc)	+20134	14 Nov 2000	2.2/0.4	212	0.437	R

[a]D: Disappearance; R: Reappearance

period variables group and the two periods are within a factor of ~ 2 (Kiss et al. 1999). Such a ratio is marginally consistent with mode switching between fundamental and first overtone in linear pulsation analysis. For example, Bedding et al. (1998) have studied the mode switching in R Dor (SRb) having two pulsation periods of 332 days and 175 days ($P_{long}/P_{short} \approx 1.9$) which switches back and forth between first and third radial pulsation mode in a time-scale of about 1000 days. The smaller amplitude semi-regulars and larger amplitude Miras may be a key to understanding the pulsation mode (Wood & Sebo 1996).

5.4 Observations

Three simultaneous events (U Ari, η Gem and μ Gem) are observed in broad K (2.2/0.40 μm) and L′ (3.8/0.60 μm) filter-bands. Z Sco, SW Vir and TV Gem occultation are recorded in the K-band only. The sampling time of the light curves was 2 milliseconds (ms) except SW Vir which was sampled at 1 ms. η Gem was observed twice during an interval of 2 months. The events were all recorded under good sky conditions except for Z Sco which is observed through thin clouds. The details of occultations are listed in Table 5.1. Details of source parameters are listed in Table 5.2.

Table 5.2: **Individual source parameters**

Parameters	U Ari	Z Sco	U Ori	η Gem	μ Gem	SW Vir	TV Gem
Spectral type	M4-9.5 IIIe	M4/5 IIIe	M6.5-9 IIIe	M3 III	M3 III	M7 III	M1-0 Iab
Visual magnitude[1] *(max-min)*	7.2-15.2	8.7-13.4	5.3-12.6	3.20-3.90	3.20	8.2-9.4	8.7-9.5
K magnitude[11]	1.59	1.48	-0.49	-1.49	-1.89	-1.87	0.99
L′ magnitude[11]	0.28	1.50	-1.41	-1.59	-2.01	-2.28	0.62
Variability type	Mira	Mira	Mira	SRa	Lb	SRb	SRc
Period (days)[1]	371	352	372	233	27[10]	150	182
Distance (pc)	775±150[2]	770±120[3]	309±60[2]	107±22[4]	71±5[4]	143±24[4]	1200±300[5]
Luminosity[11] *(10^3 $L_\odot$)*	8.4±3.5	8.3 ±3.3	9.7±4.0	2.3±1.0	1.8±0.36	4.7±1.7	68.5±34.9
Mass loss *(10^{-8} $M_\odot/yr$)*	57[6]	-	28[7]	1.4[8]	0.44[8]	3.4	200[9]
Outflow velocity *(km/s)*	6.0[6]	-	7.5[7]	-	-	7.2	12[7]

Table References: 1. SIMBAD database; 2. van Belle et al. 2002; 3. Whitelock et al. 2000b; 4. Hipparcos catalog (Perryman et al. 1997); 5. Ragland et al. 1997; 6. Winters et al. 2003; 7. Young 1995; 8. Drake et al. 1986; 9. Loup et al. 1993; 10. Percy et al. 2001; 11. Gezari et al. 1999.

[11] Luminosity is estimated using the relation $L = 4\pi d_*^2 F_{bol}$.

5.5 Result and Discussions

Table 5.3: **Derived Infrared angular diameters**

Star	Date	Phase	$\lambda/\Delta\lambda$ (μm)	Ang. Dia (UD) (mas)
U Ari	19 Feb 2002	0.57	2.2/0.4	7.3±0.3
Z Sco	22 Mar 2003	0.26	2.2/0.4	5.0±1.0
η Gem	08 Jan 2001		2.2/0.4	12.7±0.3
	08 Jan 2001		3.8/0.6	12.7±1.0
	04 Mar 2001		2.2/0.4	12.8±0.3
	04 Mar 2001		3.8/0.6	12.8±2.0
μ Gem	04 Mar 2001		2.2/0.4	13.7±0.5
	04 Mar 2001		3.8/0.6	14.8±1.0
SW Vir	01 Jun 2001	0.56	2.2/0.4	15.9±0.6
TV Gem	14 Nov 2000		2.2/0.4	4.8±0.2

5.5.1 Angular diameter measurements

U Ari

U Ari is a bright galactic Mira variable of period 371 days and the spectral type is ranges from M4-9.5 IIIe over variability phase (Keenan et al. 1989). The visual magnitude varies from 7.20 to 15.20 (SIMBAD database) over period. The distance to the source found in the literature is in the range of 530 (Wyatt & Kahn 1983) to 779 pc (van Belle et al. 2002). We have adopted the distance to the source to be 775±150 pc using reddening corrected mean K-band magnitude and period-luminosity relation found in Whitelock & Feast 2000a. The mass-loss rate and outflow velocity had been estimated from CO (3-2) line at 345 GHz to be 6.5×10^{-8} $M_{\odot}$/yr and 4.2 km/s respectively (Young 1995). In contrast recent estimation of mass-loss from CO (1-0, 2-1) lines at 230 GHz and 115 GHz is 5.7×10^{-7} $M_{\odot}$/yr and expansion velocity 6.0 km/s (Winters et al. 2003). The details about source parameters are listed in Table 5.2.

Lunar occultation of U Ari was observed on 19 February 2002 simultaneously in the K

Table 5.4: **Multi-wavelength Angular size measurements from Optical to Near-IR**

Star	Date of Obs.	Method[a]	Phase	$\lambda/\Delta\lambda$ (μm)	Ang. Dia(UD) (mas)	Reference
U Ari (Mira)	03 Sep 1977	LO	0.49	1.62/0.42	6.11 $\pm$0.34	Ridgway et al. 1979
U Ori	15 Oct 2000	LBI	0.88	2.20/0.40	15.59$\pm$0.06	Mennesson et al. 2002
(Mira)	15 Nov 2000	LBI	0.96	3.75/0.70	25.66$\pm$0.69	Mennesson et al. 2002
SW Vir	26 Jan 1981	LO	0.02	1.62/0.04	16.82 $\pm$0.34	Ridgway et al. 1982
(SRb)	01 Sep 1981	LO	1.48	2.17/0.03	16.11$\pm$0.13	Schmidtke et al. 1986
	29 Jun 1982	LO	3.48	2.28/0.40	16.77$\pm$0.23	Schmidtke et al. 1986
	29 Feb 2000	LBI	0.51	2.20/0.40	16.24$\pm$0.06	Mennesson et al. 2002
	12 Mar 2000	LBI	0.56	3.75/0.70	22.88$\pm$0.33	Mennesson et al. 2002
η Gem	22 Feb 1964	LO		0.53	9.50$\pm$1.50	Bohme et al. 1978
(SRa)	05 Nov 1982	LO		0.47	8.50$\pm$1.02	Schmidtke et al. 1984
	1988-90	LBI		0.55/0.02	11.43$\pm$0.55	Mozurkewich et al. 2003
	1988-90	LBI		0.80/0.02	10.91$\pm$0.11	Mozurkewich et al. 2003
	1993	LBI		0.712/0.012	11.75$\pm$0.27	Quirrenbach et al. 1993
	1993	LBI		0.754/0.005	10.70$\pm$0.15	Quirrenbach et al. 1993
	31 Mar 2001	LO		2.20/0.40	12.57$\pm$0.04	Richichi et al. 2003
μ Gem	1988-90	LBI		0.55/0.02	13.48$\pm$0.19	Mozurkewich et al. 2003
(Lb)	1988-90	LBI		0.80/0.02	13.99$\pm$0.14	Mozurkewich et al. 2003
	1987	LBI		2.2/0.40	13.50$\pm$0.15	Di Benedetto et al. 1987
	1993	LBI		0.754/0.005	13.50$\pm$0.13	Quirrenbach et al. 1993
	1993	LBI		0.712/0.012	13.97$\pm$0.28	Quirrenbach et al. 1993
TV Gem	15 Aug 1982	LO		0.55	5.31$\pm$0.91	Radick et al. 1984
(SRc)	30 Mar 1993	LO		2.2/0.40	4.9$\pm$0.30	Ragland et al. 1997
	03 Feb 1993	LO		2.2/0.40	4.46$\pm$0.07	Richichi et al. 1998b

[a]LO: Lunar Occultation; LBI: Long Baseline Interferometry

and L′ bands. The visual variability phase of our observation was 0.57 (AFOEV database). A good occultation trace has been recorded in K-band (Fig. 5.2) while L′ profile (Fig. 5.3) is noisy. The signal to noise ratio (S/N) is limited by atmospheric scintillation noise in K-band. Thermal noise with low frequency fluctuations noise is seen in the L′ observations. The low frequency noise in L′ trace is cleaned only in the background regions (before and after occultation fringes) using higher-order polynomial before the fit. Improvement of S/N in L′ data is adequate to fit uniform disk diameter. In Fig. 5.3 the original raw data are shown along low-frequency fluctuations removed data used for UD fit.

The K-band light curves are fitted with the UD model and yielded the UD value of 7.3±0.3. The model fit light curves along with observed data points are shown in Fig. 5.2 and the derived value is listed in Table 5.3.

Multi-wavelength angular diameter measurements of U Ari are listed in Table 5.4. Prior to our observation only one angular diameter measurement is reported in the literature and the value is 6.11±0.34 mas by LO in the broad H-band (Ridgway et al. 1979). Our measured K-band angular diameter (7.3±0.3) is about 20% higher than earlier one though both observations were done at nearly minimum light of Mira phase. Such diversity in the near-infrared angular diameter measurements also seen earlier in Miras and the detailed is discussed in section 5.1. Such an enhancement is much more than conventional limb darkening changes between H and K. The apparent size difference of U Ari between H and K bands appears to be real as it is few sigma above the errors involved in measurements . The K-band size may be enhanced by the presence of hot water layer of temperature around 1500 - 2000 K surrounding the source and such difference in apparent size between H and K has appeared in the simple two-layer model of Mennesson et al. (2002).

L′ light curve is noisy. It was possible to trace out the L′ occultation inside the large noise because of simultaneous observations in the K-band. The low frequency noise in the sky region data is cleaned up before model fit by higher order polynomial. The large fluctuations in the sky background cleaning is done by modeling with 7th order Legendre polynomials and then subtracted from the sky background regions. The raw data and cleaned data is also shown in Fig. 5.3 which shows the portions in the data cleaned up. The UD value of 7.3 mas for K-band is superimposed which shows not a proper fit. A model fit to the cleaned data yields the UD value in the range of 12 mas with a large uncertainty. Our expectation was that the L′ diameter would be substantially higher than K-band and would be measurable. However the quality of L′ data precludes such conclusions to be drawn.

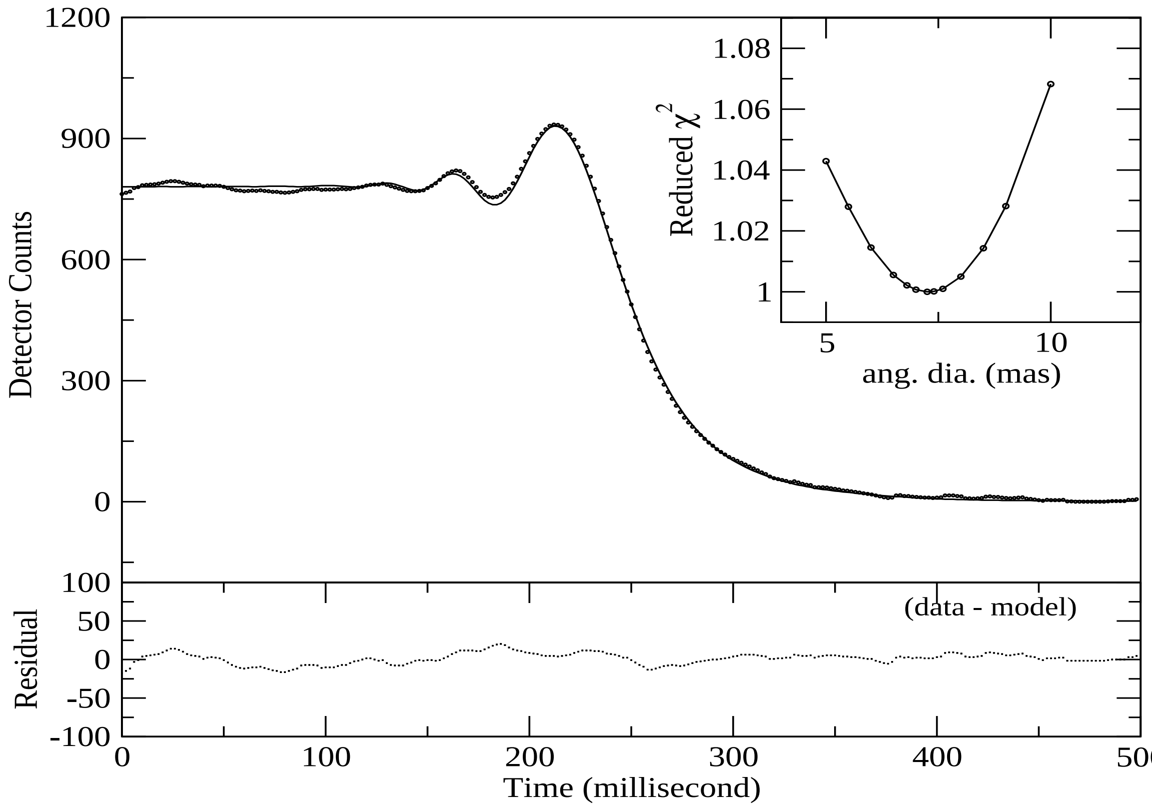

Figure 5.2: *Lunar Occultation light curve of U Ari at K is shown as observed on 19 February 2002 at variability phase 0.57. The dotted line is the observed data and the solid line is the model-fitted curve. The derived uniform disk angular diameter is 7.3±0.3 mas. The lower panel shows residuals (data -model) of fit and inset graph shows the convergence of the fit.*

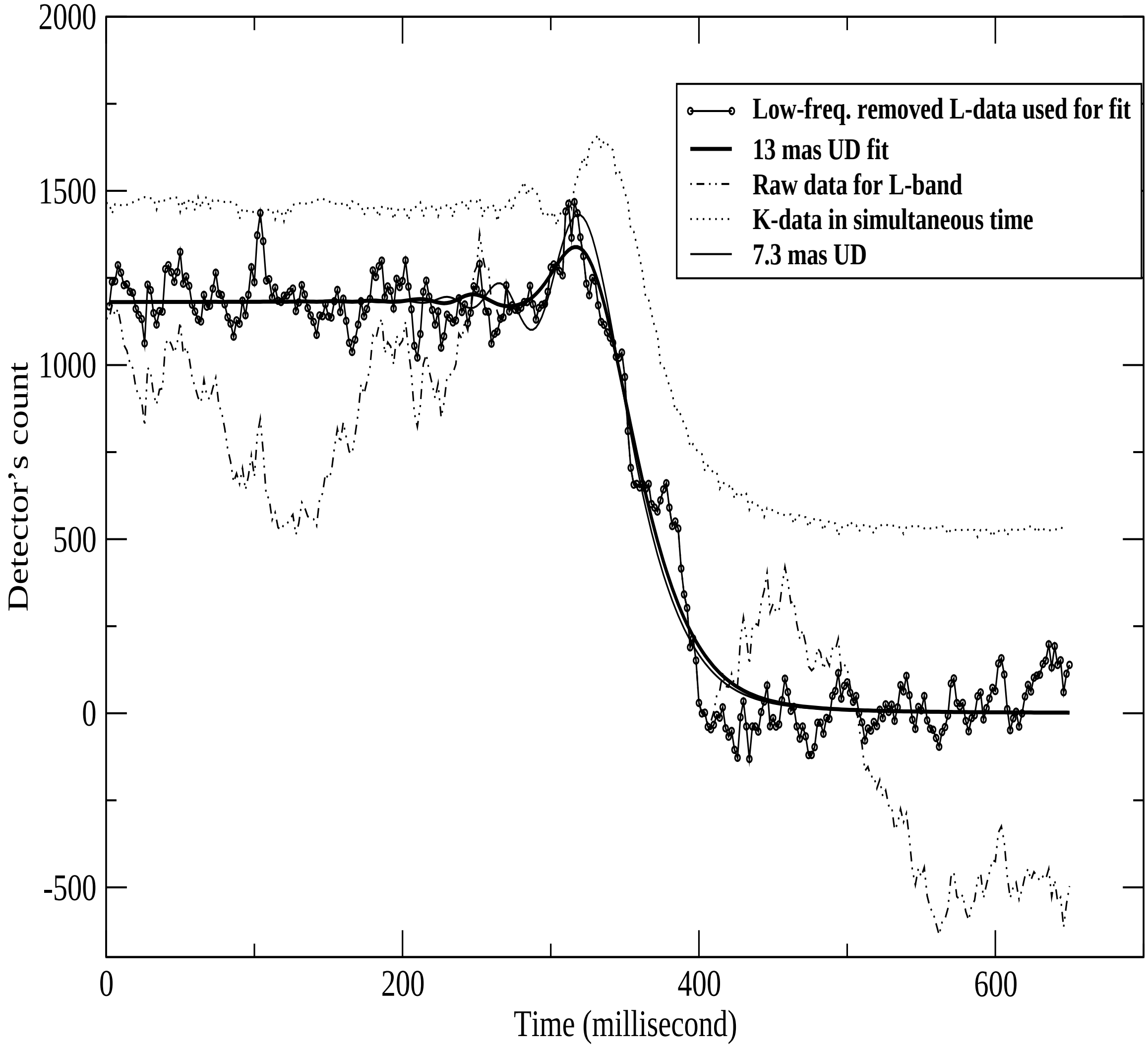

Figure 5.3: *Lunar Occultation light curves of U Ari at L′ is shown simultaneously observed with K-band on 19 February 2002. The model fit value of uniform disk diameter is about 12 mas. The solid line (thick solid line) is the model curve fit and the dotted-solid line is observed data. The dotted-dashed line is the original raw data. A model curve of angular diameter 7.3 mas (solid line) is also superposed on the fit. Simultaneously observed K-band light curve is also shown. It has been shifted in Y-axis for better comparison.*

Z Sco

Z Sco is a galactic Mira variable of period 352 days (Kukarkin et al. 1969) The spectral type is M4/5 IIIe. The visual magnitude varies from 8.7 to 13.4 (SIMBAD database) over period. The distance to the source found in the literature is in the range of 511 pc (Celis 1995) to 770 pc (Whitelock et al. 2000a). We have adopted the distance to the source to be 778±145 pc using reddening corrected mean K-band magnitude and period-luminosity relation found in Whitelock & Feast (2000b). No dust signature is detected in the LRS spectra of *IRAS* (Sloan & Price 1998). The maser emission lines of CO and SiO are not also detected in the atmosphere of Z Sco (Young 1995; Cho et al. 1996). The detailed source parameters are listed in Table 5.2.

The occultation of Z Sco was recorded on 22 March 2003 in the K band. The visual variability phase of our observation was 0.26 (AFOEV database). The sky condition during observations was poor (thin passing clouds) but event was possible to record. Fringe distortion is also evident in the occultation trace from Fig. 5.4 but four fringes are recorded in the trace. The signal is appeared about 10% less in occultation trace compared to that under clear sky conditions which was taken before that the event. Over all the quality of data is poor because of sky condition.

The light curves are fitted with the UD model of five parameters and varying background is modeled with a 5th order Legendre polynomial. We derive the UD value to be 3.8±1.0 mas. The model fit light curves along with observed data points are shown in Fig. 5.4 and the derived value of angular diameter is listed in Table 5.3.

No angular diameter measurements for Z Sco are reported earlier in the literature. We estimate the probable angular diameter of the source $\sim$ 5.1 mas at phase of our observation from empirical relation of angular diameter and (V-K) established by van Belle (1999). The expression used is given in the eqn.(6.3) of chapter 6. The uncertainty of the predicted value is about 25% as suggested by the author. The visual magnitude of the source is found in AAVSO archives to be 11.6 mag near the phase of our measurement (Mathei 2004). We measure the K-band photometric magnitude of the source is to be 1.33±0.1 mag. Our derived angular diameter is less than the predicted value but errors are large due to poor quality of the light curve.

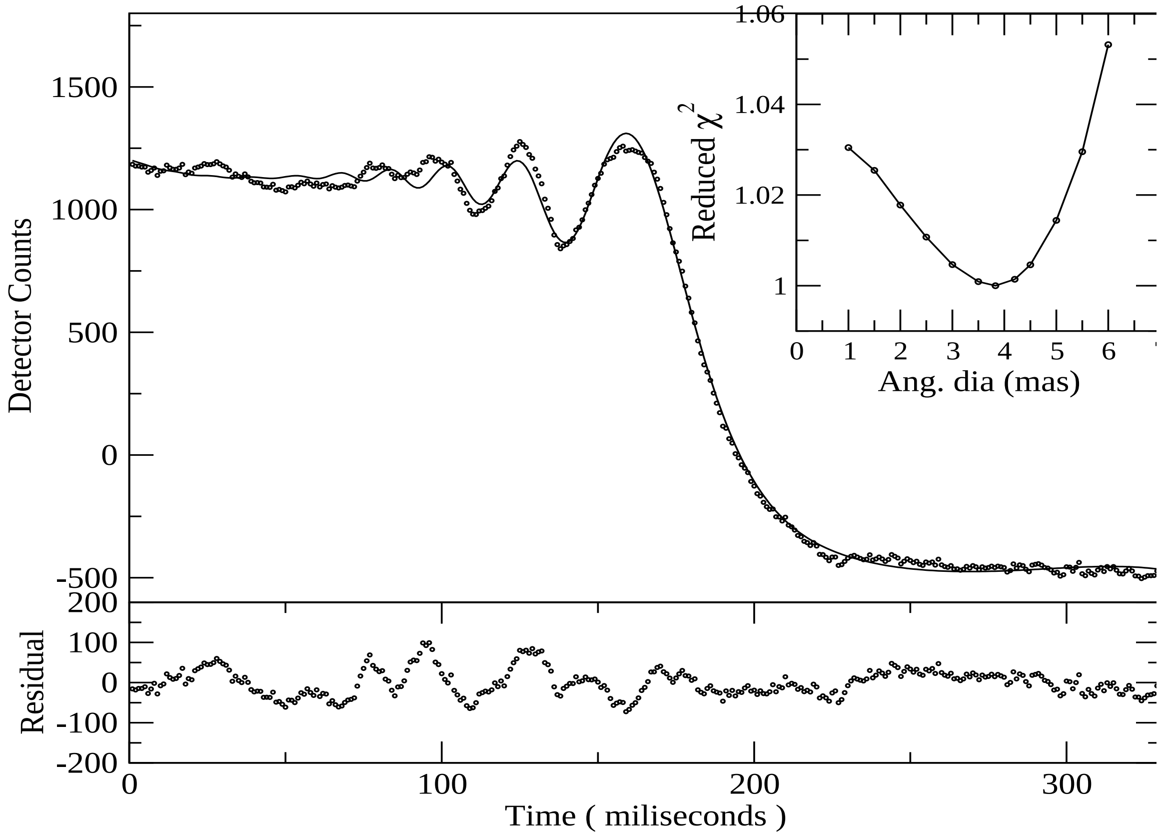

Figure 5.4: *The light curve of Z Sco observed in K is shown above. The open circles are observed data and the solid line is the model-fit curve of UD angular diameter 3.8±1.0 mas. The lower panel of the graph shows residuals (data -model) of the fit and inset graph shows the convergence of the fit.*

η Gem

η Gem is a giant semi-regular variable bright in both visual and infrared bands. The spectral type is M2.5 III (Keenan et al. 1989). The variability is classified as 'blue' SRa with small visual amplitude of 0.75 mag. The period of photometric variability is 233 days (Hipparcos catalog: Perryman et al. 1997). No dust signature is detected from mid-IR LRS spectra of *IRAS* (Sloan & Price 1998). The mass-loss rate estimated from SiO maser emission at 43 GHz is 1.4×10^{-8} $M_{\odot}$/yr (Drake et al. 1991).

Two lunar occultations of η Gem (M2.5 III) have been observed on 08 January 2001 and 4 March 2001. The best-fit UD model curves with observed data points are shown in Fig. 5.5 and Fig. 5.6. Both the events were recorded simultaneously in the K and L$'$-bands. The UD model fits yield the angular diameters of 12.7$\pm$0.3 mas at K and 12.7$\pm$1.0 mas at L$'$ for 08 Jan 2001 light curves and 12.8$\pm$0.3 mas at K and 12.8$\pm$2.0 mas at L$'$ for 04 Mar 2001. There is no difference in angular diameter between K and L$'$ bands. All our derived values of angular diameters are listed in Table 5.3.

We have two good sets of observations in both K and L$'$ bands separated by a two month interval. In this period a good K-band measurement of angular diameter has been made (Richichi & Calamai 2003). Our result in K is in good agreement with these of Richichi & Calamai (2003). Our multiband size measurements of η Gem show no variation between K and L$'$ bands unlike those in U Ori (Mira) or SW Vir (SRb). No temporal variation is also seen over and above the measurement errors between the observations in the two months interval. Given the angular diameter and bolometric flux of (7.6$\pm$1.0) $\times$ 10^{13} W cm^2, we find the effective temperature of the source to be 3450$\pm$125 K.

Previous angular diameter measurements of η Gem are listed in Table 5.4. The source has a well determined angular diameter from the wavelength range 0.55 to 2.2 μm. The optical (0.55 μm and 0.80 μm) interferometric determinations yield the UD diameters of 11.43$\pm$0.55 and 10.91$\pm$0.11 mas respectively (Mozurkewich et al. 2003). The limb darkening diameter is reported by these authors (Mozurkewich et al. 2003) to be 11.79$\pm$0.12 mas. The angular diameter at 0.712 μm (in strong TiO band) and at 0.754 μm (in adjacent continuum) yield the UD diameters of 11.75$\pm$0.27 mas and 10.70$\pm$0.15 mas respectively (Quirrenbach et al. 1993). These optical diameters are slightly lower than our measured IR diameter.

Following Sudol et al. (2002) we have converted UD diameters to limb-darkened diameters. Sudol et al. (2002) estimated the scaling factor to convert UD diameters to limb- dark-

Table 5.5: **Limb-darkened diameter of η Gem**

$\lambda/\Delta\lambda$ (μm)	Feature	θ_{UD} (mas)	$(\theta_{LD}/\theta_{UD})$	θ_{LD} (mas)
0.55/0.02	Weak TiO	11.43±0.55	1.180	13.48±0.65
0.712/0.012	Weak to Strong TiO	11.75±0.27	0.917	10.77±0.24
0.754/0.005	Weak TiO	10.70±0.15	1.100	11.77±0.16
0.80/0.02	Weak TiO	10.91±0.11	1.074	11.71±0.12
2.2/0.4	Near-continuum	12.80±0.30	1.063	13.60±0.32

ening diameters for M4 giant δ^2 LYRAE in the wavelength region 0.55 to 2.2 μm. Those scaling factors was established using static, spherically extended M giant class model of Hofmann & Scholz (1998a) which is considered here also. Being the effective temperature of δ^2 LYRAE (about 3460 K) and the spectral type close to η Gem the estimated scaling factors can be used safely to verify the limb-darken effects. In Table 5.5 we have listed the wavelength dependent scaling factors and the corresponding limb-darkened diameters of η Gem. Table 5.5 illustrates that the limb-darkening corrections disagree in all wavelength regions and it appears that such model is inadequate to correctly remove the observed angular diameter differences. Such corrections have worsened the agreement between different wavelength measurements. Sudol et al. (2002) have found such disagreement for δ^2 LYRAE for seven sets of angular diameters in the same wavelength region. These authors (Sudol et al. 2002) concluded that dynamic mechanisms in the atmosphere have a significant effects on temperature-density stratification such that a static model cannot provide the adequate description of the atmosphere. This is the case for η Gem also and being a small-amplitude variable star the dynamic mechanisms have a significant effects on angular diameter dispersions.

η Gem is also identified as a spectroscopic binary. The spectral type of the companion is G0 III which has visual magnitude of 11.3 and the separation of 0.9 to 1.08 arcsec from primary at position angle (PA) of 29^o (Philips et al. 1980; Baize et al. 1989). The *Hipparcos* catalog shows a binary separation of 1.7 arcsec at PA of 261^o (Perryman et al. 1997). The variation of separation in several observations is attributed to the ellipticity of the orbit. No binarity signature is detected in any of our LO light curves and it was also undetected from previous LO observations. The brightness ratio between the primary and secondary is estimated $\sim$ 1:1600 in the visual band. The K magnitude of the companion would be $\sim$ 13 mag which is well below the limit of our detection.

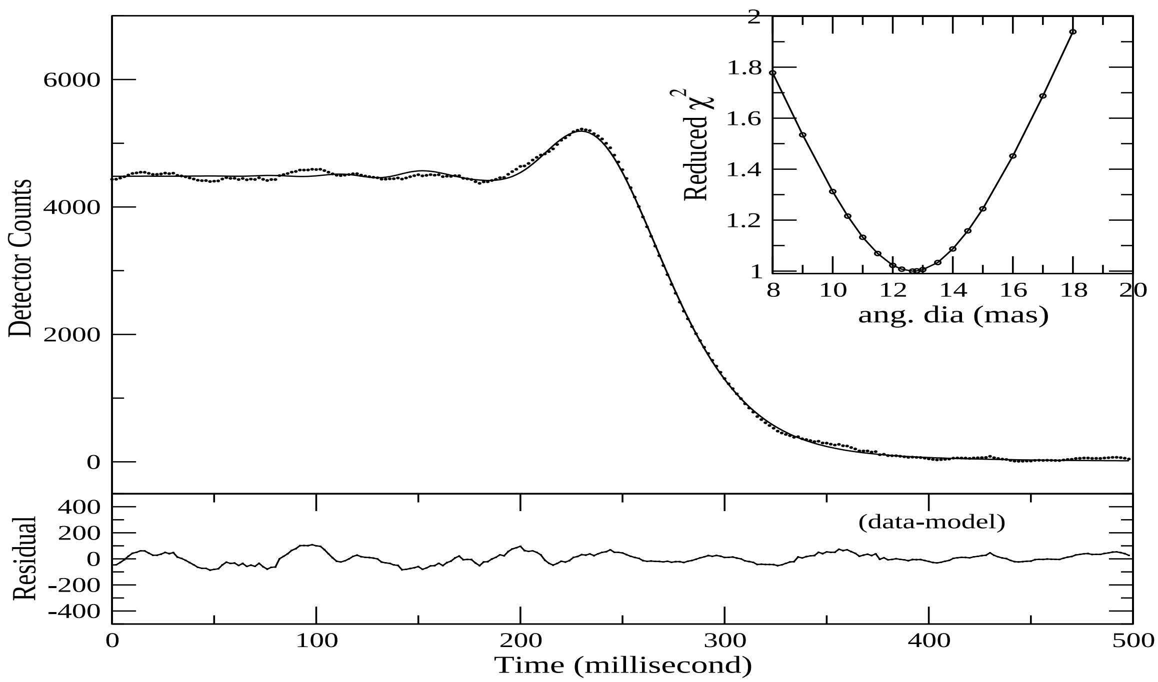

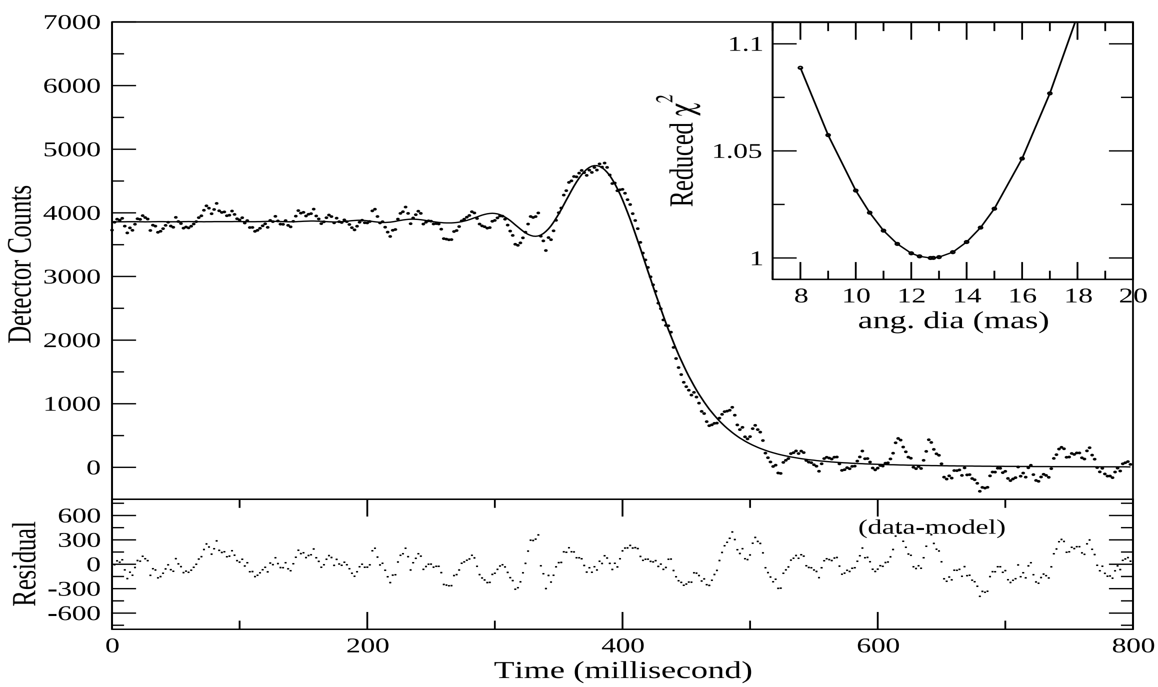

Figure 5.5: *Lunar Occultation light curves of η Gem observed simultaneously in the K-band (right) and L'-band (left) on 08 January 2001. The dotted lines are observed data points and the solid lines are the model fitted curves. The best-fit uniform disk diameters yield 12.7±0.3 mas at K and 12.7±1.0 mas at L'. The lower panels and in sets of the graphs are residuals and convergence parameters of the models respectively.*

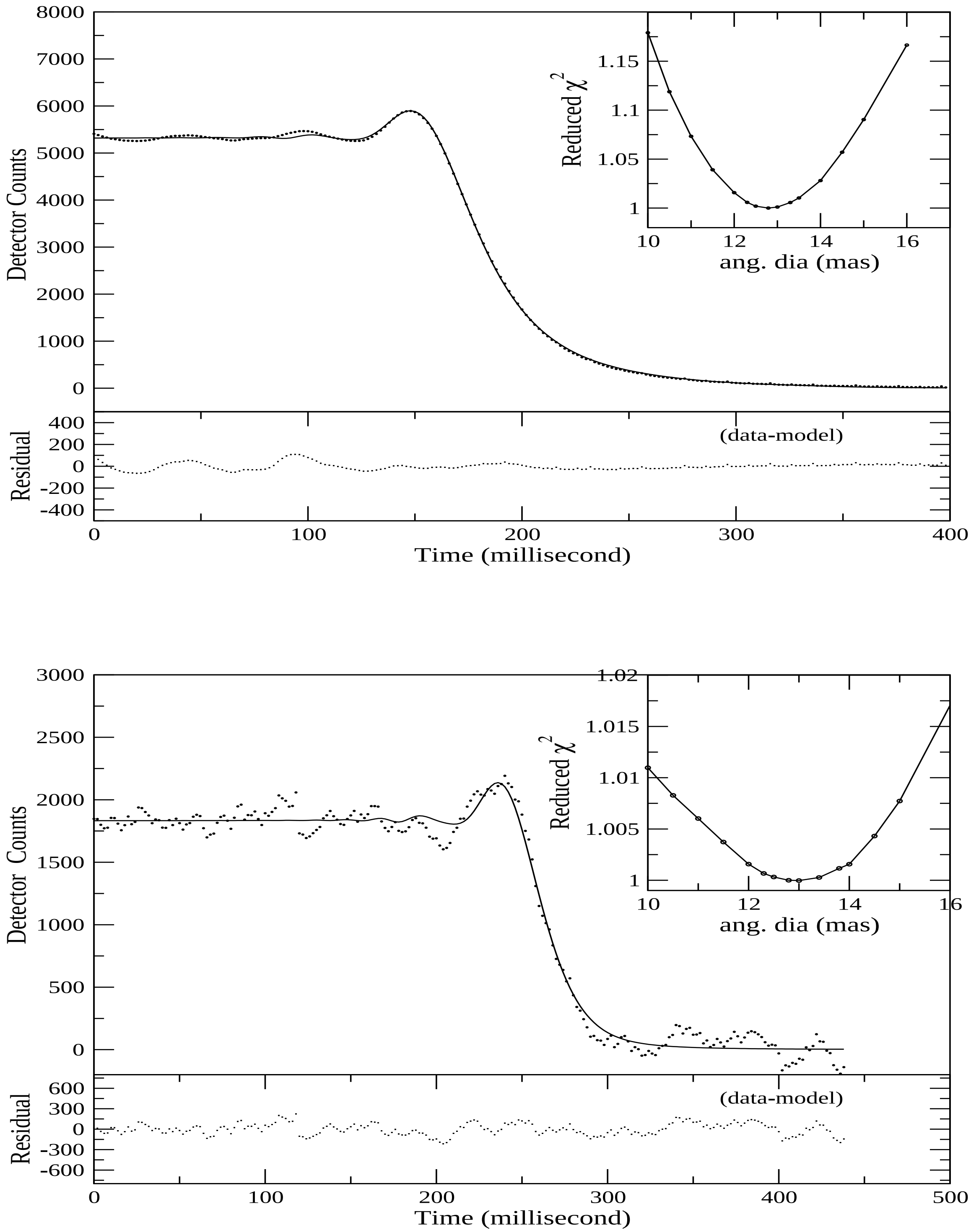

Figure 5.6: *Lunar Occultation light curves of η Gem observed simultaneously in the K-band (right) and L'-band (left) on 4 March 2001 are shown. The dotted lines are observed data points and the solid lines are the model fitted curves. The best-fit uniform disk diameters yield 12.8±0.3 mas at K and 12.8±2.0 mas at L'. The lower panels and in sets of the graphs are residuals and convergence parameters of the models respectively.*

μ Gem

μ Gem is an infrared bright (m_k =-1.87, m_L =-2.0) irregular variable and classified as 'Lb'. The spectral type of source is M3 III (Keenan et al. 1989). No dust was found from *IRAS* LRS spectra (Sloan & Price 1998). The *Hipparcos* estimation of distance to the source is 68$\pm$4 pc (Perryman et al. 1997). The mass loss is estimated to be 4.4$\times$ 10^{-9} $M_\odot$/yr (Drake et al. 1986).

The lunar occultation of μ Gem (M3 III) was observed simultaneously in the K and L$'$-bands on 04 Mar 2001. The UD model light curves are fitted to the observed occultation traces. The best-fit UD angular diameters yielded the values of 13.7$\pm$0.5 and 14.8$\pm$1.0 mas in the K and L$'$-band respectively. The best-fit model light curves along with observed data points are shown in Fig. 5.7 and the measured UD values are listed in Table 5.3.

There are thirteen observations of lunar occultation in the wavelength range 0.4 to 0.82 μm listed in the catalog of White & Feierman (1987) and the mean UD value in that wavelength range is 13.06$\pm$0.42 mas. Recently UD angular size in the optical bands using long baseline interferometry (LBI) has been reported (Mozurkewich et al. 2003). The value of 13.98$\pm$0.14 mas (at 0.80 μm) and 13.48$\pm$0.19 mas (at 0.55 μm). Only one LBI measurement in the K-band was available with the reported UD value of 13.50$\pm$0.15 mas (Di Benedetto & Rabbia 1987). Other LBI measurements at TiO absorption band (0.712 μm) and nearby continuum (0.754 μm) have reported UD values of 13.97$\pm$0.28 mas and 13.50$\pm$0.13 mas respectively (Quirrenbach et al. 1993). Mira like enlargement in angular size (a factor of $\sim$2) in TiO band compared to the adjacent continuum has not been noted in μ Gem. Some earlier previous measurements are listed in the Table 5.4. The measurements before 1987 can be found in the LO catalog of White & Feierman (1987).

Considering all available measurements including our own it appears that the UD diameter of μ Gem has not shown any substantial variation from optical to near-IR over many years. Our UD angular diameters show no significant (above few σ) variation between K and L$'$ band. We have estimated the effective temperature of 3675$\pm$140 K.

In case of Mira and evolved stars (later than spectral type M5), enhancement in angular diameter at L$'$ were observed compared to K and cause of such enhancement was attributed to warm extended gaseous layers (Mennesson et al. 2002). Such any warm layers ($\sim$ 2000K) exist in case of η Gem and μ Gem would not be closer than 3R_*, considering their estimated effective temperature as photospheric temperature and the temperature distribution in the shell to be T(r) $\propto$ $r^{-0.5}$. The radial velocity variation of semi-regular variable was found to be small ($\sim$ 4 km/s) compared to Miras ($\sim$ 25 km/s) (Hinkle et al. 1997). Again the mass loss of η Gem is small (1.4×10^{-8} $M_{\odot}$/yr) in comparison to Mira stars ($\sim 10^{-6}$ $M_{\odot}$/yr). Owing to low mass loss rate compared to Miras the density at $3R_{*}$ may not be that much sufficient to make any substantial bias in L′ measurement which are seen in Miras or spectral type later than M5.

SW Vir

SW Vir is a infrared bright semi-regular pulsating variable (SRb) of pulsation period of 150 days (Lebzelter & Horn 1999). The spectral type is M7 III (Keenan et al. 1989). The visual amplitude (max-min) is 1.5 mag which is smaller than that of Miras ($\sim$ 5 mag). The *Hipparcos* estimation of distance to the source is 142 pc (Perryman et al. 1997). The 10μm speckle observations (Benson, Turner & Dyck 1989) detected a dust shell around SW Vir and the angular extension of the shell was measured to be 280 mas (or $17R_{*}$). The corresponding shell temperature of $\sim$ 600 K was derived considering the stellar temperature of 2950 K. The evidence of dust shell around SW Vir was also found from mid-IR LRS spectra of *IRAS* (Sloan & Price 1998). The optical thickness of the shell at 2.2 μm was estimated to be $\sim$ 0.02 (Ivezic & Elitzur 1995).

The disappearence event of lunar occultation of SW Vir (M7 III) was recorded on 01 June of 2001. The S/N of data is limited by the atmospheric scintillation. It was observed only in the broad K-band. The best-fit UD model yields the value of 15.9$\pm$0.6 mas. The best-fit UD model light curve along with observed data-points are shown in Fig. 5.8 and the result is included in Table 5.3.

The angular diameter measurement of SW Vir was reported previously thrice in the near-IR region by LO and the reported values are in the range of 16.11 to 16.82 mas (Ridgway et al. 1982; Schmidtke et al. 1986). Details of those measurements are listed in the Table 5.4. Recently using LBI the reported values of angular diameters are 16.24$\pm$0.06 mas in the K′ band and 22.88$\pm$0.33 mas in the L′ band (Mennesson et al. 2002). Our measurement in the broad K-band is consistent with previous measurements. From previous reported measurements (in Table 5.4) at different phase we can see that phase-dependent variations are not observed in SW Vir. We estimate the effective temperature to be 3060$\pm$130 K.

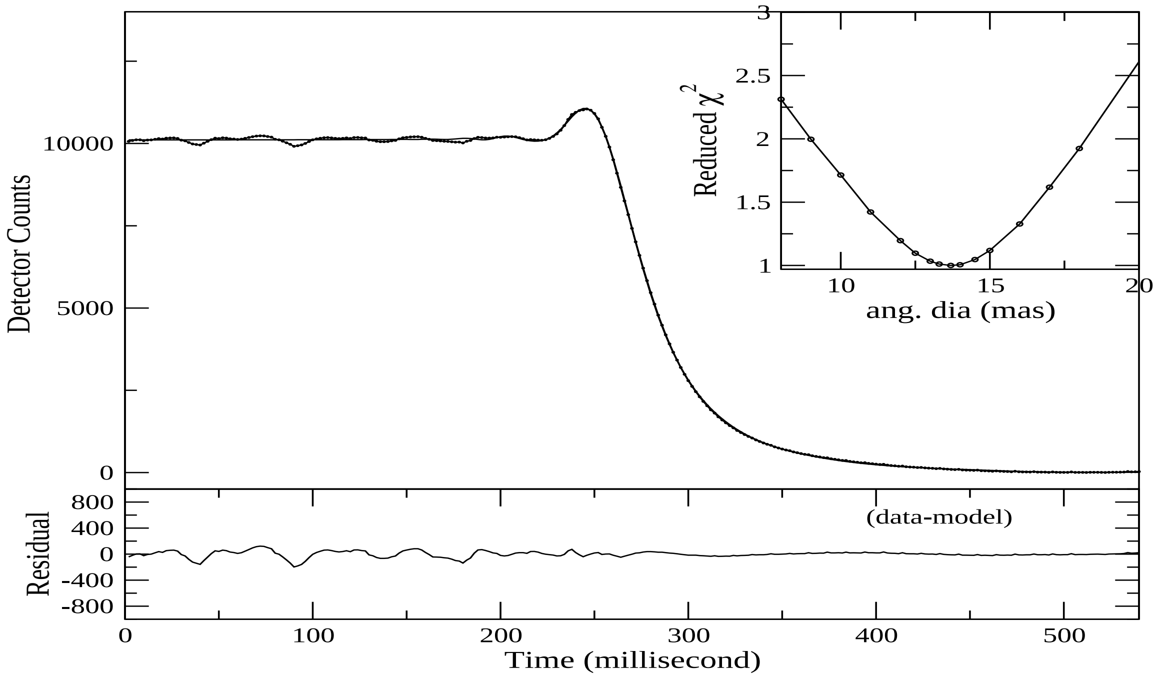

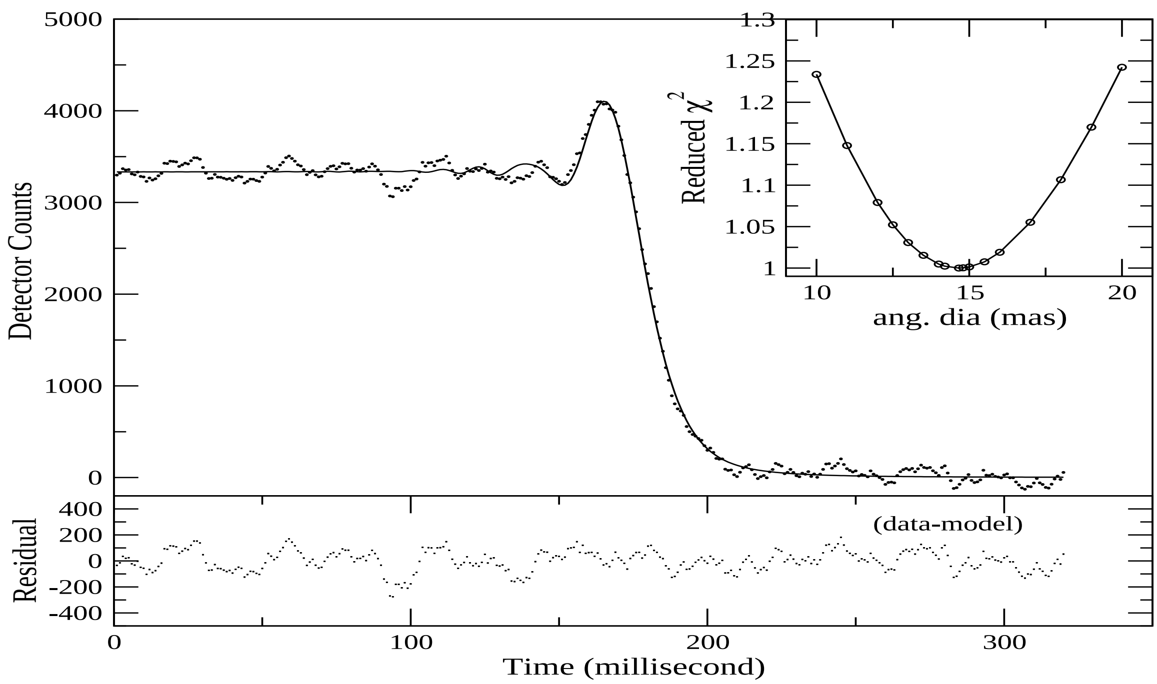

Figure 5.7: *Lunar Occultation light curves of μ Gem in the K- and L′-band are shown observed on 4 March 2001. The circles are observed data and the solid line is the model fit curve. The best-fit uniform disk angular diameter yields 13.7±0.5 mas at K-band and 14.8±1.0 mas at L′-band. The lower panels of both graphs show residual of the fit and inset graphs show the convergence of the fit.*

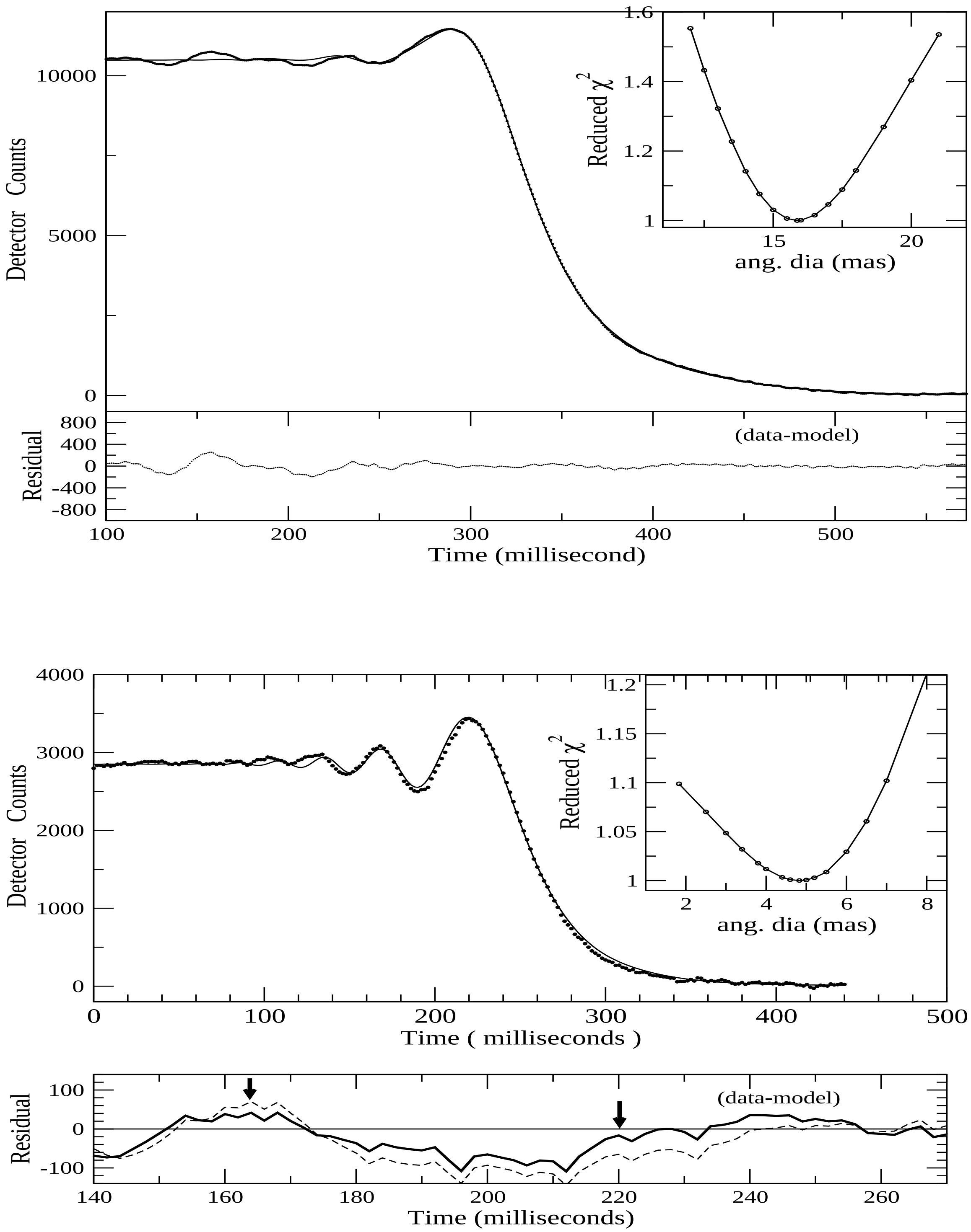

Figure 5.8: *Lunar occultation light curves in the K-band of SW Vir (upper graph) and TV Gem (lower graph). The dotted lines are observed data and the solid line is the UD model fit. The derived UD angular diameters are 15.9±0.6 (SW Vir) and 4.8±0.2 (TV Gem). In the upper graph the lower panel and inset graph shows residual (data -model) and convergence of the fit. In the lower graph, the lower panel shows residual of the fit particularly on 1st and 2nd fringes and arrow is indication the position of fringes. Inset of lower graph shows the convergence of the fit.*

TV Gem

TV gem is a short period oxygen-rich supergiant semi-regular variable (SRc). The spectral type is M1-0 Iab (Keenan et al. 1989). The visual magnitude varies from 7.0 - 7.8 over the pulsation period of 182 days (Kukarkin et al. 1969). The distance to TV Gem is 1200 $\pm$ 300 pc based on interstellar extinction towards Gem OB1 association (Underhill 1984; Ragland 1996). The mass loss rate from CO lines was estimated to be 2×10^{-6} $M_{\odot}$/yr and the outflow velocity of 12 km/s (Loup et al. 1993).

The lunar occultation of M1 supergiant TV Gem was observed on 14 Nov 2000 in the K-band. The event was a reappearance one and recorded under clear sky condition. The S/N is limited by atmospheric scintillation. The UD model fit of the light curve with usual five free parameters was not satisfactory. In UD fit we have considered two additional free parameters; parameters are the dust shell diameter (with initial guess $\sim$ 20R_*) and the shell flux (with initial guess $\sim$ 4% of stellar signal). The UD model fit appears much better than only five parameter fitting. We estimate the UD value of 4.80 $\pm$ 0.20 mas. The UD model fit of the light curve along with observed data points are shown in Fig. 5.8. A better fit to the data is obtained by including a star plus shell model rather than a single star model. The JHK photometric observation of the source was done on 16 Nov of 2000. The JHK magnitudes are 2.31$\pm$0.05, 1.39$\pm$0.05 & 1.16$\pm$0.06 respectively.

Angular diameter measurements by lunar occultation were reported several times and are listed in Table 5.4. The optical lunar occultation measured the UD value of 5.31 $\pm$ 0.91 mas (Radick et al. 1984); the infrared lunar occultations in the K-band reported the UD values of 4.9 $\pm$ 0.3 mas (Ragland et al. 1997) and 4.46 $\pm$ 0.07 mas (Richichi et al. 1998b). From LO observations in the K-band Ragland et al. (1997) had reported the double shell structure of TV Gem like another supergiant α Ori (Danchi et al. 1994). The inner dust shell was estimated to be at 20$\pm$5 R_*. The outer shell was estimated to be at $\sim$ 500R_* based on LRS spectra of *IRAS* and *IRAS* photometry (12, 25 60 μm). They found the shell contribution in the K-band to be $\sim$3%. We measure the UD angular diameter of the source 4.8$\pm$0.2 mas. We estimate the effective temperature to be 3750$\pm$120 K in good agreement with earlier values (Richichi et al. 1998). We obtain a better fit by including dust shell contribution. We estimated the dust shell to be at 13$\pm$5 R_*. The shell contribution to the K-band flux is $\sim$5% . These results are consistent with earlier measurements by Ragland et al. (1997).

5.5.2 Bolometric flux and effective temperatures

Table 5.6: **Derived angular diameters, bolometric flux and effective temperatures**

Star	Spt.Type	m_k	m_v	UD (K-band) mas	$F_{bol} \times 10^8$ (erg cm^{-2} s^{-1})	T_{eff} (K)
U Ori	M8 IIIe	-0.88	10.89	11.9±0.3	336±33	2905±80
U Ari	M9 IIIe	1.26	14.50	7.3±0.3	45±5	2250±80
Z Sco	M4/5IIIe	1.33	11.6	3.8±1.0	46±5	3120±420
SW Vir	M7 III	-1.74	7.90	15.9±0.6	735±110	3060±130
η Gem	M2.5 III	-1.49	3.70	12.8±0.3	760±105	3450±125
μ Gem	M3 III	-1.89	3.20	13.7±0.5	1140±170	3675±140
TV Gem	M1 Ia	1.16	6.83	4.8±0.2	153±15	3750±120

The bolometric fluxes are estimated by fitting a blackbody curve to available broad-band IR photometry measurements (JHKLM) compiled in the Infrared catalogue of Gezari et. al.(1999) and 12, 25 & 60 μm *IRAS* PSC measurements including our JHK measurements in some cases. In some cases two-temperature blackbody is required to best fit all observed points (1.25 -60 μm) especially additional blackbody curve with cooler temperature ($\sim$500 K) fits excess in *IRAS* flux. Such fits are shown in Fig. 5.9-5.10 in case of U Ari, U Ori and Z Sco, while for η Gem a single temperature blackbody curve is fitted to all observed fluxes (Fig. 5.10). The observed broad-band photometric magnitudes (JHKLL$'$) are converted to flux densities using the zero magnitude to flux density calibration established by Bessell, Castelli & Plez (1998). The blackbody flux is normalized with the observed flux in K-band. In case of two-temperature blackbody fit the shell flux is normalized with continuum subtracted 25 μm flux of *IRAS*. By numerically integrating the single (or resultant of double temperature) blackbody fitted curve in the wavelength range 0.4 to 100 μm the bolometric flux is calculated. The evolved stars have a peak emission in the wavelength range of 1 - 2 μm and the wavelength range of (0.4 -100 μm) of integration are adequate to calculate bolometric fluxes. No reddening corrections were applied to estimate bolometric fluxes. These were deemed unnecessary, since typical magnitude of the corrections of our sample will be less than 0.05 mag in K-band. For example, the largest visual extinction was found in U Ori, $A_v \sim 0.25$ mag (Whitelock et al. 2000a) and correspondingly $A_k \sim 0.03$ mag using the wavelength-dependent extinction relation, $A_k = 0.11A_v$ established by Bessell et al. (1998). Our own infrared JHK photometric measurements of U Ari are used to estimate the bolometric flux at that particular phase (near minimum) while others are taken from Catchpole et al. (1979) at a similar phase. In case of SW Vir and TV Gem the bolometric fluxes were taken from the literature (Perrin et al 1998; Ragland et al. 1997) while for other sources (U Ari, U Ori, Z Sco, μ Gem and η Gem) our estimated bolometric fluxes are used to calculate the effective temperature which are listed in the Table 5.6. The typical error in bolometric flux is estimated to be about 15%. The effective temperature of the sources using our derived K-band UD diameters are listed in Table 5.6.

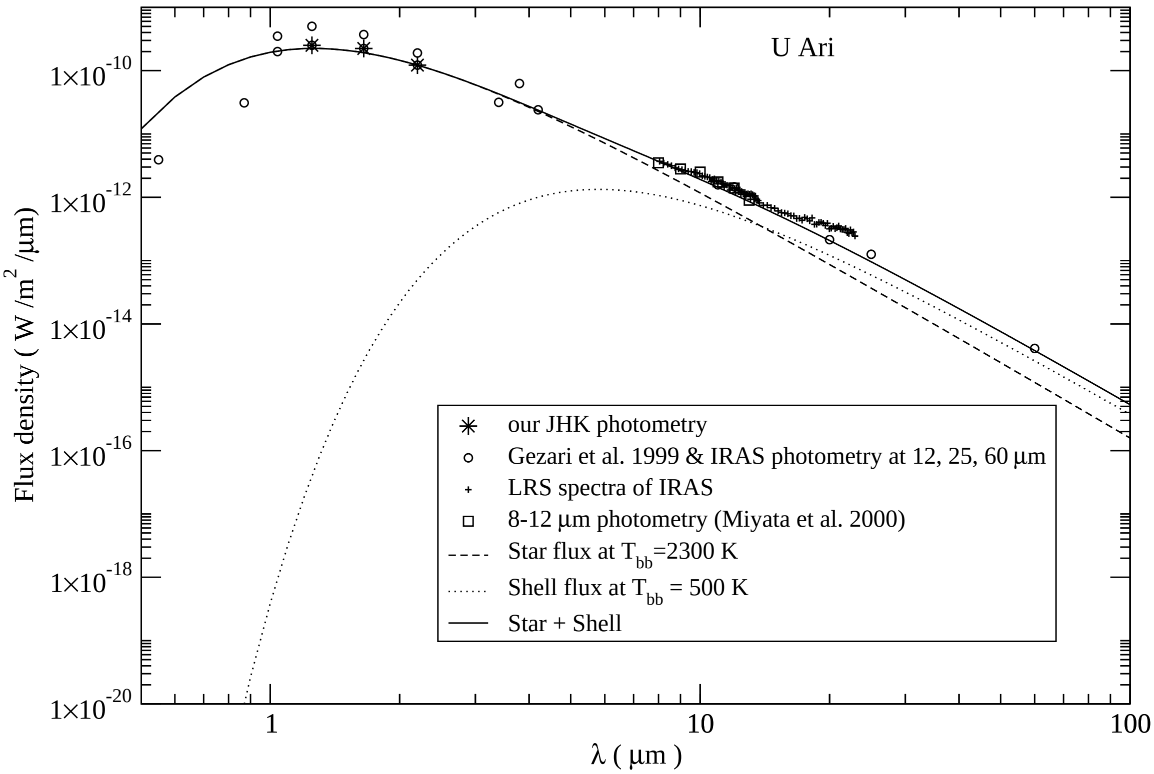

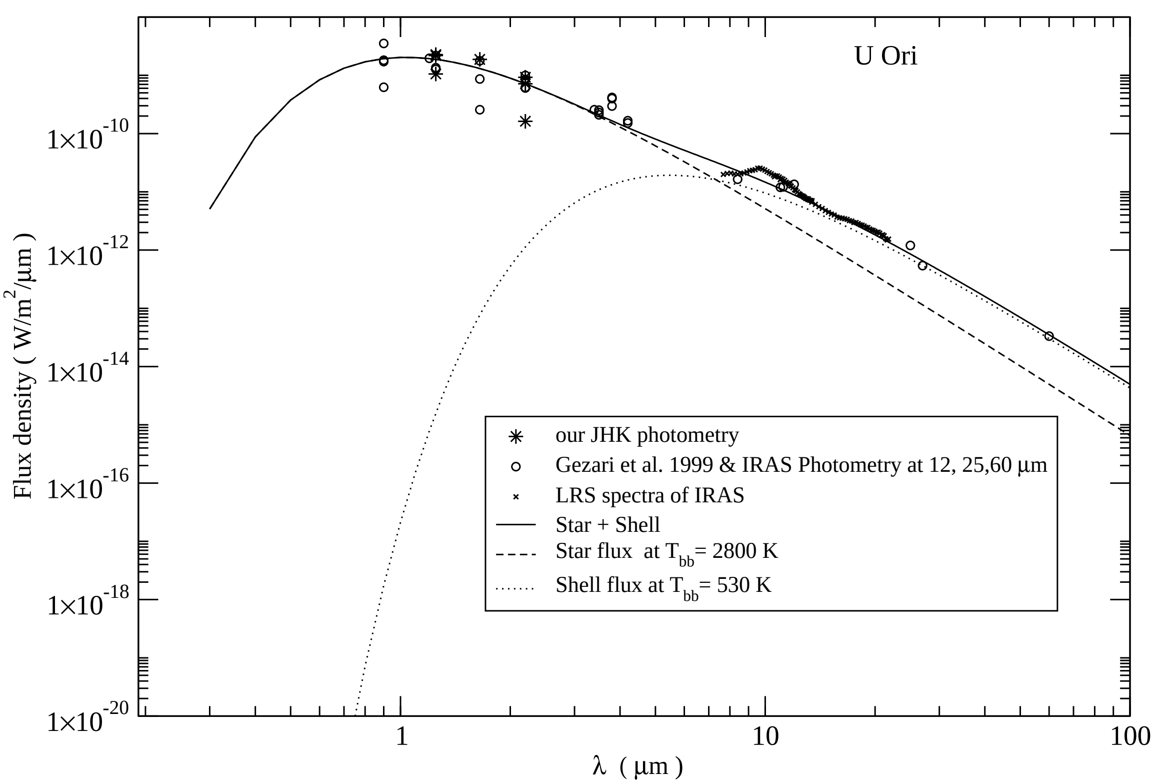

Figure 5.9: *The blackbody fit to available photometry data in the literature for U Ari and U Ori.*

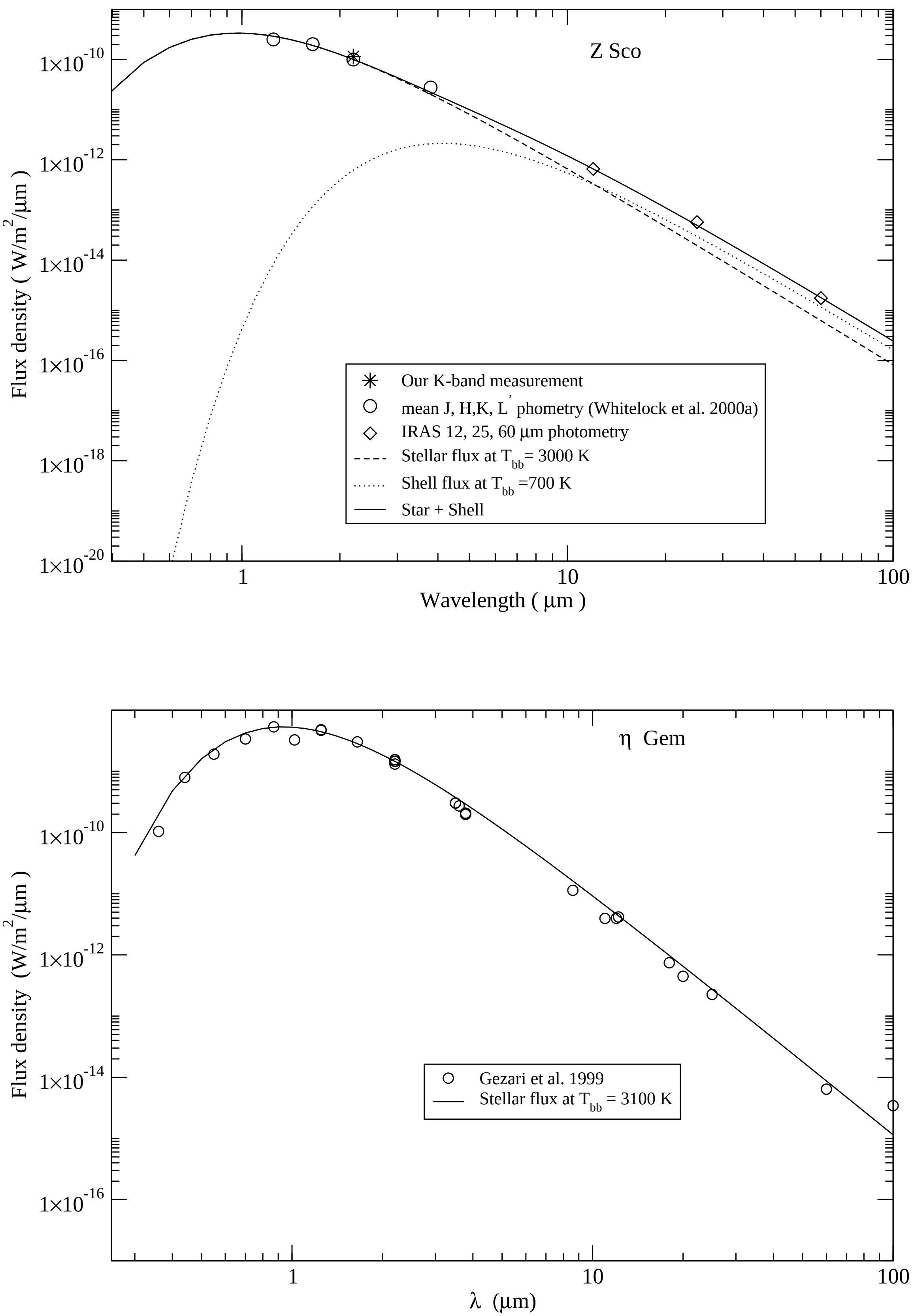

Figure 5.10: *The blackbody fit to available photometry data in the literature for Z Sco and η Gem.*

5.5.3 Linear radii and mode of pulsation

To investigate the pulsation mode it is essential to know the true photospheric radius of these variables. The K-band angular diameters for non-Miras are close to true photospheric diameter where limb-darkening is negligible (Hofmann et al 1998a). Wood (1990) had suggested that in principle one combined equation for the position of low mass AGB stars included both Miras and semi-regular variables can be used for comparing the observational results. The standard pulsation equation is written as,

$$Q = P\left(\frac{M}{M_\odot}\right)^{1/2}\left(\frac{R}{R_\odot}\right)^{-3/2} \tag{5.1}$$

Where Q is a constant quantity (unit of days) and it has distinct value for each mode of pulsation. Theoretical model predicted Q-values vary with period, mass and luminosity (Fox & Wood 1982). Typically Q-value for fundamental mode is $\approx$ 0.105 day and for the first overtone mode Q$\approx$ 0.04 (Fox & Wood 1982). Following Ostile & Cox (1986) we have considered the following expressions for fundamental and overtone modes respectively,

$$\log P = 1.86\log(R/R_\odot) - 0.73\log(M/M_\odot) - 1.92 \quad \text{Fundamental} \tag{5.2}$$

$$\log P = 1.59\log(R/R_\odot) - 0.51\log(M/M_\odot) - 1.60 \quad \text{1st overtone} \tag{5.3}$$

Where P is the period in days. M and R are in solar units.

Our derived K-band angular diameters are converted to linear radii. The distance were estimated using the post-*Hipparcos* Period-Luminosity (PL) relation between period and absolute K-band magnitude, $M_k = -3.47\log P + 0.84$ established by Whitelock & Feast (2000a). The uncertainty in distance measurements from PL relation is about 19%. Unfortunately there is no reliable *Hipparcos* parallax measurement of Miras except a few nearby Miras (within 200pc). The large uncertainties in *Hipparcos* distances are due to several causes as discussed in van Leeuwen et al. (1997). We estimate the distance using the well-known relation, $\log$d (pc) = 1 + 0.2 (m$_k^o$ - M$_k$). The reddening-corrected mean K-band apparent magnitude (m$_k^o$) is used in case of Miras owing to large amplitude ($\sim$ 0.5 mag). The mean apparent K magnitude of U Ori was found -0.64 mag (Whitelock et al. 2000b) and that of U Ari and Z Sco are respectively 1.37 mag (Feast 1996) and 1.46 mag (Whitelock et al. 2000b). The distances of SW Vir, μ Gem and η Gem were adopted from *Hipparcos* parallax measurements (Perryman et al. 1997).

Table 5.7: **Linear radii and distance of Mira and SRs**

Star	K-band UD (mas)	Period (days)	PL Dist[a] (pc)	Hip. dist (pc)	adopted Dist. (pc)	Lin. Radii ($R_\odot$)	Q-value (for 1 $M_\odot$)
U Ori	11.9±0.3	372	306±61	658±606	306±61	391±78	0.048
U Ari	7.3±0.3	371	776±155	-	776±155	610±125	0.025
Z Sco	3.8±1.0	352	778±145	405±330	778±145	320±100	0.062
SW Vir	15.9±0.6	150	98±19	143±24	143±24	244±42	0.039
η Gem	12.8±0.3	233 20[b]	150±30	107±22	107±22	146±30	0.130 0.012
μ Gem	13.7±0.5	27	-	71±5	71±5	104±8	0.025
TV Gem	4.8±0.2	182	-	1492±2340	1200±300[c]	623±158	0.012

[a]*Period-Luminosity(PL) relation of Whitelock & Feast (2000a) is used here.*
[b]*This secondary period is determined from visual photometric observations by Percy et al. (2001).*
[c]*Adopted from Ragland et al. 1997.*

Masses of Miras of moderate ($\leq$400 days) period are reasonably well constrained $\sim$ 1 $M_\odot$ (Wyatt & Cahn 1983). As semi-regular variables are progenitor of Miras then such masses may be applicable for them also. Jura & Kleinmann (1992) suggested that the main-sequence masses of Mira progenitor are in the range 0.8 - 2.0 $M_\odot$ for Miras having period less than 400 days. Wyatt & Cahn (1983) estimated the main sequence masses of 124 Miras considering available data of radial velocity measurements. The mass of one Mira (U Ari) in our sample has been determined by Wyatt & Cahn (1983) and it is 1.3$M_\odot$. In this mode analysis we have considered the mass range of 1.0 - 2.0$M_\odot$.

The linear radius-period plot in Fig. 5.11 and Q-value in Table 5.7 lead to the conclusion that Miras U Ari & U Ori in our sample are pulsating in first overtone while other Mira Z Sco is a borderline case. The angular diameter determination of Z Sco was not possible precisely because of noisy data which precludes a more definitive conclusion. The semi-regular variables SW Vir and μ Gem favour the overtone mode. Percy et al. (2001) found from photometric monitoring of η Gem that it has two periods of variability. The longer period corresponds to 234 days, which is the period considered here while the shorter period is 20 days. Such period ratio ($P_{long}/P_{short} \approx 10$) can switch the mode from fundamental to higher overtone mode. This period ratio has been found in many semi-regular variables

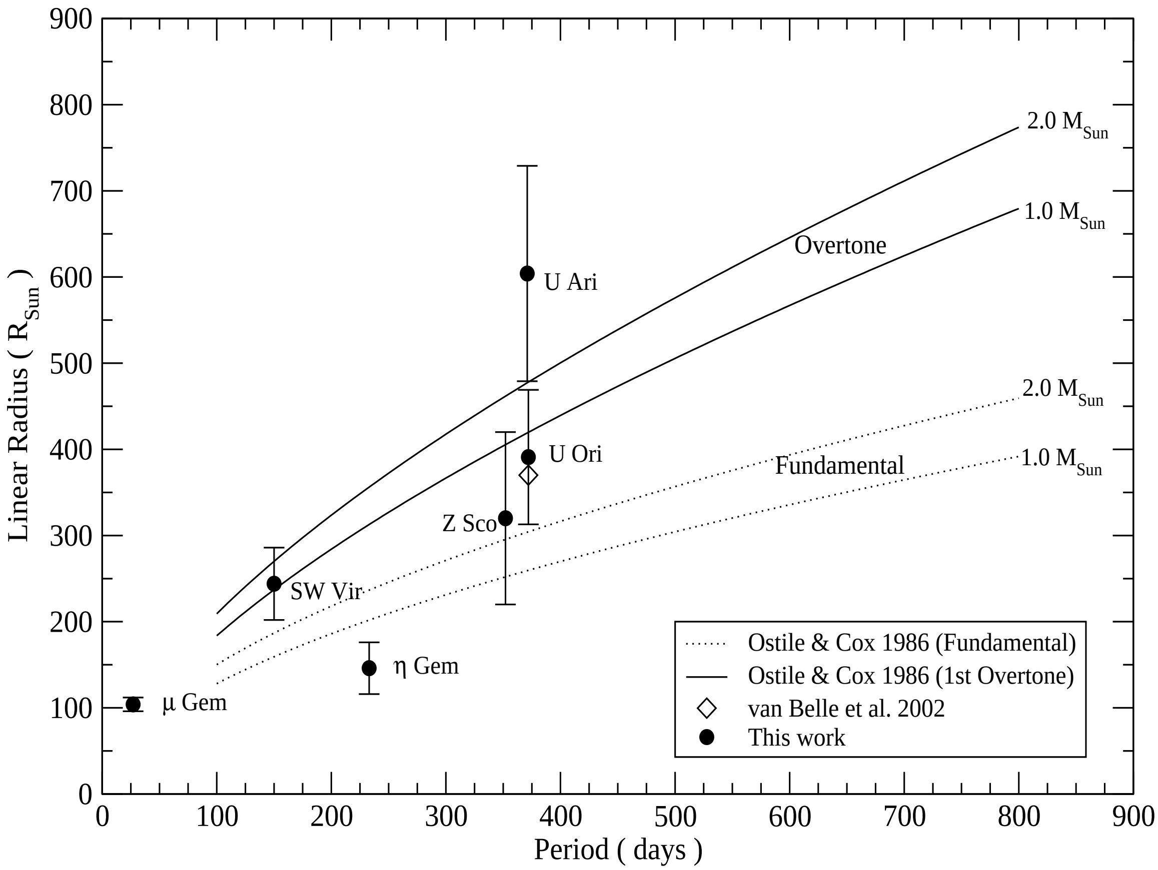

Figure 5.11: *Linear radius vs. period plot for the Miras and semi-regular variables . The filled circles represent our LO measurements in the K-band. The fundamental and first-overtone curves in the mass range 1.0 $M_\odot$ - 2.0 $M_\odot$ are derived from the radius-period relation found in Ostile & Cox (1986). The overplotted open diamond is the interferometric measurements of U Ori in the 2.2 μm found in van Belle et al.(2002).*

(Percy et al. 1998; Kiss et al. 1999). η Gem show mixed mode of pulsation. The longer period (234 days) corresponds to fundamental mode while shorter period (20 days) favours 1st overtone mode. Studies on most of the galactic SR variables found them to be 1st overtone or higher overtone pulsators (Percy et al. 1998). However, some SR variables in LMC have been found to be pulsating in fundamental mode (Wood et al. 1999).

5.6 Conclusion

UD Angular diameter of U Ari in K-band shows substantial larger value ($\sim$ 20%) compared to H-band at nearly same phase observed earlier. Such an enhancement is attributed to hot extended layers close to the photosphere (Mennesson et al. 2002). The enhancement in L$'$-band is expected to be more prominent even show an increase in size, by a factor of $\sim$ 2. But the excessive noise inL$'$-band data precluded such a determination of an accurate angular diameter. This could be confirmed in future by interferometric observations at 3.8 μm.

Two M3-giants η Gem and μ Gem are observed in both K and L$'$ bands. Their sizes are consistent with earlier IR measurements. Between K and L$'$ no difference in sizes are observed. There is no evidence of any dust around η Gem and μ Gem from *IRAS* LRS spectra.

Our K-band UD diameter of SRb variable SW Vir is consistent with earlier measurements. The effective temperature we estimate 3060$\pm$130 K. The increment of diameter in L$'$ has been again attributed to extended gaseous layers ($\sim$ 1500 - 2000K) by Mennesson et al. (2002).

Supergiant TV Gem in the K band yields the angular size of 4.80$\pm$0.20 mas consistent with previous measurements. The dust shell around TV Gem is re-confirmed by our high quality light curve. We measure the dust shell size to be 13$\pm$5 R_* in good agreement with earlier estimation (20$\pm$5 R_*). We have observed the flux from dust shell in the range of $\sim$ 5% of stellar flux which is slightly higher than earlier estimation($\sim$ 3%). The effective temperature derived is 3750$\pm$120 K, consistent with earlier value.

We estimate linear radii of three Mira variables (U Ari, U Ori and Z Sco) from the K-band angular diameter measurement. Comparing theoretical Period-Radius linear plots (Fig. 5.11) and estimating pulsation constant Q-value we find that two Miras (U Ari& U Ori) favour first overtone mode of pulsation while Z Sco is a borderline case between fundamental and 1st overtone. The large errors in angular diameter determination of Z Sco precludes any conclusion about mode. Results of pulsation mode in semi-regular variables are more complicated. Semi-regular variable SW Vir (SRb) favours first overtone mode, while irregular variables μ Gem (Lb) is likely to be pulsating in higher overtone. η Gem (SRa) has two period with ratio (P_{long}/P_{short} $\approx$ 10), longer period corresponds to fundamental mode while shorter period to higher overtone.

Chapter 6

Angular diameter of K - M Giants and Supergiants

This chapter focuses on the angular diameter measurements of *late giants and supergiants*, obtained in the K (2.2 μm) filterband. These include eleven oxygen-rich giants of spectral type in the range K0-M6 and one M3 supergiant. The effective temperature (T_{eff}) is derived from the angular diameter and calculated bolometric flux. T_{eff} values are superposed on the existing spectral type-T_{eff} calibration and discussed.

6.1 Introduction

Empirically, it has long been established that effective temperature of spectral type similar to or hotter than Sun can well described by temperature-colour relation (Barnes & Evans 1976). However, for spectral types of K - M ($T_{eff} \leq 4500$ K), such a calibration is not satisfactory. Initial attempts to define a relationship between temperature and visual colour indices were less successful for cooler star, mainly because of presence of broad molecular bands in the V, R and I filters.

Theoretically study of red giant stars (K-M) stars has proved difficult to model accurately because these objects are cool and thus have a wealth of molecules in their stellar atmospheres. This means that a variety of phenomena that can be ignored in the modeling of hotter stars are important in the atmospheric structure of these evolved stars. The most critical of these are the molecular opacities, which depend not only on the accuracy of the (sometimes nonexistent) laboratory data (Brett 1990; Jorgensen 1994).

The effective temperature of a stellar source is a fundamental parameter which is measure of the total radiation integrated over all wavelengths. The effective temperature is estimated from measured angular diameter and the bolometric flux using the basic relation,

$$T_{eff} = \left(\frac{4F_{bol}}{\phi^2\sigma}\right)^{1/4} \tag{6.1}$$

Where F_{bol} is the bolometric flux, which can be estimated from the spectral energy distribution of the observed fluxes. ϕ is uniform disk angular diameter and σ is the Stefan-Boltzmann constant. In this work we have measured resolved angular diameters of 9 late-type giants in the spectral type range K0 - M6. Three stars are unresolved. Bolometric fluxes are estimated from the spectral energy distribution of observed fluxes.

The scale of temperatures of giant stars has been the target of a number of previous studies based on both direct and indirect methods (e.g. Richichi et al. 1999; Blackwell & Lynas-Gray 1998). The indirect method of Blackwell et al. (1998) is based on stellar atmosphere models. The extensive work of Blackwell et al. (1998) studied 420 stars (A0 -K3) with luminosity class between II and V.

The direct methods, for measuring stellar angular diameters, lunar occultations and long baseline interferometry, have established the calibration of effective temperature scale of K-M type stellar sources. Ridgway et al. (1980) first established such a calibration from lunar occultation angular diameter measurements at near-infrared wavelengths of twenty giants in the spectral range K0 -M6. Later, Dyck et al.(1996) measured interferometric angular diameters of 34 stars at 2.2 μm and extended the scale to M7. Perrin et al. (1998) extended it to M8. Again by lunar occultation measurements of 32 giants in the K-band Richichi et al. (1999) extended the scale upto M9. Dyck et al. (1996) estimated the uncertainty in their effective temperature at a given spectral type to be approximately 95 K. Richichi et al. (1999) estimated the errors in the empirical relation in the range 185 to 70 K.

6.2 Observations & Results

All lunar occultations pertaining to this chapter have been been carried out in the broad K-band. The observation log is given in Table 6.1. The source are arranged according to their spectral type. The cross-identifications and source parameters are listed in Table 6.2 and 6.3 respectively. Observations are generally made under good sky conditions with exception of IRC+20128 where the sky was poor. Our derived UD angular diameters by model fit are listed in Table 6.4. Near-Infrared JHK photometry on most of the occulted sources are obtained and are listed in Table 6.5.

Of the 12 sources, 9 sources are resolved and three sources (IRC+20071, IRC+20137

Table 6.1: **Log of Observations**

Star	Spt. Type	Date of observation	Sampling (millisec)	PA (deg.)	v_{comp} (km/s)	Event[a] type	Lunar Phase[b]
IRC+20205	K0 III	12 Apr 2000	2	165	0.527	D	8.1
IRC+20071	K5 III	06 Jan 2001	1	59	0.654	D	12.0
IRC-20516	K5 III	21 May 2000	2	256	-0.541	R	17.7
IRC+20178	M0 III	16 Feb 2000	2	97	0.925	D	11.3
IRC+10245	M1 III	03 May 2001	2	57	0.375	D	10.2
IRC+10245	”	27 Mar 2002	2	87	0.655	D	13.8
IRC+10245	”	14 Apr 2003	2	135	0.763	D	12.8
IRC+10228	M1 III	11 May 2000	2	70	0.439	D	7.4
IRC-20570	M2/3 III	22 May 2000	2	259	-0.545	R	18.7
IRC+10046	M3/4	09 Dec 2000	1	55	0.800	D	13.6
IRC+20137	M5 III	15 Mar 2000	1	83	0.737	D	10.2
IRC+20153	M5 III	10 Apr 2000	1	102	0.761	D	5.9
IRC+20128	M5/6 III	13 Mar 2000	2	105	0.924	D	7.5
IRC-20418	M3pe I	10 May 2001	1	287	-0.574	R	17.3

[a] D : Disappearance ; R: Reappearance; [b]Days after new Moon.

Table 6.2: **Cross-identification for the Sources**

TMSS	SAO	*IRAS*	HD	HR	Other Names
IRC+20205	98087	08418+1820	74442	3461	Del Cnc
IRC+20071	93777	04051+1712	26038	1280	HIP 19284
IRC-20516	187255	-	173460	7046	28 Sgr
IRC+20178	79328	07189+2032	57423	2795	56 Gem
IRC+10245	119035	11432+0648	102212	4517	Nu Vir
IRC+10228	99034	10140+1358	89056	4035	37 Leo
IRC-20570	188355	19344-2204	184921	-	BD-22 5169
IRC+10046	93489	03307+1430	22031	-	V1122 Tau
IRC+20137	-	06101+2039	-	-	NSV 2869
IRC+20153	-	06341+2109	260525	-	AX Gem
IRC+20128	-	05539+2016	-	-	NSV 2736
IRC-20418	-	17593-2328	-	-	Hen 3-1560

Table 6.3: **Source parameters.**

Name	RA(2000) hr min sec	Dec(2000) ^{o} $'$ $''$	Spectral type	V (mag)	K (mag)	HIP para. (mas)
IRC+20205	08 44 41.10	+18 09 15.5	K0 III	3.94	1.52	23.97±0.83
IRC+20071	04 07 59.42	+17 20 23.6	K5 III	5.94	2.32	9.46±1.06
IRC-20516	18 46 20.61	-22 23 31.8	K5 III	5.39	1.50	2.55±1.03
IRC+20178	07 21 56.86	+20 26 37.2	M0 III	5.10	1.29	7.61±0.83
IRC+10245	11 45 51.56	+06 31 45.8	M1 III	4.05	0.08	10.42±0.75
IRC+10228	10 16 40.74	+13 43 42.0	M1 III	5.41	1.29	6.53±0.87
IRC-20570	19 34 27.61	-22 04 00.7	M2/3 III	7.72	2.39	-
IRC+10046	03 33 35.92	+14 40 42.6	M3/4	7.62	2.05	1.14±1.06
IRC+20137	06 13 07.0	+20 38 18	M5 III	7.2	2.71	-
IRC+20153	06 37 06.76	+21 07 03.5	M5 III	9.47	1.69	-
IRC+20128	05 56 55.4	+20 17 17	M5/6 III	6.30	2.14	-
IRC-20418	18 02 23.6	-23 28 35	M3pe I	13	1.89	-

& IRC+10046) are unresolved for which we put an upper limit of angular diameter of 2 mas. The spectral types of the sources are mostly taken from SIMBAD database. Alternative spectral classification is also discussed in the section of the individual source details. Along with our derived angular diameters the predicted and previously measured values are also given in Table 6.4 for comparison. The predicted angular diameter is based on the relation between V=0 zero-magnitude angular size and V-K colour empirically established from available database of angular diameter measurements by van Belle (1999). The empirical expression was established considering 92 angular diameters for 67 carbon stars and Mira variables and 197 angular diameters for 190 giant and supergiants measured by lunar occultation and interferometric observations in the near-IR. These are used here for evolved non-variable giants and supergiants (eqn. 6.2) and variable stars (eqn. 6.3) respectively,

$$\log \phi_{V=0} = (0.669 \pm 0.052) + (0.223 \pm 0.0010) \times (V-K) \quad \text{non-variable stars} \tag{6.2}$$

$$\log \phi_{V=0} = (0.789 \pm 0.119) + (0.218 \pm 0.014) \times (V-K) \quad \text{variable stars} \tag{6.3}$$

The zero magnitude angular sizes are scaled to angular size at source distance by the relation $\phi_{\mathbf{V=0}} = \phi \times \mathbf{10^{V/5}}$. According to van Belle the accuracy of the expressions in the predictions of angular sizes are 12% for giants and supergiants while 26% for variable sources. van Belle (1999) suggested that these relationship valid over a V - K range of 2.0 - 8.0 (non-variable stars) and 5.5 - 13.0 (variable stars).

Table 6.4: **Derived UD angular diameter in the K-band**

Star	Spectral type	ϕ_{UD} (measured) (mas)	ϕ^{a} (pred.) (mas)	Prev. result	Ref.
IRC+20205	K0 III	**2.5±0.5**	2.6	2.45±0.26	5
IRC+20071	K5 III	<2.00	1.9	2.71±0.15	4
IRC-20516	K5 III	**3.2±0.5** *	2.9		6
IRC+20178	M0 III	**3.1±0.3**	3.2	4.4±0.9	2
IRC+10245	M1III	**5.2±0.3**	5.6	5.20±0.16	1
IRC+10245	M1III	**5.7±0.2**	-	-	
IRC+10245	M1III	**5.5±0.3**	-	-	
IRC+10228	M1 III	**3.7±0.5** *	3.2		6
IRC-20570	M2/3 III	**2.8±0.7** *	2.1		6
IRC+10046	M3/4	<2.00 *	2.4		6
IRC+20137	M5	<2.00 *	1.7		6
IRC+20153	M5 III	**3.2±0.2**	3.2	3.02±0.07	4
IRC+20128	M5/6	**4.2±0.7**	2.2	4.13±0.13	3
IRC-20418	M3 peI	**5.5±0.4**	3.5	4.73±0.47	1

*First observations of the source.

[a]The angular diameter are predicted from the empirical relation (angular diameter versus (V - K) colour) of van Belle (1999).

Table Reference : 1. Schmidtke et al. (1986); 2. Beavers et al (1981); 3. Richichi et al. (2001); 4. Richichi et al. (1998a); 5. Ridgway et al. (1982); 6. This work.

6.2.1 Bolometric Flux and Effective Temperature

Bolometric fluxes are usually obtained by a bolometric correction to the measured V magnitude. However, such estimations for late-type stars have failed because of large corrections due to their blanketing atmospheres. To calculate bolometric fluxes of these sources, the approach taken is by integrating of the spectral energy distribution in the optical to far-infrared region. These sources radiate predominately in the near-IR wavelengths. Photometry in this spectral region where the flux distribution peaks, gives the most effective estimate of bolometric flux. Photometric points in the infrared regions are usually fitted well by a single temperature Planck blackbody . In some cases (like IRC+20128 and IRC-

Table 6.5: **JHK magnitudes from our observations**

Star	Date	J	H	K
IRC+20205	24 Nov 2000	2.00±0.03	1.50±0.03	1.39 ±0.04
IRC+20178	23 Nov 2000	2.23 ±0.03	1.46±0.02	1.29±0.03
IRC+10245	22 Feb 2002	0.97±0.05	0.26±0.05	-0.26±0.05
IRC+10228	24 Nov 2000	2.29 ±0.03	1.49±0.03	1.21±0.03
IRC-20570	03 May 2001	3.49±0.09	2.36±0.06	2.12±0.06
IRC+20137	24 Nov 2000	3.67±0.03	3.14±0.04	2.71±0.03
IRC+20153	11 Dec 2000	2.93±0.02	1.95±0.03	1.67±0.02
IRC+20128	23 Nov 2000	3.38±0.02	2.44±0.02	2.00 ±0.03

20418 in Fig. 6.5 and Fig. 6.11) at certain wavelengths (i.e. mainly 10 μm and long-ward wavelengths.) the measured value deviates from single temperature fit. This is mainly due to re-emission of dust and molecules from absorbed photospheric radiation and appears as an infrared excess. Such excesses are fitted with additional cooler temperature blackbody component.

We have carried out JHK photometry of the most of the occulted sources. The JHK magnitudes of our observations are listed in Table 6.6. In few cases we do not have JHK values and have taken them from literature. To complete the flux distribution curve we have taken other wavelength region data (i.e. mainly optical and far infrared data) from published sources. Such measurements in the infrared are compiled in the catalog of infrared (Gezari et al. 1999). Recent all sky released data from 2MASS was also useful to get JHK_s measurements (Cutri et al. 2003).

Table 6.6: **Bolometric flux and Effective temperatures**

Star	Spectral type	Ang. Dia (UD) (mas)	Bol. flux $\times 10^{-8}$ erg cm^2 sec^{-1}	T$_{eff}$ (K)
IRC+20205	K0 III	2.5±0.5	101±20	4690±520
IRC-20516	K5 III	3.2±0.5	70±10	3820±330
IRC+20178	M0 III	3.1±0.3	69±8	3830±220
IRC+10245	M1 III	5.5±0.3	214±40	3835±200
IRC+10228	M1 III	3.7±0.5	95±10	3790±270
IRC-20570	M2/3 III	2.8±0.7	24±5	3100±420
IRC+20153	M5 III	3.2±0.2	39±3	3240±120
IRC+20128	M5/6	4.2±0.7	24±4	2530±240
IRC-20418	M2-5 Ipe	5.5±0.4	71±10	2900±150

6.2.2 Individual Source details

Resolved Sources

IRC+20205

This disappearence event is recorded in the K-band. The spectral type is K0 III (SIMBAD database) and the *Hipparcos* measured distance to the source is 41pc (Perryman et al. 1997). The observed light curve is noisy because of scintillation. The UD model is fitted to the observed trace with five parameters. Model fit is shown in Fig. 6.1. We derive UD angular diameter of 2.5±0.5 mas. Previous reported UD value is 2.45±0.26 mas by LO in near-IR (Ridgway et al. 1982). We estimate the bolometric flux to be 101±20 $\times 10^{-8}$ erg cm^2 sec^{-1} using blackbody model of photometric data (Fig. 6.1). We derive an effective temperature of 4690±520 K.

IRC-20516

The reappearance of IRC-20516 has been recorded in the K-band. The source is classified as K5 III (SIMBAD database). The *Hipparcos* distance to the source is 392±158 pc (Perryman et al. 1997). We report the first HAR observation of this sources. The observed light curve fitted with UD model using 5 parameters is shown in Fig. 6.2. We derive the UD angular diameter of 3.2±0.5 mas. We estimate the bolometric flux of the source to be 70±10 $\times$ 10^{-8} erg cm^2 sec^{-1} (Fig. 6.2) and the effective temperature to be 3820±330 K.

IRC+20178

The lunar occultation of IRC+20178 (56 Gem) occurred on 16 Feb 2000 and was obtained in the K-band. The event was a disappearance. The spectral type of the source is M0 III (SIMBAD database). The observed light curve is fitted with UD model using 5 parameters and a 5th order polynomial is used to fit varying background. The model fit curve is shown in Fig. 6.3. Three fringes are well recorded in the light curve. We derive the UD value of 3.1±0.5 mas. Previous reported fully limb darkened angular diameter is 4.4±0.9 mas by LO at 0.57 μm (Beavers et al. 1981). We measure JHK magnitudes of the source listed in Table 6.5. We estimate the bolometric flux of the source to be 69±8 $\times$ 10^{-8} erg cm^2 sec^{-1} by fitting the blackbody function to observed fluxes available in the literature and our measured JHK values (Fig. 6.3). We derive the effective temperature of the source of 3830±220 K.

IRC+10245

The spectral type of the source is M1 III (Keenan et al. 1989). The lunar occultations (LO) of Nu Vir were observed thrice in K-band on 03 May 2001, 27 Mar 2002 and 14 Apr 2003. On 27 Mar 2002 simultaneous K and L$'$ light curves are observed. But L$'$ data is noisy and is not included in the present analysis. The observed light curves fitted with five parameters UD model are shown in Fig. 6.4 and Fig. 6.5. We derive the UD values of 5.2±0.3, 5.70±0.2 and 5.5±0.3 mas for respective date of light curves. The direction of lunar occultation on the source for three observations varies from position angle 57^o to 135^o (Table 6.1) shown by schematic diagram in Fig. 6.6. The observations can be used for studying asymmetric nature, if any, of the source. However our observations clearly rule out any large spatial asymmetry in the source, unlike what was deduced for U Ori (chapter 4). The angular diameter of the source had been measured several times previously in the optical-infrared wavelengths by LO. The reported LO angular diameters are in the range 5.60 - 5.24 mas (White & Feierman 1987). We estimate the bolometric flux of 214$\pm$40 $\times$ 10^{-8} erg cm^2 sec^{-1} from the blackbody function fit to photometric data in the range from visible to far infrared wavelengths. Stellar effective temperature has been derived to be 3835$\pm$200 K (Table 6.6.)

IRC+10228

The disappearence of IRC+10228 is recorded in the K-band. The source is classified as M1 III (SIMBAD database). Alternative spectral classification is M0 III (Buscumbe 1999). The *Hipparcos* distance to the source is 153$\pm$20 pc (Perryman et al. 1997). The observed light curve is noisy. The UD model is fitted to the observed trace with five parameters and 5th order polynomial is needed to fit varying background. The model fit is shown in Fig. 6.7. No angular diameter measurements exist for the source. We report a UD value of 3.7$\pm$0.5 mas. We estimate the bolometric flux of 95$\pm$10 $\times$ 10^{-8} erg cm^2 sec^{-1} from blackbody fit to the observed fluxes (Fig. 6.7) and the effective temperature of 3790$\pm$270 K.

IRC-20570

The reappearance of IRC-20570 is recorded in K-band. The source is classified as M2/3 III (SIMBAD database). We report the first HAR observation of this sources. The observed trace is noisy. The observed light curve is fitted with UD model using 5 parameters and a 5th order polynomial is needed to fit varying background which is shown in Fig. 6.8. It is barely resolved. We derive the UD value of 2.8$\pm$0.7 mas. We estimate the bolometric flux of the source to be 24$\pm$5 $\times$ 10^{-8} erg cm^2 sec^{-1} using a blackbody to fit observed fluxes (Fig. 6.8). The effective temperature is derived to be 3100$\pm$420 K.

IRC+20153

The disappearance LO event of the source was observed on 10 April 2000 in the K-band. The source is a pulsation variable giant with spectral type of M5 III (Kukarkin et al. 1971) but there is no estimation of its period of variability. The observed light curve is fitted with five parameters which is shown in Fig. 6.9. Four fringes are recorded well in the trace. We derive the UD value of 3.2$\pm$0.2 mas. Previous reported UD value is 3.02$\pm$0.07 mas by LO in the K-band (Richichi et al. 1999). We estimate the effective temperature to be 3235$\pm$120 K adopting a value for bolometric flux of 39$\pm$2 $\times$ 10^{-8} erg cm^2 sec^{-1} (Richichi et al. 1999).

Our derived temperature is good agreement with the value of 3320$\pm$73 derived by Richichi et al. (1999). These authors have used the limb- darkened diameter of 3.09$\pm$0.007. The scaling factor used to convert LD to UD diameter was 1.02 and this factor for K-band is derived based on non-variable M giant model atmosphere of Hofmann & Scholz (1998a).

IRC+20128

The disappearance LO event of IRC+20128 was obtained on 13 Mar 2000 in the K-band. The over all light curve is effected by scintillation noise. The observed light curve are fitted with UD model of 5 parameters which is shown in Fig. 6.10. Additional 2nd order polynomial is used to fit varying background in the model. However, the fit is not completely satisfactory because of noise. We derive the UD value of 4.2 $\pm$0.7 mas. Previously reported angular diameter by LO in K-band is 4.13$\pm$0.11 (Richichi et al. 2001). We obtain JHK photometry of the source (Table 6.5).

The spectral type of IRC+20128 is assigned as M6/7 on the basis of $IRAS$ LRS spectra (Kwok et al. 1997). Search for OH and Si0 maser emission yielded no detection (Chengalur et al. 1983, Jiang et al. 1996). A two-temperature blackbody fit to photometric data (Gezari et al. 1999; our JHK flux; IRAS 12, 25, 60 μm fluxes of point source catalog (PSC)) yielded a value of bolometric flux of 24$\pm$4 $\times$ 10^{-8} erg cm^2 sec^{-1}. From this we derive the effective temperature of 2530$\pm$240 K. The estimated temperature is quite low in comparison to its spectral classification. However, we find the spectral type of the source is consistent with our observed color (J-K) (Koornneef 1983).

IRC-20418

This reappearance event was observed on 10 May 2001 in the K-band. The observed light curve is fitted with a UD model using 5 parameters and a 4th order polynomial is needed to fit varying background. The light curve and fit is shown in Fig. 6.11. We derive the UD angular diameter of 5.5$\pm$0.4 mas. Previous reported UD value is 4.73$\pm$0.47 mas by LO in the near-IR narrowband filter ($\lambda/\Delta\lambda$ = 2.17/0.03 μm) (Schmidtke et al.1986).

IRC-20418 was first discovered as an infra-red source by Neugebauer & Leighton (1969) during two-micron sky survey. This source is listed as a Hα emission line star in the survey of Sanduleak & Stephenson (1973). Sanduleak et al. (1973) surveyed 179 stars which are mostly located in the direction of Galactic center. This source also lies in the direction of Galactic center. Hansen & Blanco (1973) found that this star had a peculiar emission at

8600 A^o and classified it as a M supergiant. However observations by Grasdalen & Sneden (1979) did not see any emission line at 8600 A^o. Grasdalen et al.(1979) and Lockwood (1985) classified it, respectively, as a M3pe and M5. Recently Pereira et al.(2003) classified it as a M2-3 supergiant using TiO band-index from optical spectra. Optical spectra also confirmed that the source is highly reddened star because the continuum below 6000 A^o is highly extinguished. We adopt here the spectral type of M3 I.

We estimated the distance to the source using the empirical relation for supergiants between absolute magnitude (M_{12}) of 12 μm flux and [12] -[25] of *IRAS* PSC measurements (Hickman et al. 1995). The distance is estimated to be 0.69 kpc with an uncertainty of 15%.

From DENIS observations the JK_s magnitudes are 3.997$\pm$0.005 and 1.675$\pm$0.025 respectively (Kimeswenger et al. 2004). Considering the spectral type of M3 I, we find the intrinsic colour (J-K) to be 1.20 mag (Koornneef 1983). The observed colour (J-K_s) being 2.322$\pm$0.025 mag, one can estimate colour excess E(J-K_s) to be 1.122$\pm$0.025 mag. To estimate extinction A_{k_s}, we use the relation A_{k_s} = 0.67 E(J-K_s) established by Dutra et al. (2003) for sources in 2MASS data within 10^o of Galactic center. Further using the relation A_k = 0.95 A_{k_s} (Dutra et al. 2003) we find the extinction in K-band is to be A_k = 0.71$\pm$0.02 mag. The visual extinction, A_v, is estimated to be 6.37$\pm$0.14 mag using the relation A_k = 0.112 A_v (Rieke & Lebofsky 1985). IRC-20418 is situated behind a obscured cloud having excess E(B-V) $\approx$ 2.0 (Lundstrom & Stenholm 1984) and shows a total line-of-sight extinction of $A_v \approx$ 6.5 mag (Williams et al. 1987; Pendleton et al. 1994). Our derived extinction towards IRC-20418 is close to those values which is result of foreground extinction towards the source.

Photometric data available in the literature (Gezari et al. 1999,JK_s of DENIS, JHK_s of 2MASS & *IRAS* PSC flux at 12, 25 & 60 μm) are dereddened considering the visual extinction A_v=6.3 mag. The wavelength dependent extinction relation is taken from Rieke & Lebofsky (1985). The dereddened fluxes are fitted with blackbody function with temperature 2800 K and the blackbody flux is normalized with observed K-band flux. To better fit far infrared points we have used another cooler temperature blackbody function of 500 K (in Fig. 6.11). We estimate the bolometric flux of the source to be 71$\pm$10 $\times$ 10^{-8} erg cm^2 sec^{-1}. We derive an effective temperature of 2900$\pm$150 K.

Unresolved Sources

IRC+20071

The disappearence of IRC+20071 has been recorded in the K-band. The spectral type of the source is K5 III (SIMBAD database). The trace is good quality which have recorded well upto fifth fringes. The UD model is fitted with five parameters and a 5th order polynomial is used to fit varying background. The fit is shown in Fig. 6.12. The source is *unresolved* in our analysis, evidenced by the convergence χ^2 of the fit (inset of Fig. 6.12). For resolved sources, the model converges towards an angular diameter which gives a minimum χ^2 value. For unresolved sources χ^2 remains flat upto the resolution limit then increases monotonically with diameter. Fig.6.12 shows model best-fit light curve with observed data points. We put an upper limit of a uniform disk (UD) angular diameter to be $\sim$2 mas.

Previous reported value of angular diameter is 2.71$\pm$0.15 mas by LO in K (Richichi et al. 1998a). IRC+20071 has been reported to be LO binary with separation of 50 mas (Dunham 1977). However no positive detection has emerged of binarity from speckle interferometric observations with an angular resolution of 30 mas in the optical and previous LO in the K-band (Hartkopf & McAlister 1984; Richichi et al. 1998a). There is also no evidence for a binary in our light curve.

IRC+20137

The lunar occultation of IRC+20137 (NSV 2869) was obtained first-time in the K-band on 15 Mar 2000. The angular diameter of the source has not been reported earlier in the literature. The spectral type of the source is M5 III (Kwok et al 1997). Being a variable the visual magnitudes (V) of the source are in the range 6.88 - 7.62 mag (NSV catalogue: Kukarkin et al. 1981). The reported K-band magnitude (K) is 2.71 mag (Neugebauer et al. 1969). We estimate the angular diameter of the source is in the range 1.6 - 1.8 mas using eqn.(6.3) of van Belle (1999).

The source is *unresolved* in our analysis of UD model fit, evidenced by the convergence parameter χ^2 of the fit (shown inset of Fig.6.13). Fig. 6.13 shows model best-fit light curve with observed data points. We put an upper limit to the uniform disk (UD) angular diameter of $\sim$2 mas.

IRC+10046

The source is classified as M3/4 from LRS spectra of *IRAS* (Kwok et al. 1997) and no luminosity class is specified. Alternative spectral classification of the source as M1 III exist in the Tycho spectral catalog (Wright et al. 2003). The predicted angular diameter is 2.43 mas using eqn.(6.2) of van Belle (1999). However in our analysis the source is *unresolved* which is clear from convergence parameter of fit shown in Fig. 6.13. We put an upper limit of the angular diameter of 2.0 mas.

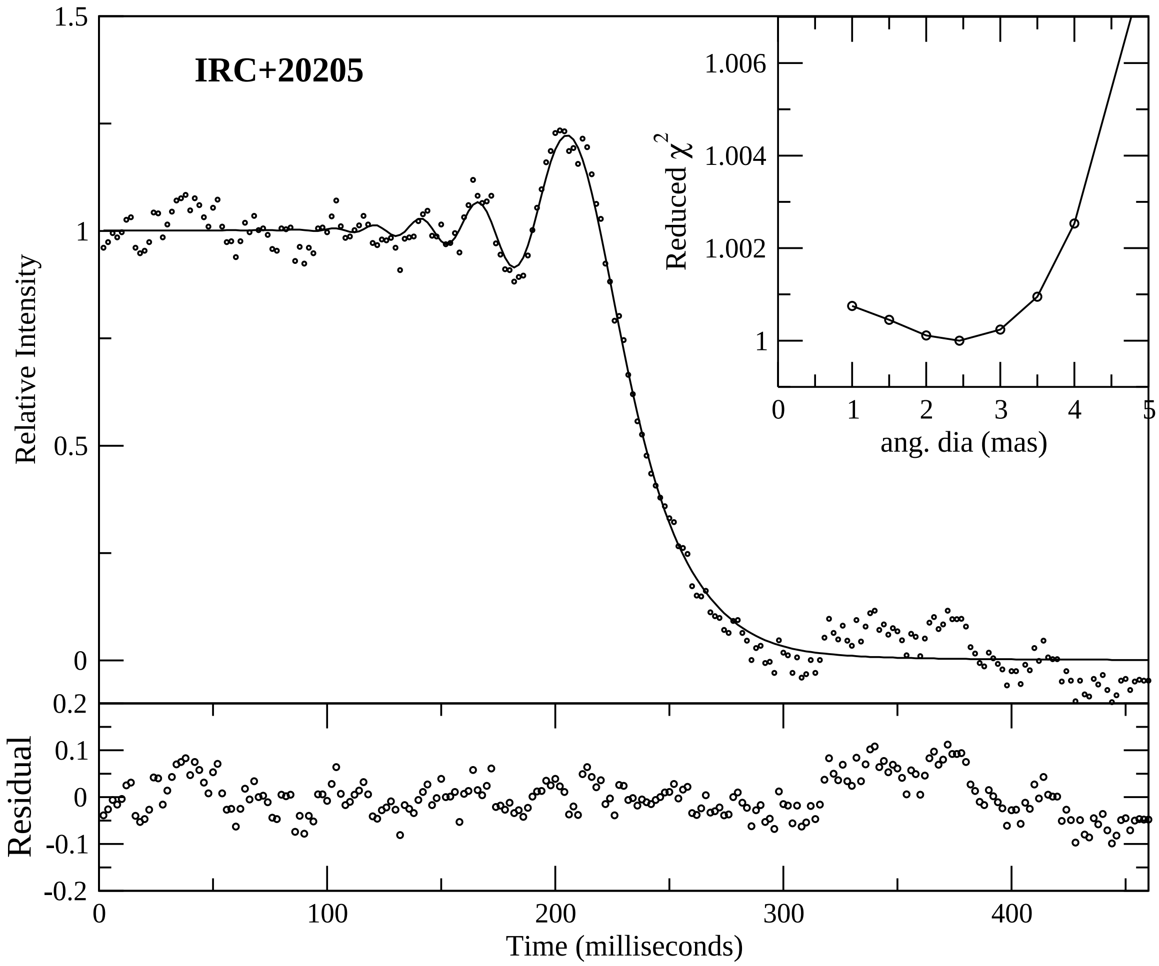

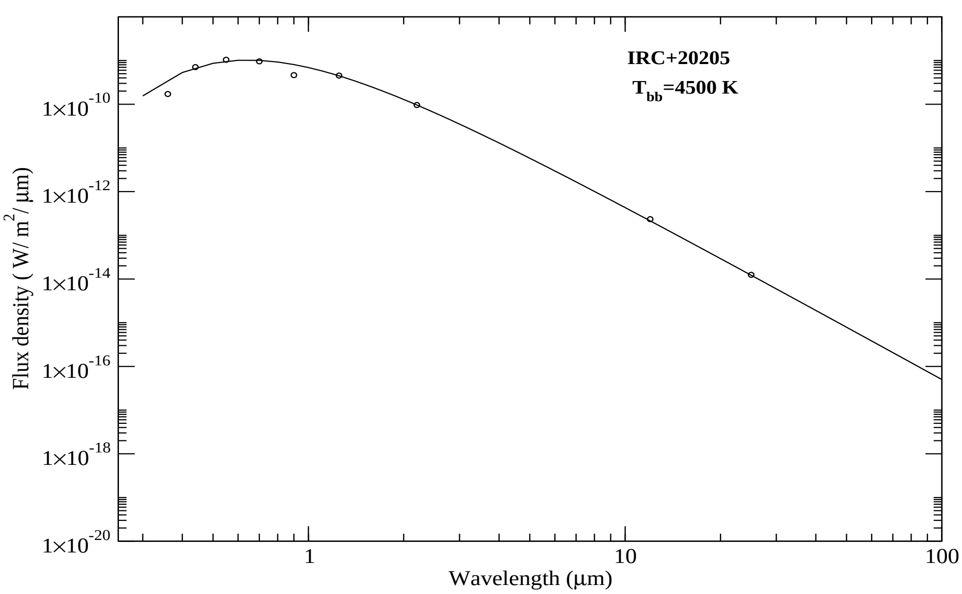

Figure 6.1: *The observed data (dots) are fitted with UD model fit for IRC+20205 (upper graph). In the upper graph the inset shows convergence of fit. Residuals (data-model) are shown in the lower panel. In the lower graph broadband fluxes available in literature and our JHK values are shown along with the blackbody fit.*

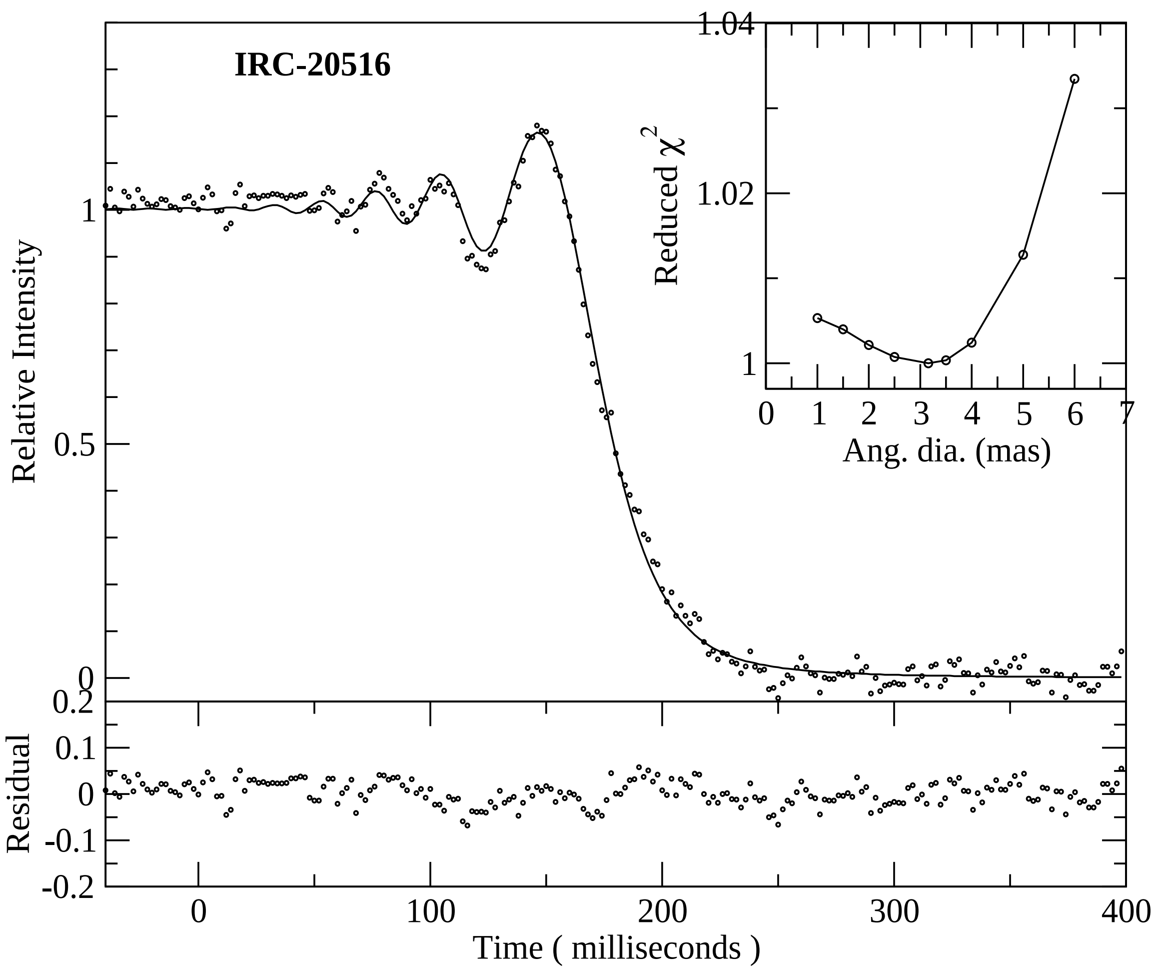

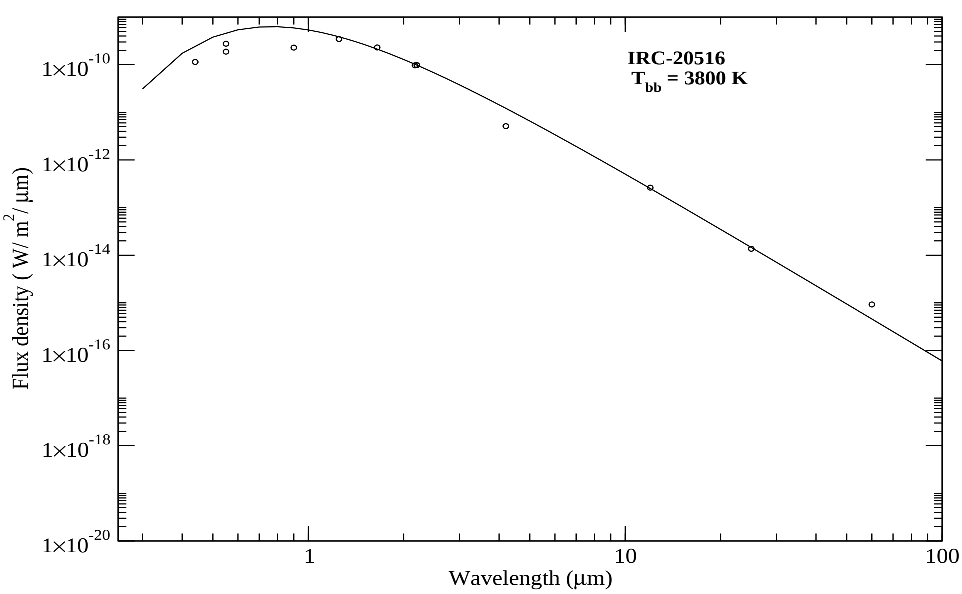

Figure 6.2: *The observed data (dots) are fitted with UD model fit for IRC-20516 (upper graph). In the upper graph the inset shows convergence of fit. Residuals (data-model) are shown in the lower panel. In the lower graph broadband fluxes available in literature are shown along with the blackbody fit.*

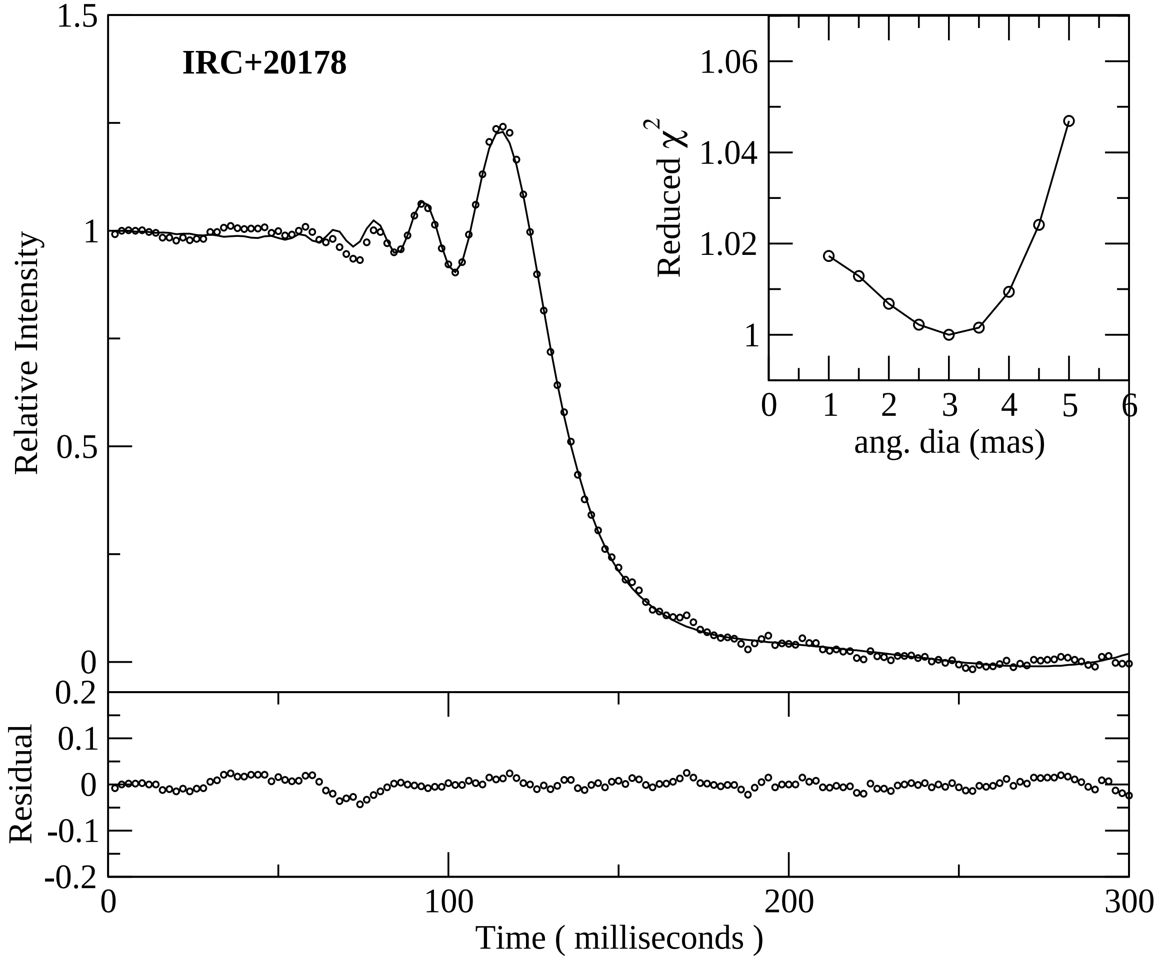

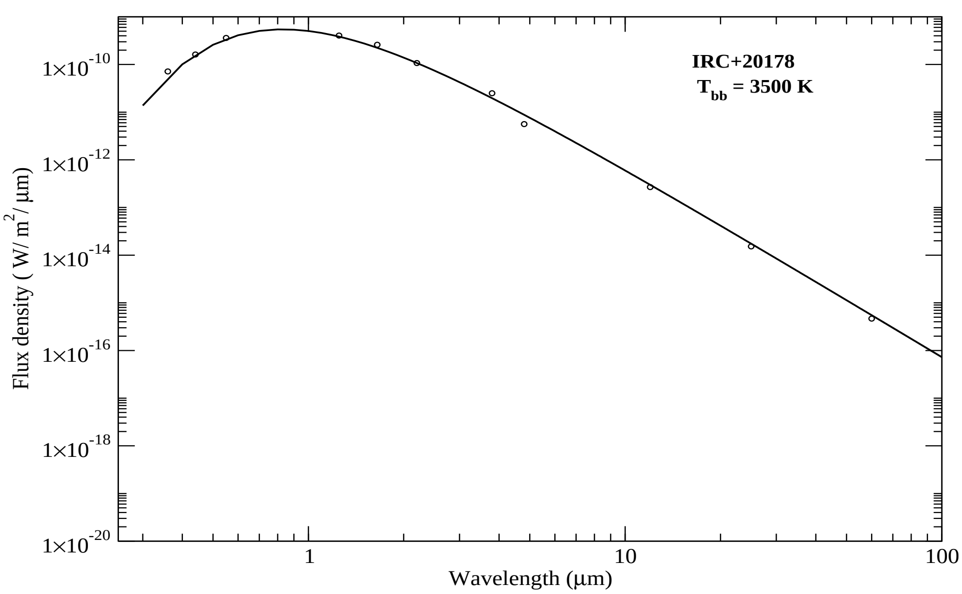

Figure 6.3: *The observed data (dots) are fitted with UD model fit for IRC+20178 (upper graph). In the upper graph the inset shows convergence of fit. Residuals (data-model) are shown in the lower panel. In the lower graph broadband fluxes available in literature and our JHK values are shown along with the blackbody fit.*

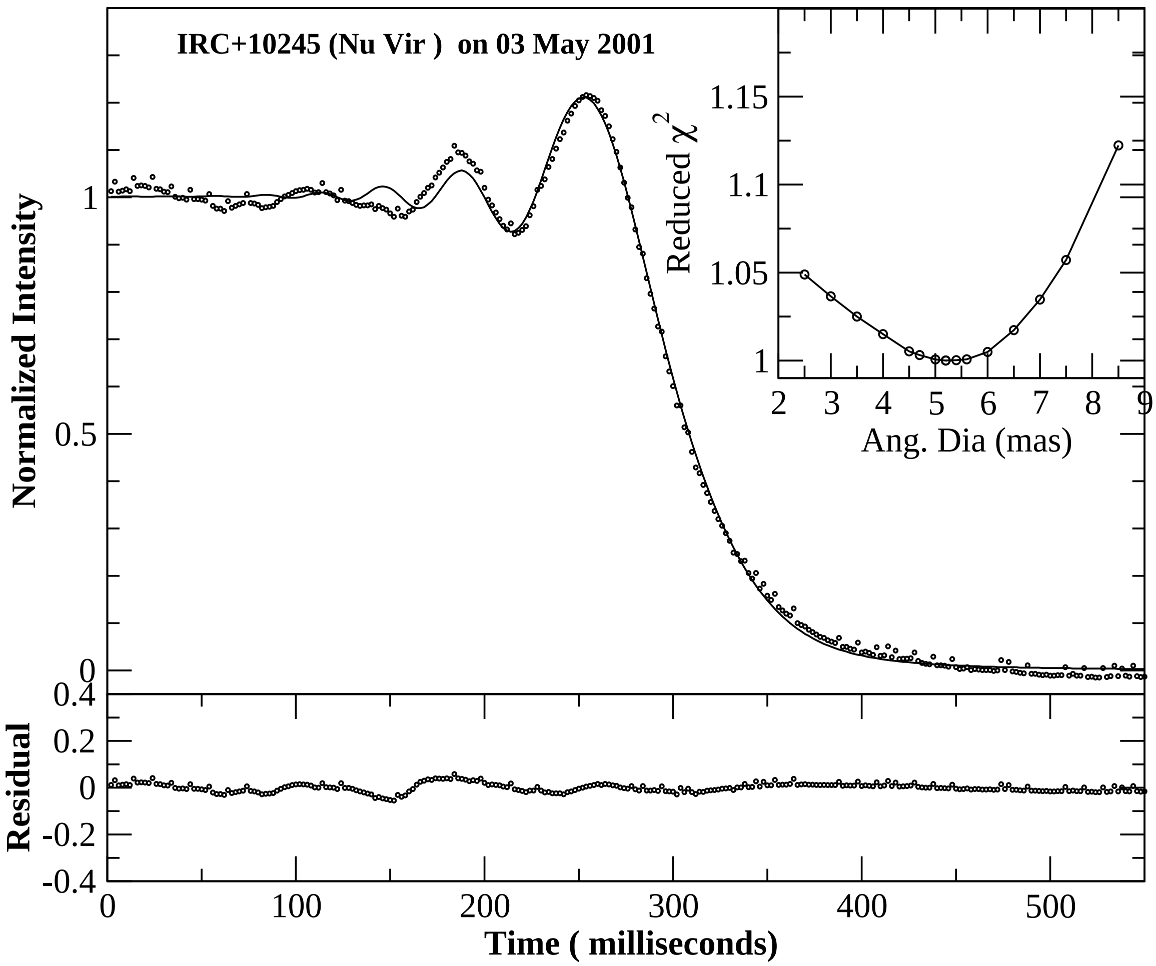

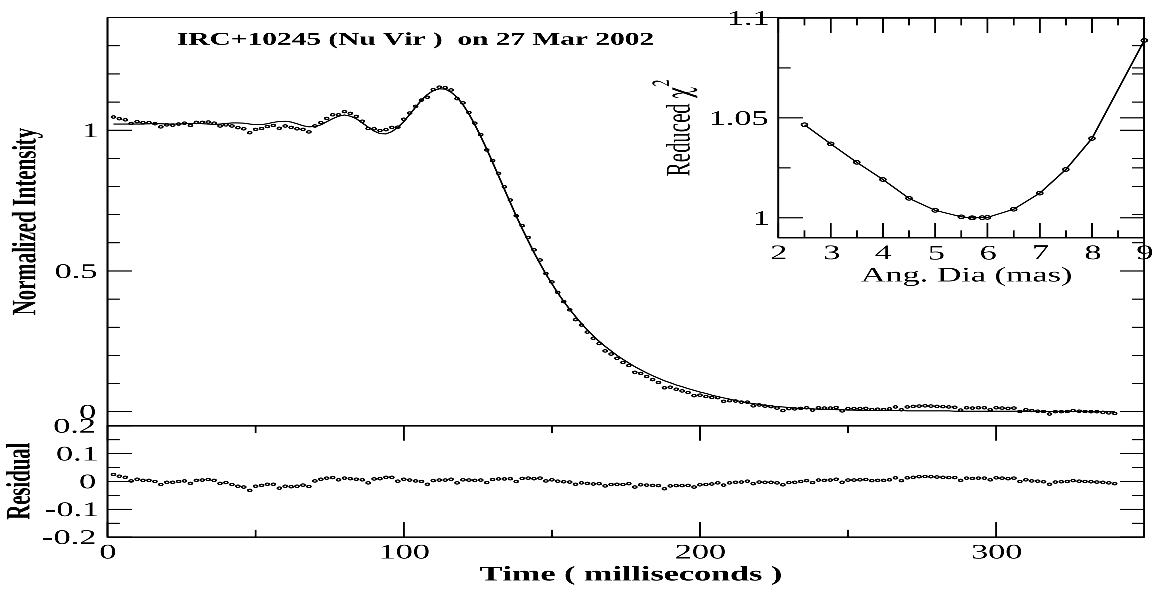

Figure 6.4: *The observed data (dots) are fitted with UD model fit for IRC+10245 (Nu Vir) observed on different dates mentioned in the graph. Insets of the graph shows convergence of fit. Residuals (data-model) are shown in the lower panel.*

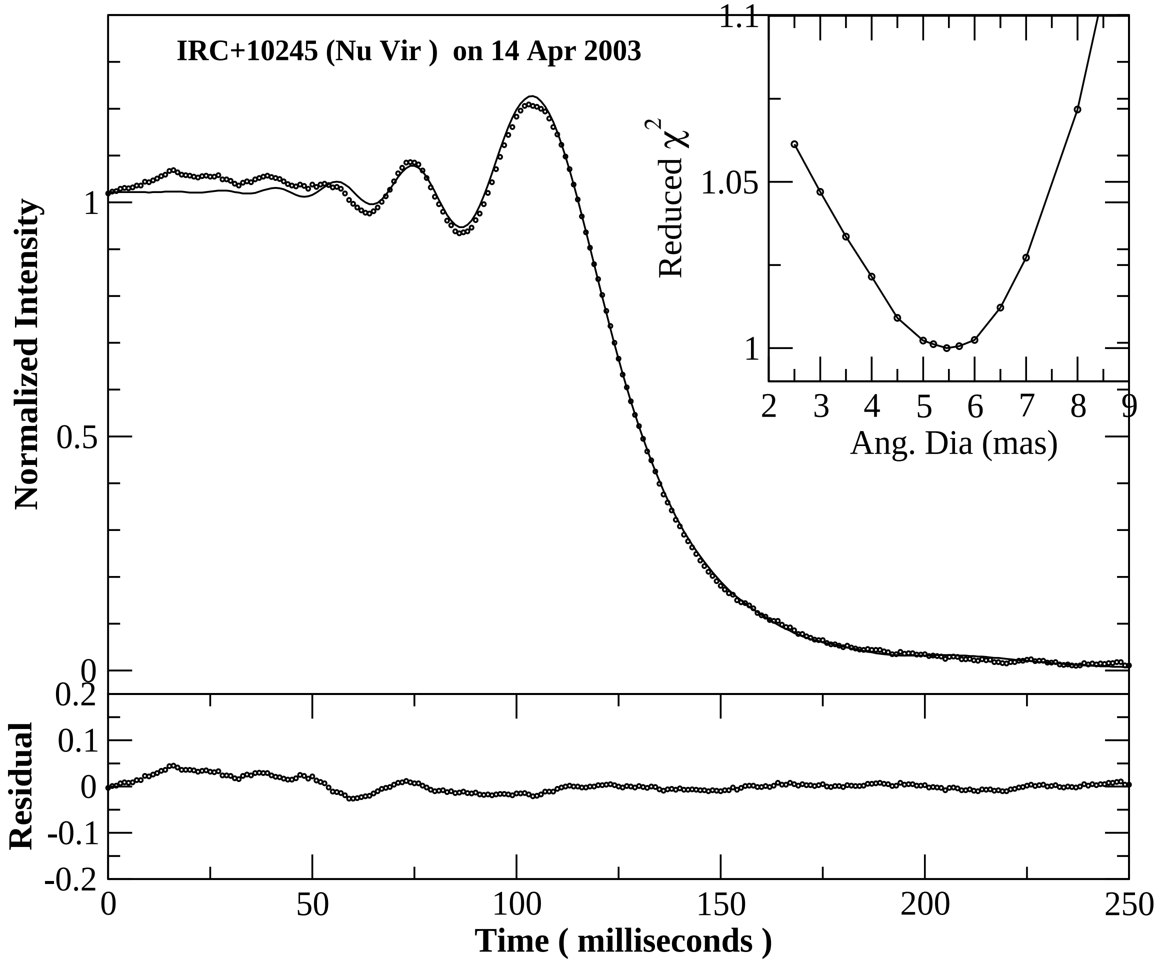

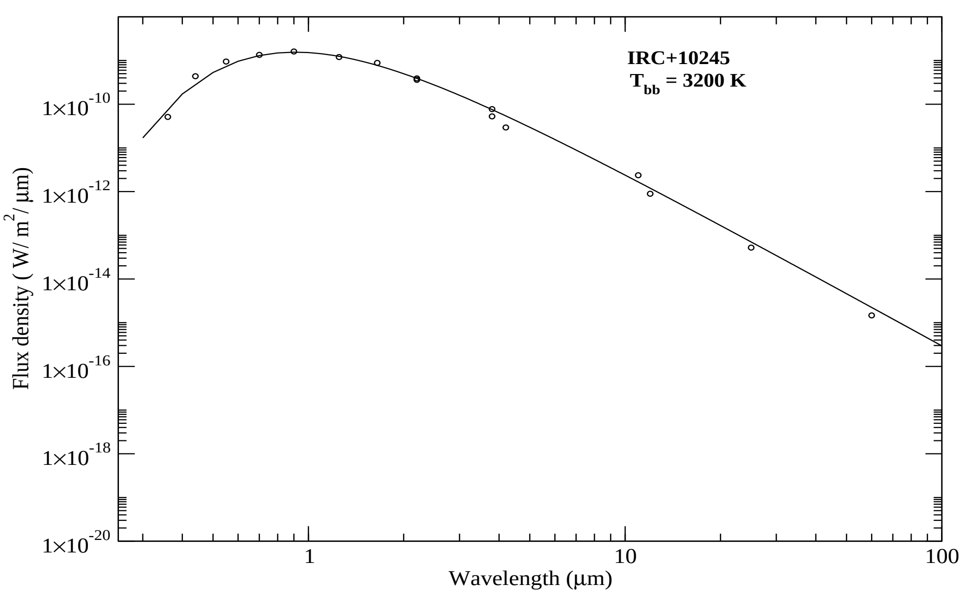

Figure 6.5: *The observed data (dots) are fitted with UD model fit for IRC+10245 (Nu Vir) observed on 14 Apr 2003 (upper graph). In the upper graph the inset shows convergence of fit. Residuals (data-model) are shown in the lower panel. In the lower graph broadband fluxes available in literature and our JHK values are shown along with the blackbody fit.*

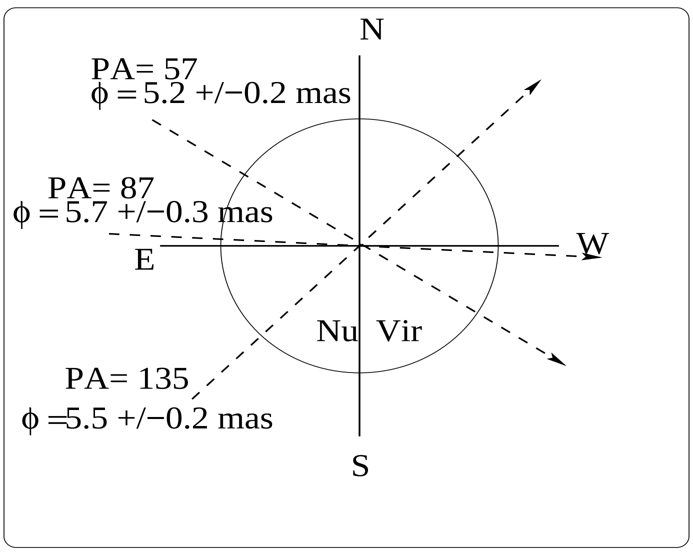

Figure 6.6: *The direction of lunar occultation for three observations of Nu Vir (IRC+10245) are shown. Position angles and derived angular diameters are also mentioned.*

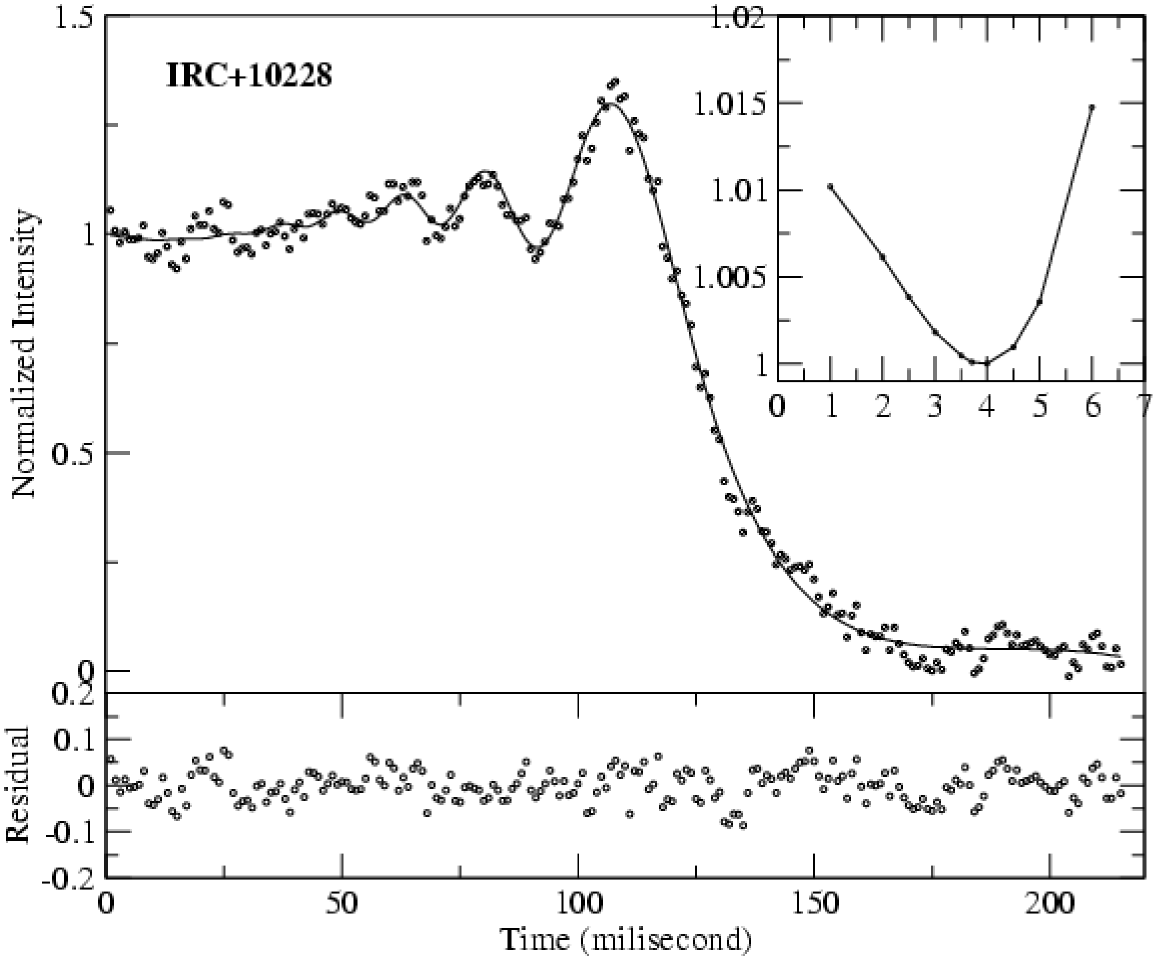

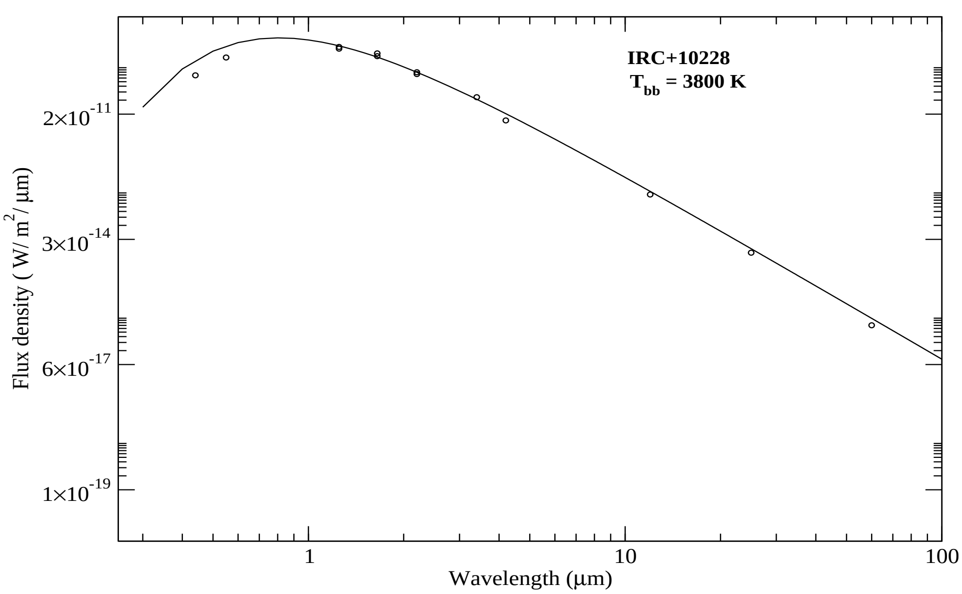

Figure 6.7: *The observed data (dots) are fitted with UD model fit for IRC+10228 (upper graph). In the upper graph the inset shows convergence of fit. Residuals (data-model) are shown in the lower panel. In the lower graph broadband fluxes available in literature and our JHK values are shown along with the blackbody fit.*

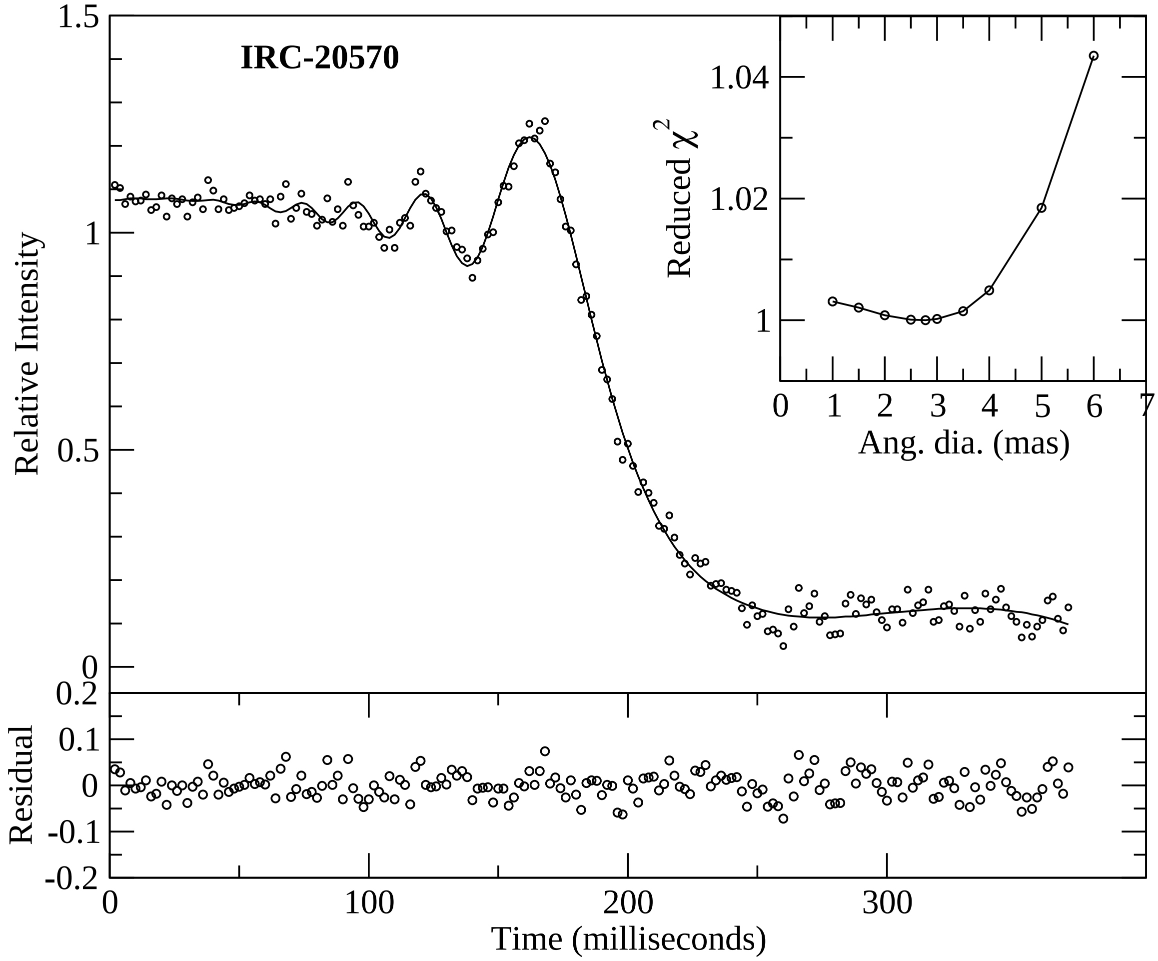

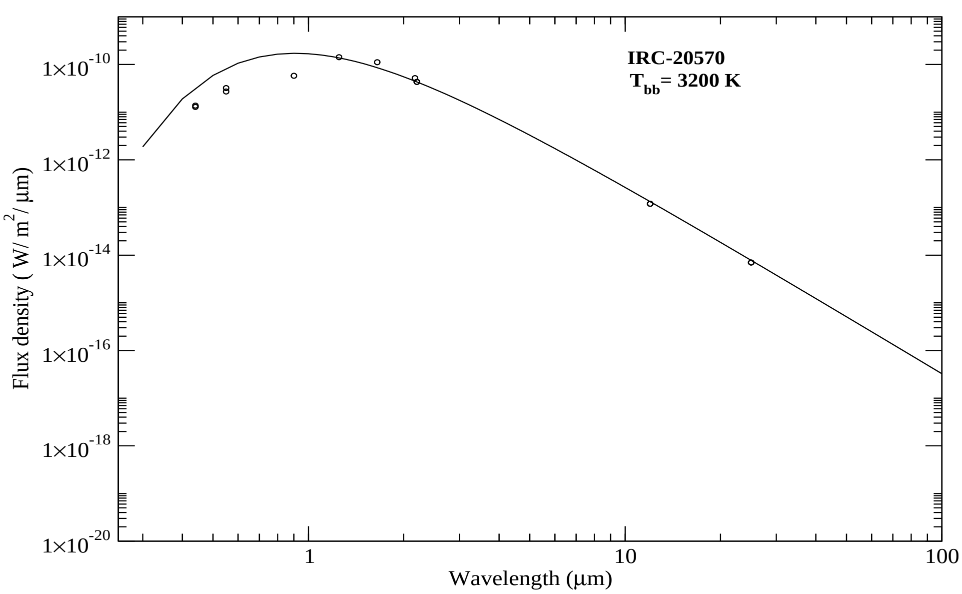

Figure 6.8: *The observed data (dots) are fitted with UD model fit for IRC-20570 (upper graph).In the upper graph the inset shows convergence of fit. Residuals (data-model) are shown in the lower panel. In the lower graph broadband fluxes available in literature and our JHK values are shown along with the blackbody fit.*

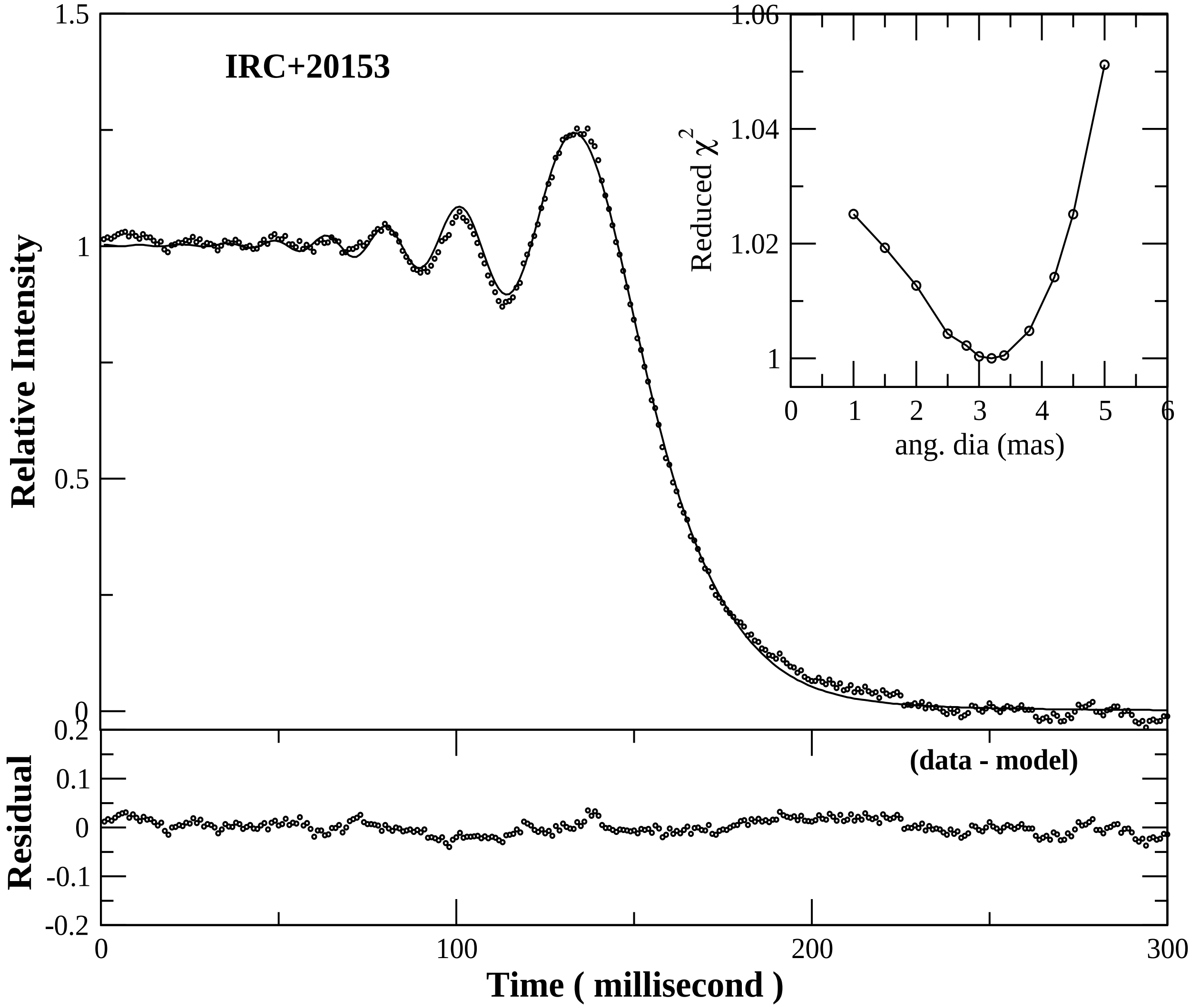

Figure 6.9: *The observed data (dots) are fitted with UD model fit for IRC+20153. The inset graph shows convergence of fit. Residuals of the fit is shown in the lower panel.*

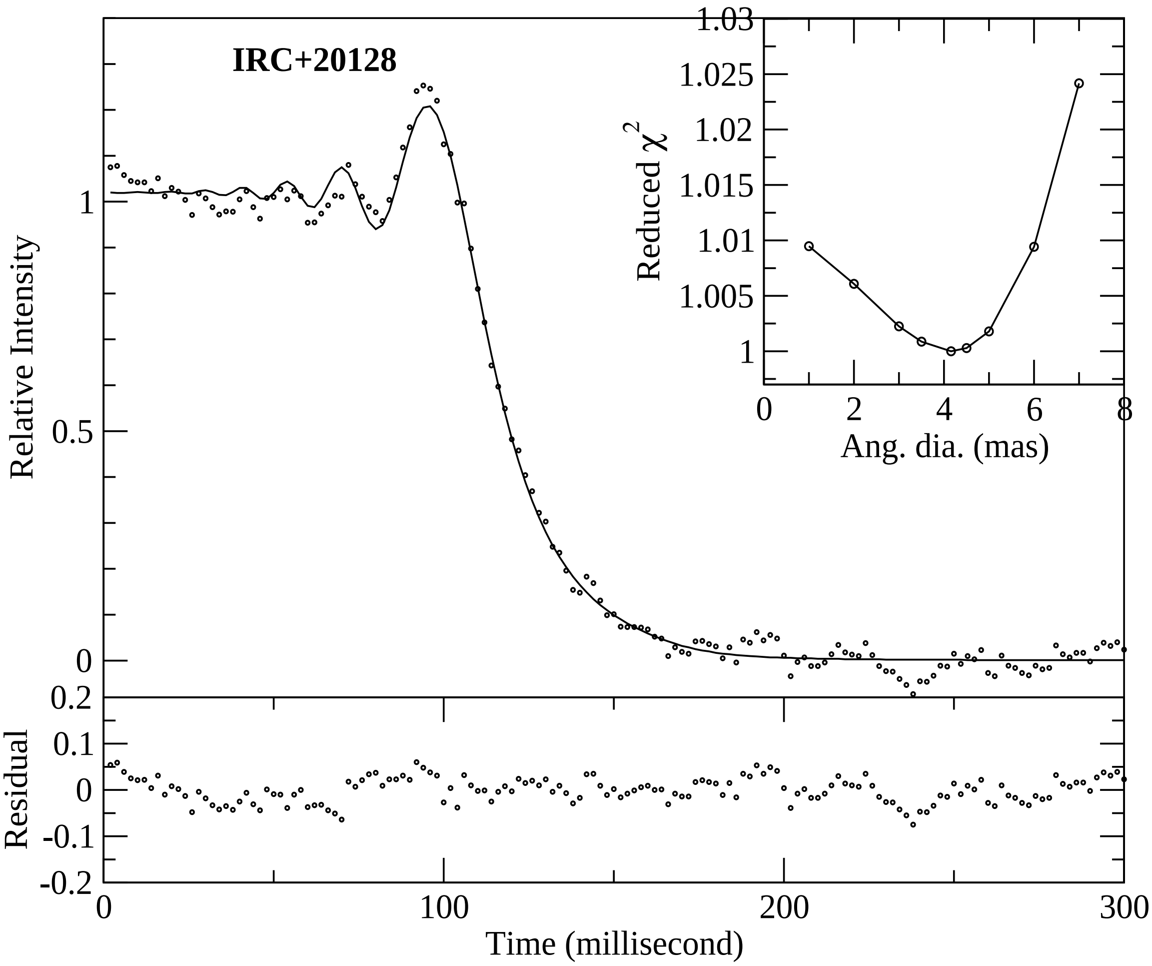

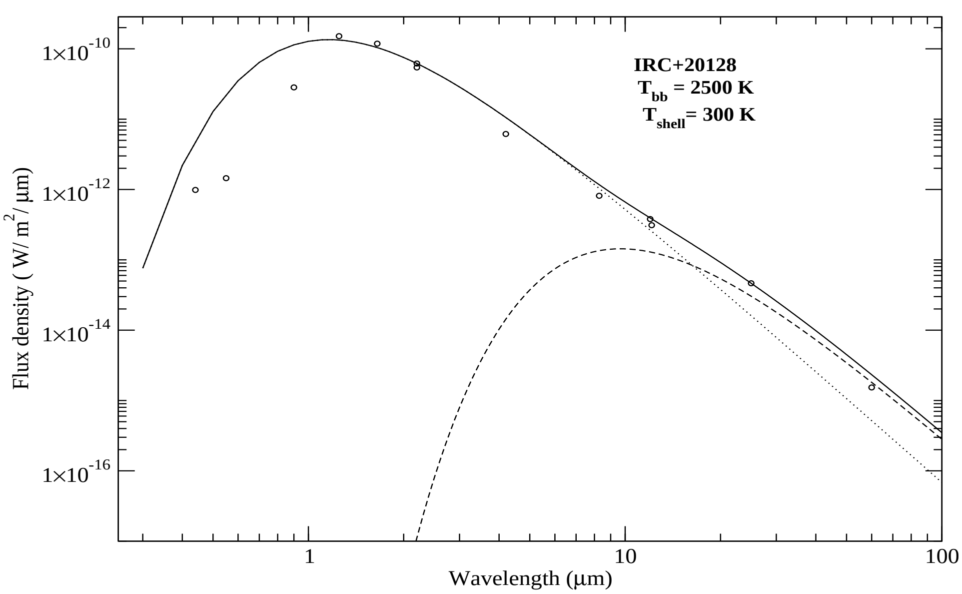

Figure 6.10: *The observed data (dots) are fitted with UD model fit for IRC+20128 (upper graph). In the upper graph the inset shows convergence of fit. Residuals (data-model) are shown in the lower panel. In the lower graph broadband fluxes available in literature and our JHK values are shown along with the blackbody fit.*

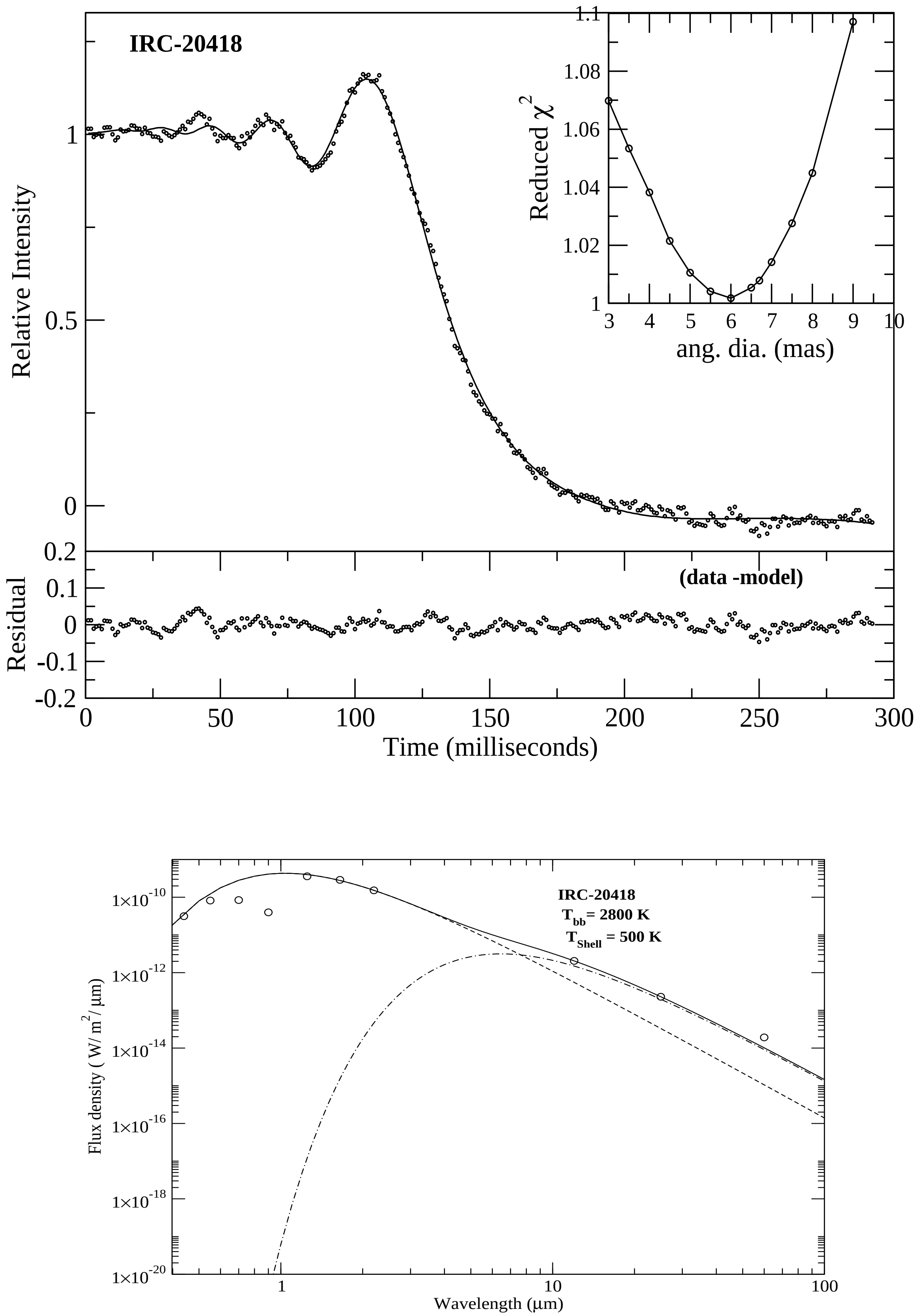

Figure 6.11: *The observed data (dots) are fitted with UD model fit for IRC-20418 (upper graph). In the upper graph the inset shows convergence of fit. Residuals (data-model) are shown in the lower panel. In the lower graph broadband fluxes available in literature are shown along with the blackbody fit.*

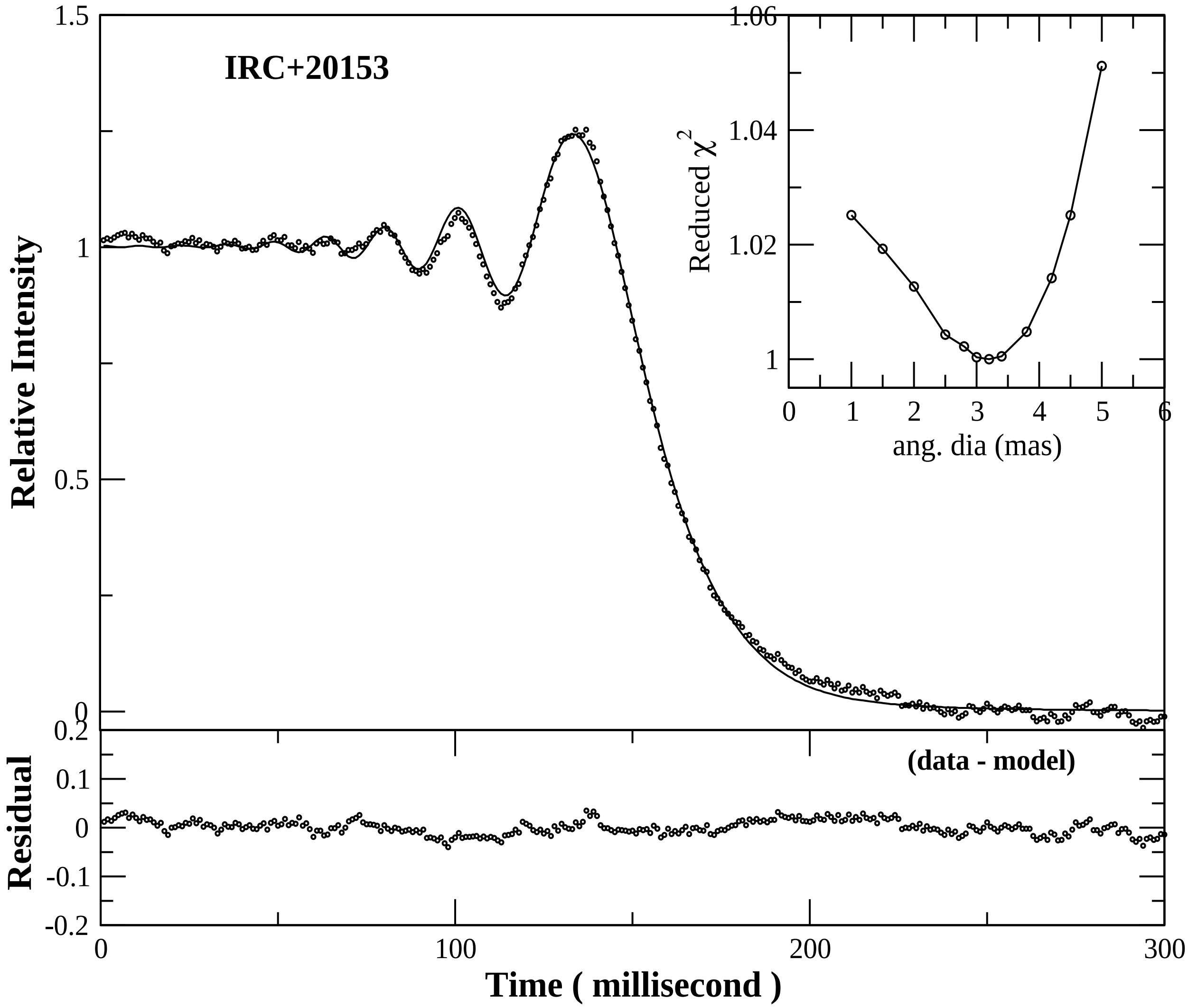

Figure 6.12: *The observed data (dots) are fitted with UD model fit for IRC+20153 (Upper graph) and IRC+20071 (Lower graph).The inset of the graphs shows convergence of fit. Residuals (data-model) are shown in the lower panel.*

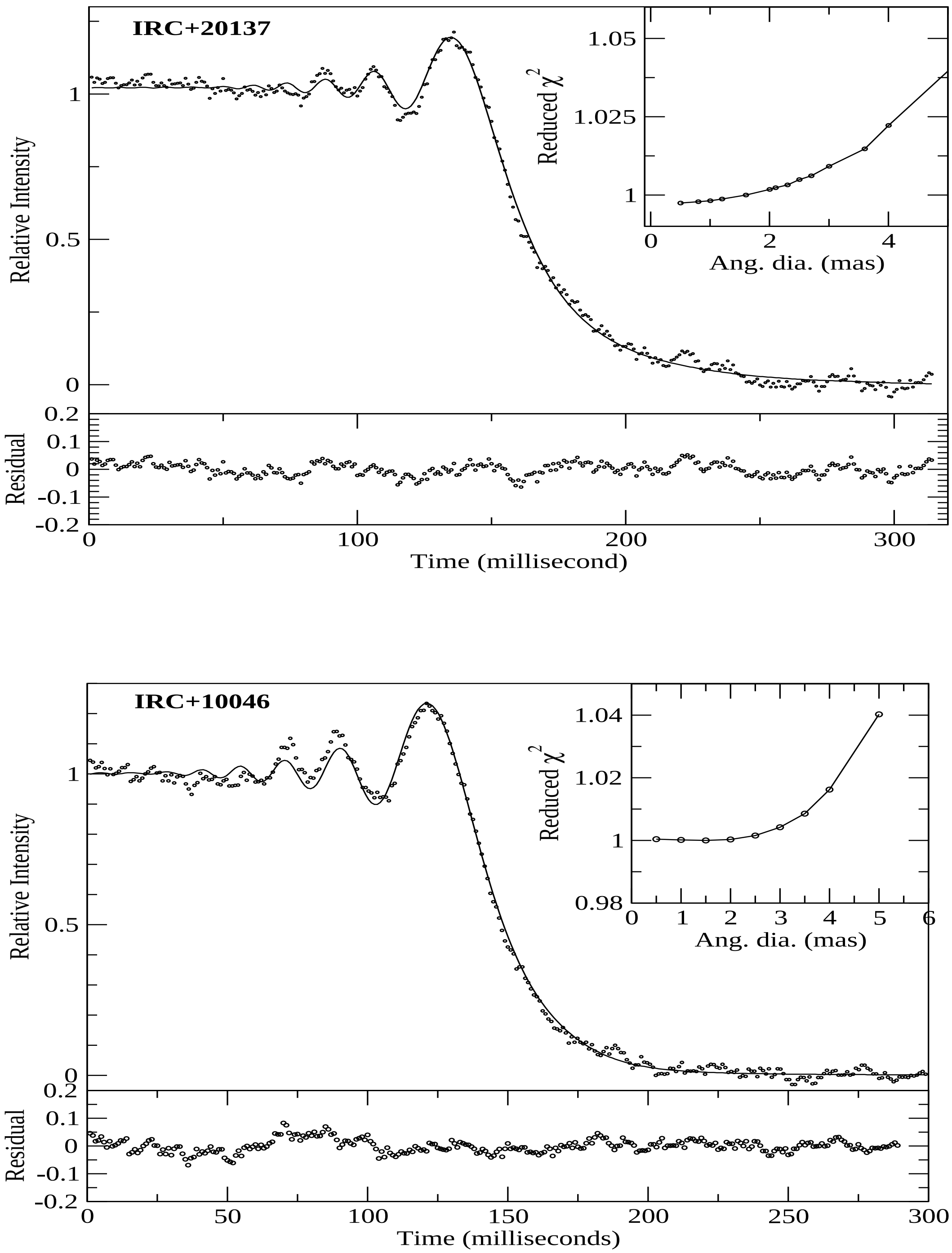

Figure 6.13: *The observed data (dots) are fitted with UD model fit for IRC+20137 (Upper graph) and IRC+10046 (Lower graph). The inset of graphs shows convergence of fit. Residuals (data-model) are shown in the lower panel.*

6.3 The Scale of Effective Temperature

The derived effective temperature of our samples (including three from chapter5) along with spectral types are listed in Table 6.7. We have also listed in Table 6.7 the existing calibration scales established by several authors (e.g. Ridgway et al. 1980; Dyck et al. 1996; Richichi et al. 1999). In Fig. 6.14. we have plotted our derived effective temperatures along these three existing calibration scales. The scatter in the plot are due to uncertainties in angular diameter measurements, spectral classification and bolometric flux estimations.

Angular diameters in our samples presented here are mostly in the range 2.5 - 5 mas. In most cases scintillation effects is the limiting source of noise. Another potential uncertainty is misclassification of the spectral type. For most of the sources in our sample MK spectral classifications are not available. In spite of weak dependence of bolometric flux on effective temperature, estimations of bolometric flux without proper knowledge of extinction of the sources can bias temperature strongly. Over all our derived effective temperatures are good agreement with the existing calibration scale.

Limb-darkening factor is not considered here. Perrin suggested the scaling factor to be 1.035 to obtain limb-darkened diameter from the UD value. Richichi et al. (1999) estimated the scaling factor for K-band in the range of 1.005 to 1.04 for spectral range M2 to M10. The limb-darkened correction may overestimate the diameter by maximum 4%, which results in only a 2% change in the effective temperature.

Fitted blackbody temperatures to the spectral energy distribution correlate well with the effective temperatures derived from angular diameters and bolometric fluxes as illustrated in the Fig. 6.15.

Table 6.7: **Comparison of our derived T$_{eff}$ with earlier calibrations**

Spt. Type	Star	Our result	Calibration		
		T$_{eff}$	R1980	D1996	R1999
K0	IRC+20205	4690±520	4790	-	4810
K1	-	-	4610	4510	4585
K2		-	4450	4370	4390
K3	-	-	4270	4230	4225
K4	-	-	4095	4090	4080
K5	IRC-20516	3820±330	3980	3920	3955
M0	IRC+20178	3830±220	3895	-	3845
M1	IRC+10245	3835±200	3810	3835	3750
	IRC+10228	3790±270			
M2	-	-	3730	3740	3655
M3	IRC-20570	3100±420	3640	3675	3560
	μ Gem	3675±140			
	η Gem	3450±125			
M4			3560	3595	3460
M5	IRC+20153	3240±120	3420	3470	3355
M6			3250	3380	3240
M7	SW Vir	3060±120	-	3210	3100
M8	-	-	-	-	2940
M9	-	-	-	-	2755

R1980 : Ridgway et al. 1980; D1996 : Dyck et al. 1996; R1999: Richichi et al. 1999.

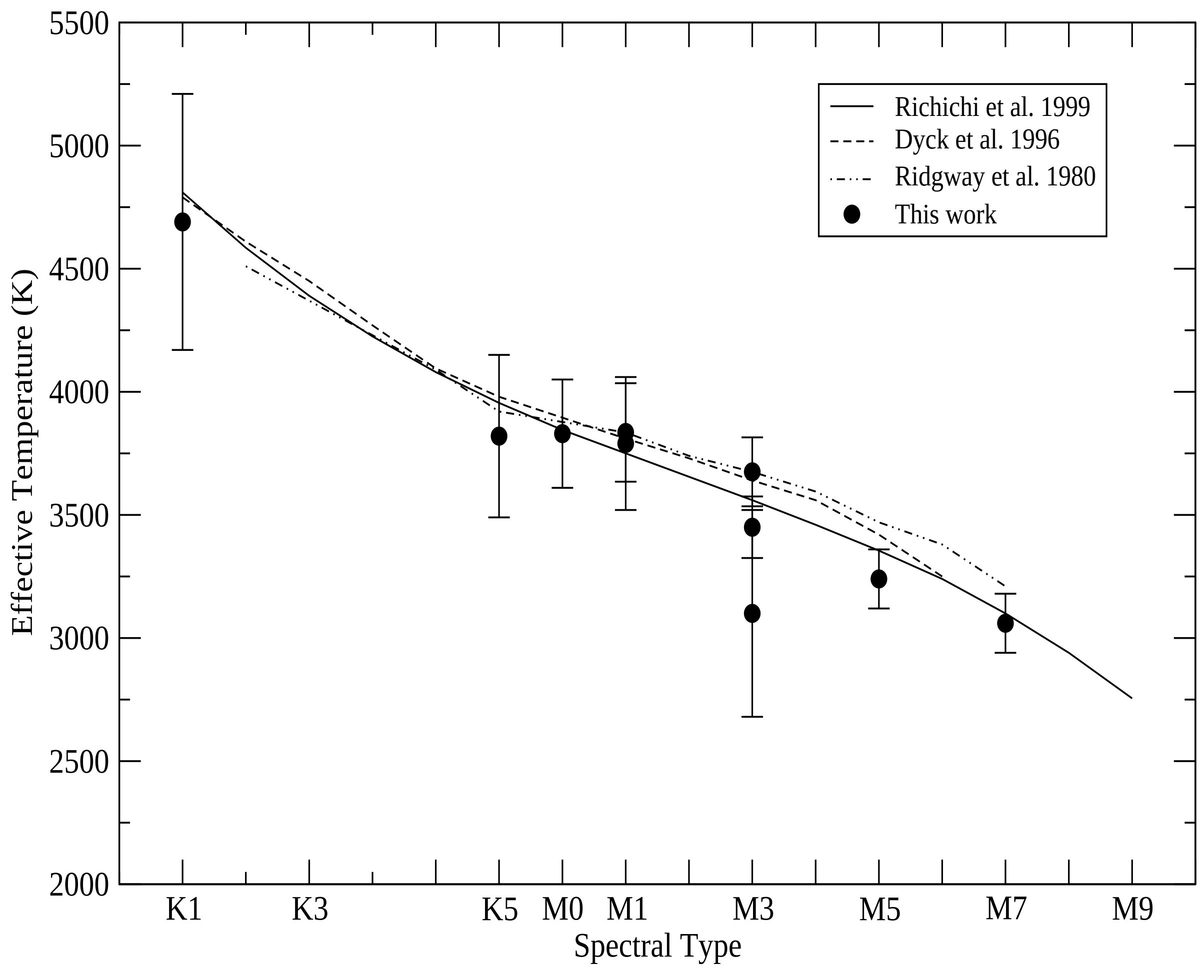

Figure 6.14: *Comparison of our derived T_{eff} with other empirically calibrated T_{eff} with spectral type. The filled circles are our derived values. The different curves are from the calibration of different authors mentioned inside legend box of the graph.*

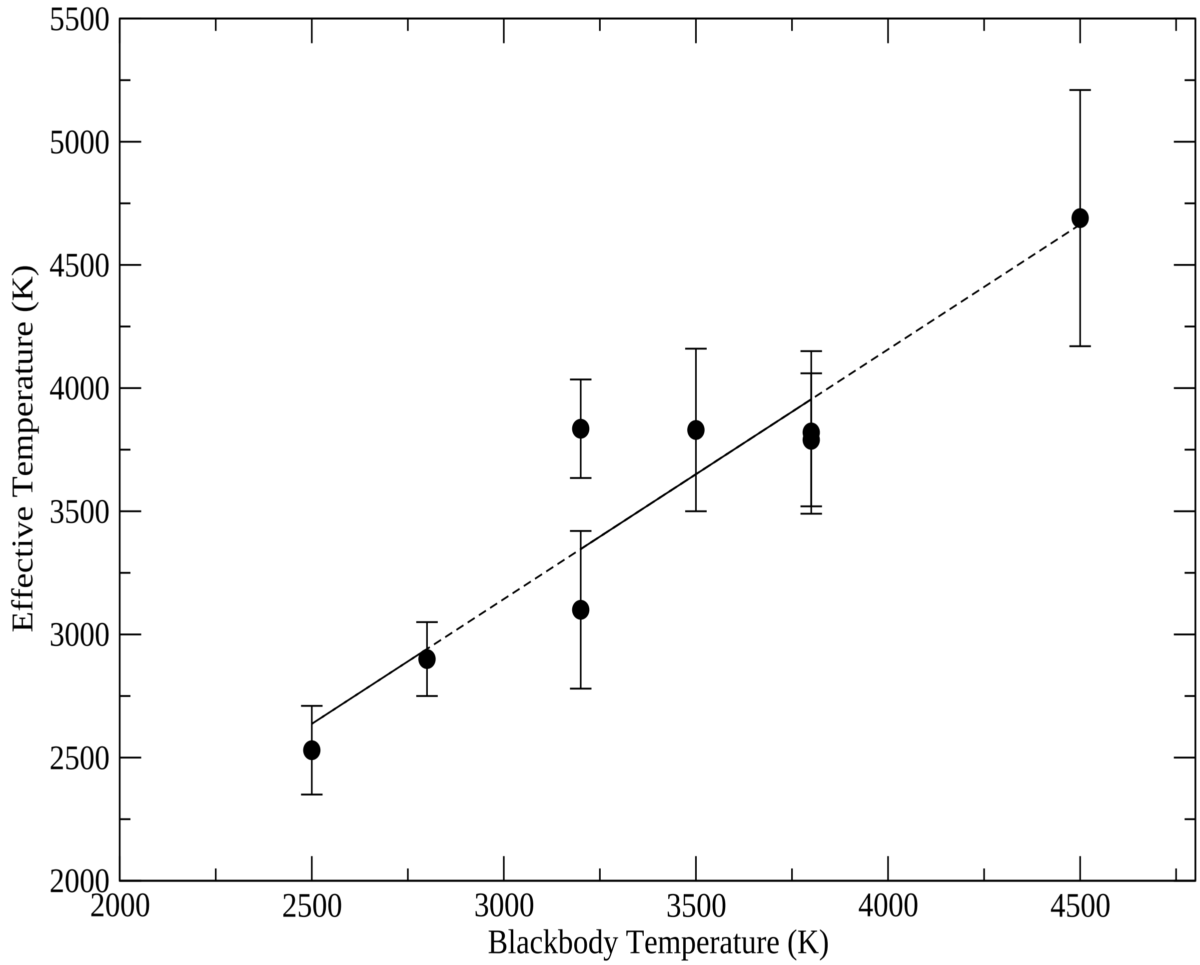

Figure 6.15: *Fitted blackbody temperature from photometry is compared with effective temperature derived from angular diameter and bolometric flux.*

Chapter 7

Summary and Future Prospects

7.1 Summary

In this thesis the lunar occultation results of 20 red giant sources are reported and discussed. Of the 20 sources 3 are unresolved and 5 are observed for the first time by high angular resolution technique. The sources comprise giants and supergiants of late spectral classes in the range of K0 - M9. This include Mira variables and semi-regular variables. One Wolf-Rayet star WR 104 is also in the list.

Considering the scientific potential of observing lunar occultations simultaneously in the K (2.2μm) and thermal L′ (3.8μm), the two channel photometer was specially developed as a part of this thesis work. Scientific motivation was that L′-band LO observations could probe more efficiently the circumstellar shell signature above the photospheric emission whereas K-band observations would more suitable to measure 'true' photospheric diameter of evolved sources. Thermal L′-band lunar occultation is very limited in literature because of observing difficulties due to a strong varying terrestrial thermal background. However the two channel mode could be operated only for a limited number of occultation events involving sources bright in the L′-band like η Gem and μ Gem. The difficulties of observing in L′-band have not been completely overcome. Added to the noisy and drift prone DC level of L′-band observations is the difficulty of aligning two dewars at right angles simultaneously. Efforts are presently on to reduce the optical-bandwidth and also correct for drifts using a more robust power supply. But these experimental innovations are beyond the scope of this thesis.

'Pinwheel' dust shell surrounding Wolf-Rayet star WR 104 was first revealed by aperture masking experiment on Keck 10m telescope. A rare lunar occultation observations of WR 104 provided the opportunity to study and compare results of earlier Keck observations. Significant departure from spherically symmetric one-dimensional brightness profile is retrieved from the lunar occultation light curve. The derived brightness profile exhibits several fine structures consistent with its higher angular resolution but not seen in the Keck profiles as their spatial resolution is 50 mas. Our one dimensional profile degraded to Keck resolution is in good agreement with Keck results. Thus our results confirm the spiral structure of the source. We derive the period of rotation of WR104 in the range 240 to 250 days again in good agreement with Keck results.

Many Mira stars show asymmetric structures in high angular resolution observations. Reason for such asymmetries is still not clear for all cases. Evidence of such asymmetric spatial structure in the atmosphere of Mira variable U Orionis emerged from two observations of lunar occultations on the same day but at different sites (different position angles). Several corollary evidences are also support the asymmetric spatial structure in U Ori.

Multiband angular diameters have been measured to study chromatic size variation of evolved sources like Mira and semi-regular (SR) variables. Three simultaneous K and L$'$ lunar occultations of variables (U Ari (Mira), η Gem (SRV) and μ Gem (SRV)) has been recorded. L$'$ band light curve of U Ari is noisy and the quality of L$'$ data precludes any conclusion. Derived UD angular diameter of U Ari from good trace at K-band shows substantial larger value($\sim$ 20%) compared to H-band at nearly same phase observed elsewhere earlier. Such an enhancement is attributed to extended layers close to the photosphere. This enhancement in L$'$ band is expected to be more prominent and even show an increase in size, a factor of $\sim$ 2 which could be confirmed in future by interferometric observations at 3.8 μm. In case of M3-giants η Gem and μ Gem, their angular sizes are consistent with earlier IR measurements. Between K and L$'$ no difference in sizes are observed.

Supergiant TV Gem in the K band yields the angular size of 4.8$\pm$0.2 mas consistent with previous measurements. The dust shell around TV Gem is re-confirmed by our high quality light curve , we measure the dust shell size to be 13$\pm$5 R_* in good agreement with earlier estimation (20$\pm$5 R_*).

The linear radii of three Mira variables (U Ari, U Ori and Z Sco) is derived from angular diameter measurements. Comparing theoretical Period-Radius and estimating pulsation constant Q-value we find that two Miras (U Ari& U Ori) favour the first overtone mode while Z Sco is a borderline case between fundamental and 1st overtone. Results of pulsation mode in semi-regular variables are more complicated. Semi-regular variable SW Vir (SRb) favours first overtone mode, while irregular variables μ Gem (Lb) is likely to be pulsating in a higher overtone. η Gem (SRa) has two period with a ratio ($P_{long}/P_{short} \approx$ 10), longer period corresponds to fundamental mode while shorter period relates to higher overtone.

Twelve AGB stars in the spectral range K0 to M6 have been observed for determination of angular diameter in the K-band. Of the 12 sources 9 are resolved while 3 are unresolved. The effective temperature is calculated from derived angular diameter and estimated bolometric flux. The calibration of effective temperature with spectral type has been compared with the existing calibration scales and found to be in good agreement.

7.2 Future Prospects

Till recently these single element IR detectors (mainly InSb) have been successfully used for lunar occultation studies of IR bright ($m_k > 3$) IR sources of Two Micron Sky Survey (TMSS) catalogue. With the advent of two dimensional IR arrays like NICMOS, PICNIC and HAWAII etc. in the 1 - 2.5 μm region single element detector is being phased out. Apart from increased sensitivity the first advantage of using an IR array in a sub-area fast readout mode is in the reduction of background noise due to a reduced field of view in the sky compared to conventional photometer. Secondly mean sky can be subtracted from object frames which improves the signal to noise. The main difficulty is in rapid sampling of the lunar occultation event with an array due to inherent delays in readout and processing electronics of the array. We have investigated the sampling of sub-area (20 $\times$ 20 pixels) of the NICMOS 256 $\times$ 256 pixels camera installed at 1.2m IR telescope of Gurushikhar Observatory. A beginning has been made in the lunar occultation with NICMOS array in the K-band with about sampling plus integration time of 16 ms. Two successful events are reported (Chandrasekhar, Shah & Mondal 2003). One source is resolved with its sampling time. It is clear that the sampling rate has to be reduced much further within 3 ms. However for binary detection and for extended sources ($\geq$ 10 mas) the present arrangement would be suitable.

Richichi (1994) has estimated that even with 1.5m telescope it should be possible to reach on S/N $\sim$ 50 for 2 millisecond integration on a array upto K-magnitude of $\sim$ 6.5. Recent two micron all sky survey (2MASS) has a large number of IR sources in the Zodiacal belts whose positions are determined well enough for lunar occultation predictions to be made for any observatory. For example in the 10 square deg. of sky around the object μ Gem, 1400 stars are available in the K-magnitude range between 3.0 - 6.0. A large database of high angular resolution observations at multiwavelengths can permit statistical studies to be carried out.

Because of the large sizes and brightness in the infrared, cool evolved stars are always favourite targets in high angular resolution observations. The improvement of the quality and size of optical telescope, and the advent of new techniques to fight the limitations due to atmospheric turbulence have allowed access to new informations on the environment of evolved stars. Spatial asymmetry has been found in the atmosphere of high mass-lossing evolved stars which are discussed in chapter 4 of this thesis. Spots may be common in evolved stars. Spot and asymmetries can be well addressed in the near future with imaging interferometers on bigger telescopes. The pulsation of long period variables has been detected and the diameter variations are monitored extensively for a few stars like R Leo (Burns et al. 1998) and S Lac (Thompson et al. 2002a). By studying pulsation important question of the mass-loss process can addressed as pulsation is one of main cause of mass loss.

Angular diameter measurements of evolved sources at multiwavelengths will verify theoretical constructed model of their dynamic atmosphere. Enhancement in L' sizes in evolved stars are well modeled by a molecular layer located at a 1-2 stellar radii with a typical temperature of about 1500K (Mennesson et al. 2002). More K and L' high angular resolution observations are needed to understand the dynamics of atmosphere in such mass-losing giants. Our initial efforts are presented in this thesis. In near future with narrow L' filter we hope to present more definitive results with better signal to noise ratio.

Wolf-Rayet stars evolve from a massive progenitor. Due to presence of strong stellar wind (about 2000 km/s) and dust shell WR stars are relatively bright in the NIR region compared to visual band. Free-free emission from wind and thermal emission from dust contributes significantly in NIR flux. There are 31 WR stars brighter than K = 7 mag (Williams et al. 1987). The sensitivity of present or near future interferometers will allow high angular resolution imaging of their environments. Several important aspects like dust shell around late-type WR stars, colliding-wind binaries and structure of WR winds can be studied in greater detail. Only a few (like WR104, WR98a, WR112, WR140 & WR118) have been observed at high angular resolution.

At near-infrared wavelengths, adaptive optics on 8 m class ground-based telescopes and the NICMOS camera on the Hubble Space Telescope (HST) can probe regions within a few arcseconds of nearby stars. Dozens of such young stars within $\sim$60 pc of Earth have been identified (Song et al. 2003 and references therein). Planet detection with current adaptive optics (AO) imaging systems on large telescopes requires planet-star separations of at least 1-2 arcseconds. In addition, a planet must be sufficiently warm to radiate at near-IR wavelengths. Long integrations on nearby stars with ages of hundreds of millions of years can probe down to a few Jupiter masses (e.g., Macintosh et al. 2003). These authors have carried out deep Keck adaptive optics imaging of two nearby stars with asymmetric dust (ϵ Eri and Vega). Lunar occultation with 8-m class telescope may be used to detect extra-solar planets around such young stars and in this matter case studies for detecting planet around solar type stars have been put forward by Richichi (2003).

References

[1] Allen, D.A., Barton, J.R. & Wallace, P.T., 1981, MNRAS, 196, 797

[2] Allen, D.A., Harvey, P.M. & Swings, J.P., 1972, A&A, 20, 333

[3] Ashok, N.M., Chandrasekhar, T., Ragland, S. & H.C.Bhatt, 1994, Exp.Astron., 4, 177

[4] Babcock, H. W., 1953, PASP, 65, 221

[5] Bains, I., Cohen, R. J., Louridas, A., Richards, A. M. S., Rosa-Gonzalez, D. & Yates, J. A., 2003, MNRAS, 342, 8

[6] Baize, P., 1980, A&AS, 39, 83

[7] Baldwin, J. E., Beckett, M. G., Boysen, R. C., Burns, D., Buscher, D. F., Cox, G. C., Haniff, C. A., Mackay, C. D., Nightingale, N. S., Rogers, J., Scheuer, P. A. G., Scott, T. R., Tuthill, P. G., Warner, P. J., Wilson, D. M. A. & Wilson, R. W., 1996, A&A, 306, L13

[8] Barnes, T.G. & Evans, D.S., 1976, MNRAS, 174, 489

[9] Beavers, W.I., Eitter, J.J.,& Cadmus, R.R., 1981, AJ, 86, 1404

[10] Bedding, T.R, Jacob, A. P., Scholz, M. & Wood, P.R., 2001, 325, 1487

[11] Bedding, T.R, Zijlstra, A.A., Jones, A. & Foster, G., 1998, MNRAS, 301, 1073

[12] Benson, J. A., Hutter, D. J., Elias, N. M. II, Bowers, P. F., Johnston, K. J., Hajian, A. R., Armstrong, J. T., Mozurkewich, D., Pauls, T. A.,Rickard, L. J., Hummel, C. A., White, N. M., Black, D. & Denison, C. S., 1997, AJ, 114, 1221

[13] Benson, J.A., Turner, N.H. & Dyck, H.M., 1989, AJ, 97, 1763

[14] Berger, J.P., Haguenauer, P., Kern, P., et al., 2001, A&A, 376, L31

[15] Bessell, M. S., Scholz, M. & Wood, P. R. 1996, A&A, 307, 481

[16] Bessell, M.S., Brett, J.M., Scholz, M. & Wood, P.R., 1989, A&A, 213, 209

[17] Bessell, M.S., Castelli, F. & Plez, B., 1998, A&A, 333, 231

[18] Bessell, M.S., Scholz, M. & Wood, P.R., 1996, A&A, 307, 481

[19] Blackwell, D.E. & Lynas-Gray, A.E., 1998, A&AS, 129, 505

[20] Böhme, D., 1978, AN, 299, 243

[21] Born, M. & Wolf, E., 1959, Principle of Optics, Pergamon Press, London

[22] Bowers, P.F. & Johnson, K.J., 1988, APJ, 330, 339

[23] Boyle, R.P., Aspin, C., Coyne, G.V. & McLean, I.S., 1986, A&A, 164, 310

[24] Bradley, A., Abramowicz-Reed, L., Story, D., Benedict, G. & Jefferys, W., 1991, PASP, 103, 317

[25] Brett, J. M., 1990, A&A, 231,440

[26] Burns, D., Baldwin, J. E., Boysen, R. C., Haniff, C. A., Lawson, P. R., Mackay, C. D., Rogers, J., Scott, T. R., St.-Jacques, D., Warner, P. J., Wilson, D. M. A. & Young, J. S., 1998, MNRAS, 297, 462

[27] Buscumbe, W., 1999, 14th General Catalogue of MK spectral classification, Northwestern Univ., USA

[28] Busher, D. F., 1988, MNRAS, 235, 1203

[29] Catchpole, R.M., Robertson, B.S.C., Lloyds Evans, T.H.H, Feast, M.W., Glass, I.S. & Carter, B.S., 1979, SAAO Circ., 1, 61

[30] Celis, S.L., 1995, APJS, 98, 701

[31] Chan, S.J. & Kwok, S., 1988, APJ, 334, 362

[32] Chandrasekhar, T., Shah, R. & Mondal, S., 2003, Bull. Astr. Soc. Ind., 31, 471

[33] Chandrasekhar, T. & Mondal, S., 2001, MNRAS, 322, 356

[34] Chandrasekhar, T., 1999, Bull. Astr. Soc. Ind., 27, 43

[35] Chandrasekhar. T., Ashok, N.M. & Ragland, S., 1992, J.Astrophys. Astr., 13, 195

[36] Chapman, J.M. & Cohen, R.J., 1985, MNRAS, 212,375

[37] Chapman, J.M., Cohen, R.J. & Saikia, D.J., 1991, MNRAS, 249, 227

[38] Chengalur, J.N., Lewis, B.M., Eder, J. & Terzian, Y., 1993, APJS, 89, 189

[39] Cho, S.-H., Kaifu, N. & Ukita, N., 1996, A&AS, 115, 117

[40] Cohen, M. & Kuhi, L.V., 1977, MNRAS, 180, 37

[41] Cohen, M., Barlow, M.J. & Kuhi, L.K., 1975, A&A, 40, 291

[42] Colavita, M. M., Boden, A.F., Crawford, S. L., Meinel, A. B., Shao, M., Swanson, P. N., van Belle, G.T., Vasisht, G., Walker, J. M., Wallace, J. K., Wizinowich, P.L., 1998, Proc. SPIE, 3350, 776

[43] Conti, P.S., 1999, New Astron., 4, 489

[44] Coyne, G. V., Magalhaes, A. M., 1977, AJ, 82, 908

[45] Crowther, P.A., 1997, MNRAS, 290, L59

[46] Crowther, P.A., De Marco, O. & Barlow, M.J., 1998, MNRAS, 296, 367

[47] Cutri, R.M., 2003, The 2MASS All-Sky Catalog of Point Sources, Infrared Processing and Analysis Center/California Institute of Technology, USA

[48] Danchi, W.C., Bester, M., Degiacomi, Greenhill, L.J. & Townes, C.H. 1994, AJ, 107, 1469

[49] Di Benedetto, G.P. & Rabbia, Y., 1987, A&A, 188,114

[50] Di Benedetto, G.P., 1993, A&A, 270, 315

[51] Diercks, H. & Hunger, K., 152, Z. Astron., 31, 182

[52] Drake, S.A., Linsky, J.L., Judge, P.G., Elitzur, M. 1991, AJ, 101, 230

[53] Drake, S.A.& Linsky, J.L. 1986, AJ, 91, 602

[54] Dunham, D.W., 1977, Occ. Newsletter, 1, 120

[55] Dutra, C.M., Santiago, B.X., Bica, E.L.D. & Barbuy, B., 2003, MNRAS, 338, 253

[56] Dyck, H. M. & Sandford, M. T., 1971, AJ, 76, 43

[57] Dyck, H.M., Simon, T. & Wolstencroft, R.D., 1984, APJ, 277, 675

[58] Dyck, H.M. & Nordgren, T.E., 2002, AJ, 124, 541

[59] Dyck, H.M., Benson, J.A., van Belle, G.T. & Ridgway, S.T., 1996, AJ, 111, 1705

[60] Eddington, A.J., 1918, MNRAS, 69, 178

[61] Eikenberry, S. S., Fazio, G. G., & Ransom, S. M., 1996, PASP, 108, 939

[62] Evans, D.S., Edwards D.A., Frueh M., McWilliam A. & Sandmann W.H.,1985, AJ, 90, 2360

[63] Feast, M.W. 1996, MNRAS, 278, 11

[64] Fizeau, A.H., 1868, C.R. Acad. Sci. (Paris), 66, 932

[65] Fox, M.W. & Wood, P.R., 1982, APJ, 259, 198

[66] Foy, R. & Labeyrie, A., 1985, A&A, 152, L29

[67] Fried, D.L., 1966, J. Opt. Soc. Am., 56, 1372

[68] Gautschy, A. & Saio, H., 1996, Ann. Rev. Astron. Astrophys., 34, 551

[69] Gehrz, R.D. & Hackwell, J.A., 1974, APJ, 194, 619

[70] Gezari, D. Y., Pitts, P. S. & Schmitz, M., 1999, Catalog of Infrared Observation, 5th Ed., NASA, Ref. Pub. 2225

[71] Gilliland, R.L. & Dupree, A.K., 1996, APJL, 463, 29

[72] Girardi, L., Bressan, A., Bertelli, G. & Chiosi, C., 2000, A&AS, 141, 371

[73] Grasdalen, G.L. & Sneden, C., 1979, PASP, 91, 337

[74] Gustafsson, B., Bell, R.A., Eriksson, K., Nordlund, A., 1975, A&A, 42, 407

[75] Hackwell, J.A., Gehrz, R.D. & Smith, J.R., 1974, APJ, 192, 383

[76] Hall, D.N.B., Aikens, R.S., Joyec, R. & McCurnin, T.W., 1975, Appl. Opt., 14, 450

[77] Hanbury Brown, R. & Twiss, R.Q., 1956, Nature, 178, 1046

[78] Hanbury Brown, R., Davis, J., Allen, L. R, 1974, MNRAS, 167, 121

[79] Hanbury Brown, R., Davis, J., Allen, L. R., Rome, J. M., 1967, MNRAS, 137, 393

[80] Haniff, C. A., Ghez, A. M., Gorham, P. W., Kulkarni, S. R., Matthews, K. & Neugebauer, G., 1992, AJ, 103, 1662

[81] Haniff, C.A., Scholz, M. & Tuthill, P.G. 1995, MNRAS, 276, 640

[82] Hansen, O.L. & Blanco, V.M. 1973, AJ 78, 669

[83] Happer, W., MacDonald, G. J., Max, C. E. & Dyson, F. J., 1994, J. Opt. Soc. Am. 11, 263

[84] Harrington, J.P., 1969, Astrophys. Letters, 3, 165

[85] Harrison, T. E., McNamara, B. J., Szkody, P., Gilliland, R. L., 2000, AJ, 120, 2649

[86] Hartkopf, W.I. & McAlister, H.A., 1984, PASP, 96, 105

[87] Hartkopf, W.I., McAlister, H.A. & Mason, B., 2001, AJ, 122, 3480

[88] Hinkle, K.H., Lebzelter, T. & Scharlach, W.W.G., 1997, AJ, 114, 2686

[89] Hofmann. K. -H., Balega. H., Scholz. M. & Weigelt, G., 2000, A&A, 353, 1016

[90] Hofmann, K, -H & Scholz, M., 1998a, A&A, 335, 637

[91] Hofmann, K, -H, Scholz, M. & Wood, P.R., 1998b, A&A, 339, 486

[92] Howrath, I.D. & Schmutz, W., 1992, A&A, 261, 503

[93] Hummel, C. A., Benson, J. A., Hutter, D. J., Johnston, K. J., Mozurkewich, D., Armstrong, J. T., Hindsley, R. B., Gilbreath, G. C., Rickard, L. J., White, N. M., 2003, AJ, 125, 2630

[94] Iben Jr., I., 1985, QJRAS, 26, 1

[95] Iben, I. Jr. & Renzini, A., 1983, Ann. Rev. Astron. Astrophys., 21, 271

[96] Ivezi$\acute{e}$, $\check{Z}$ & Elitzur, M., APJ, 1995, 445, 415

[97] Jacob, A.P. & Scholz, M., 2002, MNRAS, 336, 1377

[98] Jenison, R.C., 1958, MNRAS, 118, 276

[99] Jiang, B.W., Weguchi, S., Yamamura, I., et al., 1996, APJS, 106, 463

[100] Jorgensen, U. G., 1994, A&A, 284, 179

[101] Jura, M & Kleinmann, S.G., 1992, APJS, 79, 105

[102] Karovska, M., Hack, W., Raymond, J. & Guinan, E. 1997, APJ, 482, L175

[103] Keenan P.C. & McNeil, R.C., 1989, APJS, 71, 245

[104] Kimeswenger, S., Lederle, C., Richichi, A., et al., 2004, A&A, 413, 1037

[105] Kiss, L.L., Szatmary, K., Cadmus, Jr., R.R. & Mathei, J.A., 1999, A&A, 346, 542

[106] Knapp, G. R. & Morris, M., 1985, APJ, 292, 640

[107] Knapp, G. R., Pourbaix, D., Platais, I., & Jorissen, A, 2003, A&A, 403, 993

[108] Knoechel, G. & von der Heide, K., 1978, A&A, 67, 209

[109] Koornneef, J., 1983, A&A,128, 84

[110] Kukarkin, B. V. et al., 1981, Cataloque of suspected variable stars . Moscow, Acad. of Sciences USSR Shternberg,1951

[111] Kukarkin, B.V. et al., 1969, *General Catague of Variable Stars*, 3rd ed. (Astronomical Council of the Academy of Sciences in the U.S.S.R, Moscow), vol.1

[112] Kukarkin, B.V., 1971, General catalogue of variable stars, 3rd ed.

[113] Kwok, S., Volk, K. & Bidelman, W.P., 1997, APJS, 112, 557

[114] Léna, P., Leburn, F. & Mignard, F., 1998, Observational Astrophysics, Spinger, 2nd ed.

[115] Labeyrie, A., 1970, A&A, 6, 85

[116] Labeyrie, A., 1975, APJL, 196, 71

[117] Labeyrie, A., Koechlin, L., Bonneau, D., Blazit, A. & Foy, R. 1977, APJ, 218, L75

[118] Lattanzi, M.G., Munari, U., Whitelock, P.A. & Feast, M.W. 1997,APJ, 485, 328

[119] Le'pine S. & Moffat A. F. J., 1999, APJ, 514, 909

[120] Lebzelter, Th. & Hron, J., 1999, A&A, 351, 533

[121] Lloyd-Hart, M., Angel, J. R. P., Groesbeck, T. D., et al., 1998, APJ, 493, 950

[122] Lockwood, G.W., 1972, APJS, 209, 305

[123] Lockwood, G.W., 1985, APJS, 58, 167

[124] Loup, C., Foryeille, T., Omont, A. & Paul, J.F., A&AS, 99, 291

[125] Lucy L.B., 1974, AJ, 79, 745

[126] Lundstrom, L. & Stenholm, N., 1984, A&AS, 58, 163

[127] Macintosh, B, Becklin, E.E., Kaisler, D., Konopacky, Q. & Zuckerman, B., 2003, APJ, 594, 538

[128] MacMohan P.A., 1909, MNRAS, 69, 126-27

[129] Mallbet, F., Kern, P., Schanen-Duport, I., Berger, J.-P., Rousselet-Perraut, K., & Benech, P., 1999, A&AS, 138, 135

[130] Marchenko, S.V., Moffat, A. F. J. & Grosdidier, Y., 1999, APJ, 522, 433

[131] Mathei, J. A., 2004, Observations from the AAVSO International Database (private communication)

[132] McAlister, H.A., 1985, Ann. Rev. Astron. Astrophys., 23, 59

[133] McArther, B.E. et al., 2001, APJ, 560, 907

[134] McLean, I. S., 1979, MNRAS, 186, 21

[135] Menduca, A., 1979, A&AS, 36, 411

[136] Mennesson, B., Perrin, G., Chagnon, G., Foresto, V. Coude du, Ridgway, S., Merand, A., Salome, P., Borde, P., Cotton, W., Morel, S., Kervella, P., Traub, W., Lacasse, M., 2002, APJ, 579, 446

[137] Michelson, A.A. & Pease, F.G., 1921, ApJ, 53, 249

[138] Miyata, T., Kataza, H., Okamoto, Y., Onaka, T. & Yamashita, T. 2000, APJ, 531, 917

[139] Moffat A. F. J. & Robert C., 1994, APJ, 421, 310

[140] Moffat A.F.J., Niemela V.S. & Marraco H.G., 1990, APJ, 348, 232

[141] Mondal, S. & Chandrasekhar, T., 2004, MNRAS, 348, 1337

[142] Mondal, S., Chandrasekhar, T. & Kikani, P.K. 2002a, Bull. Astr. Soc. Ind., 30, 811

[143] Mondal, S. & Chandrasekhar, T. 2002b, MNRAS, 334, 143

[144] Mondal, S., Chandrasekhar, T., AShok, N.M. & Kikani, P.K., 1999, Bull. Astr. Soc. Ind., 27, 335

[145] Monnier, J.D., Traub, W. A., Schloerb, F. P., et al., 2004a, ApJL, 602, 57

[146] Monnier, J.D., Millan-Gabet, R., Tuthill, P. G., Traub, W. A., et al., 2004b, arAix:astro-ph/0401363

[147] Monnier, J.D., 2003, Rep. Prog. Phys., 66, 789

[148] Monnier, J.D., 2000, in Principle of Long baseline Stellar Interferometry, NASA-JPL (Publication 00-009), p203

[149] Monnier, J. D., Tuthill, P. G. & Danchi, W. C., 1999a, APJL, 525, 97

[150] Monnier, J.D., Tuthill, P.G., Lopez, B., Cruzalebes, P., Danchi, W.C. & Haniff, C.A., 1999b, APJ, 512, 351

[151] Monnier, J.D., 1999, Ph.D. Thesis, Univ. of California at Berkeley, USA

[152] Mozurkewich, D., Armstrong, J.T., Hindsley, R.B. et al., 2003, AJ, 126, 2502

[153] Nather, R. E. & Evans, D. S.,1970, AJ, 75, 575

[154] Nather, R. E. & McCants, M. M.,1970, AJ, 75,963

[155] Neckel, T. & Krale, G. 1980, A&AS, 42, 251

[156] Neff, J. E., O'Neal, D. & Saar, S. H., 1995, APJ, 452, 879

[157] Neugebauer, G.A. & Leighton, R.B., 1969, NASA SP-3047

[158] Ostile, D.A. & Cox, A.N., 1986, APJ, 311, 864

[159] Padmanabhan, T., *Theoretical Astrophysics, volume II. Star and Stellar Systems*, Cambridge Univ. Press, 2001

[160] Paresce, F., 2003, AP&SS, 286, 297

[161] Pataki, L. & Kolena, J., 1974, Bull. Am. Astr. Soc., 6, 340

[162] Pendleton, Y.J., Sandford, S.A., Allamondola, L.J., Tielen, A.G.G.M. & Sellgreen, K., 1994, APJ, 437, 683

[163] Percy, J. R. & Parkes, M. 1998, PASP, 110, 1431

[164] Percy, J. R. & Wilson, B.J., 2001, PASP, 113, 983

[165] Pereira, C.B., Franco, C.S. & de Araujo, F. X., 2003, A&A, 397, 927

[166] Perl, M.& Tuchman, Y.,1990, ApJ, 360, 554

[167] Perrin, G., Coudè du Foresto, V., Ridgway, S.T., Mariotti, J.-M., Traub, W.A., Carleton, N.P. & Lacasse, M.G. 1998, A&A, 331,619

[168] Perryman, M.A.C. et al., 1997, The Hipparcos and Tyco Catalogs (ESA SP-1200)(Noordwijk: ESA)

[169] Phillips, J. P., Selby, M. J., Wade, R. & Sanchez Magro, C.,1980, MNRAS, 190, 337

[170] Quirrenbach, A., 2001, Ann. Rev. Astron. Astrophys., 39, 353

[171] Quirrenbach, A., Mozurkewich, D., Armstrong, J.T., Buscher, D.F. and Hummel, C.A. 1993, APJ, 406, 215

[172] Quirrenbach, A., Mozurkewich, D., Busher, D.F., Hummel, C.A., Armstrong, J.T., 1994, A&A, 286, 1019

[173] Radick, R.R., Henry, G.W & Sherlin, J.M., 1984, AJ, 89, 151

[174] Ragland, S. & Richichi, A., 1998, MNRAS, 302, L13

[175] Ragland, S., 1996, Ph.D. Thesis, Devi Ahilya Univ., India

[176] Ragland, S., Chandrasekhar, T. & Ashok, N.M., 1997, A&A, 319, 260

[177] Ragland, S., Chandrasekhar, T., Ashok, N. M., 1998, MNRAS, 287, 681

[178] Reid, M. J., Moran, J. M., Leach, R. W., Ball, J. A., Johnston, K. J., Spencer, J. H. & Swenson, G. W., 1979, APJ, 227, L89

[179] Richichi, A., 1989, A&A, 226, 366

[180] Richichi, A., Chandrasekhar, T., Lisi, F., Howell, R. R., Meyer, C., Rabbia, Y., Ragland, S. & Ashok, N. M., 1995, A&A, 301, 439

[181] Richichi, A., 2003, A&A, 397,1123

[182] Richichi, A. & Calamai, G. 2003, A&A, 399, 275

[183] Richichi, A. & Paresce, F., 2003, Msngr, 114, 26

[184] Richichi, A., Chandrasekhar, T., & Leinert, Ch., 2003, New Astron., 8, 507

[185] Richichi, A. & Calamai, G. 2001, A&A, 380, 526

[186] Richichi, A., Ragland, S., Calamai, G., Richter, S., Stecklum, B. 2000, A&A, 361, 594

[187] Richichi, A., Fabbroni, L., Ragland, S.& Scholz, M., 1999, A&A, 344, 511

[188] Richichi, A., Ragland, S.& Fabbroni, L., 1998a, A&A, 330, 578

[189] Richichi, A., Ragland, S., Stecklum, B. & Leinert, Ch., 1998b, A&A, 338, 527

[190] Richichi, A., Baffa, C., Calamai, G. & Lisi, F., 1996, AJ, 112, 1

[191] Richichi, A., 1994, IAU Sym. 158, Very High Resolution Imaging, eds. Robertson, J.G. & Tango, W.J., p71

[192] Richichi, A., Lisi, F. & Di Giacomo, A., 1992, A&A, 254, 149

[193] Ridgway, S.T., Jacoby, G.H., Joyce, R.R. Siegel, J.M. & Wells, D.C., 1982, AJ, 87, 808

[194] Ridgway, S.T., Joyce, R.R., White, N.M. & Wing, R.F., 1980, APJ, 235, 126

[195] Ridgway, S.T., Wells, D.C., Joyce, R.R.& Allen, R.G., 1979, AJ, 84, 247

[196] Ridgway, S.T., Wells, D.C. & Joyce, R.R. 1977, AJ, 82 ,414

[197] Ridgway, S.T., Wells, D.C. & Joyce, R.R. 1974, AJ, 79 ,1079

[198] Rieke, G. H. & Lebofsky, M. J., APJ, 1985, 288, 618

[199] Roddier, F., ed. 1999, Adaptive Optics in Astronomy, Cambridge Univ. Press

[200] Saha, S.K., 2002, Rev. Mod. Phys., 74, 551

[201] Sanduleak, N. & Stephenson, C.B., 1973, APJ, 185,899

[202] Schmidtke, P.C., Africano, J.L., Jacoby, G.H., Joyce, R.R. & Ridgway, S.T., 1986, AJ, 91, 961

[203] Schmidtke, P.C.& Africano, J.L., 1984, AJ, 89, 1371

[204] Scholz, M. & Takeda, Y. 1987, A&A, 196, 342

[205] Schwarz, H.E. & Clarke, D., 1984, A&A, 132, 370

[206] Schwarzchild, M., 1975, APJ, 195, 137

[207] Sedlmayr, E., 1994, in Proc. of IAU Col. No. 146 : Molecules in the Stellar Environment, ed. U.G. Jorgensen (Springer-Verlag), p440

[208] Serkowski, K., 1970, APJ, 160, 1107

[209] Shawl, S.J.,1975, AJ, 80, 602

[210] Shu, F. H., 1982, The Physical Universe, University Science Books, Mill Valley, California, USA

[211] Sloan, G.C. & Price, D.S. 1998, APJS, 119, 141

[212] Sloan, G.C. & Price, D.S., 1998, APJS, 119, 141

[213] Smith, L.F., 1968, MNRAS, 140, 409

[214] Smith, L.F., shara, M.M. & Moffat, A.F.J., 1990, APJ, 358, 229

[215] Soker, N, 1998, MNRAS, 299, 1242

[216] Song, I., Zuckerman, B. & Bessell, M.S., 2003, APJ, 599, 342

[217] Sudol, J.J., Benson, J.J., Dyck, H.M. & Scholz, M., 2002, AJ, 124, 3370

[218] Svatoš, J. & Šolc, M., 1981, Astrophys. Space Sci., 77, 511

[219] Tej, A., 1999, Ph.D. Thesis, Gujarat Univ., India

[220] Tej, A., Chandrasekhar, T., Ashok, N.M., Ragland, S., Richichi, A., Stecklum, B., 1999, AJ, 117, 1857

[221] Thompson, R.R., Creech-Eakman, M.J. & van Belle G.T. 2002a, APJ, 577, 447

[222] Thompson, R.R., Creech-Eakman, M.J. & Akeson R.L. 2002b, APJ, 570, 37

[223] Tomaszewski, L., Landstreet, J.D., McLean, I.S., Coyne, G.V., 1980, APJ, 238, 935

[224] Torres, A.V. & Massey, P., 1987, APJS, 65, 459

[225] Tuthill, P.G., Monnier, J.D & Danchi, W.C., 2002, in Moffat A.F.J. and St-Louis N., eds, ASP conf. Ser., Vol. 260, Interacting Winds from Massive Stars, Astron. Soc. Pac., San Francisco, p. 321

[226] Tuthill, P.G., Monnier, J.D & Danchi, W.C., 2001, Nature, 409, 1012

[227] Tuthill, P.G., Danchi, W.C., Hale, D.S., Monnier, J.D.& Townes, C. H., 2000a, APJ, 534, 907

[228] Tuthill, P.G., Monnier, J.D., Danchi, W.C., Wishnow, E.H & Haniff, C.A., 2000b, PASP, 112, 555

[229] Tuthill, P.G., Monnier, J.D & Danchi, W.C., 1999a, Nature, 398, 487

[230] Tuthill, P.G., Haniff, C.A. & Baldwin, J.E. 1999b, MNRAS, 306, 353

[231] Tuthill, P.G., Monnier, J.D. & Danchi, W.C., 1999c, in ASP Conf. Ser. 194, Optical and IR Interferometry from Ground and Space eds. S.C. Unwin & R. Stachnik (San Francisco: ASP), 188

[232] Tuthill, P. G., Haniff, C. A. & Baldwin J. E., 1995, MNRAS, 277, 1541

[233] Tycner, C., Hajian, A. R., Mozurkewich, D., Armstrong, J. T., Benson, J. A., Gilbreath, G. C., Hutter, D. J., Pauls, T. A., Lester, J. B., 2003, AJ, 125, 3378

[234] Underhill, A.B., 1984, PASP, 96, 305

[235] Usov, V.V., 1991, MNRAS, 252, 49

[236] van Belle, G.T., 1999, PASP, 111, 1515

[237] van Belle, G.T., Dyck, H.M., Benson, J.A. & Lacasse, M.G., 1996, AJ, 112, 2147

[238] van Belle, G.T., Thompson, R.R. & Creech-Eakman, M.J. 2002, AJ, 124, 1706

[239] van Leeuwen, F., Feast, M. W., Whitelock, P. A., Yudin, B., 1997, MNRAS, 287, 955

[240] van der Hucht, K.A., 1992, A&A Rev., 4, 123

[241] van der Hucht, K.A., 2001, New Astron. Rev., 45, 135

[242] van der Hucht, K.A., Morris P.W., Williams P.M., Setia Gunawan D.Y.A., Beintema D.A., Boxhoorn D.R., de Graauw T., Heras A., Kester D.J.M., Lahuis F., Leech K.J., Roelfsema P.R., Salama A., Valentijn E.A. & Vandenbussche B., 1996, A&A, L193

[243] Veen, P. M., Van Genderen, A. M., van der Hucht, K. A., Li, A., Sterken, C. & Dominik, C., 1998, A&A, 329, 199

[244] Warner, B., 1988, in High Speed Astronomical Photometry, Cambridge Univ. Press

[245] Weidemann, V. & Schönberber, D., 1990, in Miras to Planetary Nebulae : which path for stellar evolution ? ed. M. O. Mennessier and A. Omont (Editions Frontières: France), 67

[246] White, N.M. & Feierman, B.H., 1987, AJ, 94, 751

[247] White, N.M., Vitas in Astronomy, 30, 13

[248] Whitelock, P.A. & Feast, M.W., 2000b, MNRAS, 319, 759

[249] Whitelock, P.A., Marang, F. & Feast, M.W., 2000a, MNRAS, 319, 728

[250] Whitford, A.E., 1939, APJ, 89, 472

[251] Williams, P.M., van der Hucht, K.A. & Thé P.S., 1987, A&A, 182, 91

[252] Williams, P.M. & van der Hucht, K.A., 1992, in Drissen L., Leitherer C., Nota A., eds, ASP conf. Ser., Vol. 22, Non-isotropic and variable outflows from Stars, Astron. Soc. Pac., San Francisco, p. 269

[253] Williams, P.M., van der Hucht, K.A., Pollock, A.M.T., Florkowski, D.R., van der Woerd, H. & Wamsteker W.M., 1990, MNRAS, 243, 662

[254] Williams, J.D., 1939, APJ, 89, 467

[255] Williams, P.M, van der Hucht, K.A. & Thé, P.S., 1987, A&A, 182, 91

[256] Wilson, L.A. & Hill, S.J., 1979, APJ, 228, 854

[257] Wilson, L.A., 2000, Ann. Rev. Astron. Astrophys., 38, 573

[258] Winters, J.M., Le Bertre, T., Jeong, K.S., Nyman, L, -A. & Epchtein, N., 2003, A&A, 409, 715

[259] Wood, P.R. 1990, in Miras to Planetary Nebulae : which path for stellar evolution ? ed. M. O. Mennessier and A. Omont (Editions Frontières: France), 67

[260] Wood, P.R. & Sebo, K.M., 1996, MNRAS, 282, 958

[261] Wood, P.R. et al., 1999, in IAU Sypm. No. 191, Asymptotic giant branch stars, eds. T. Le Bertre, A. Lebre, and C. Waelkens (San Francisco: ASP), p151

[262] Wright, C.O., Egan, M.P., Kraemer, K.E. & Price S.D., 2003, AJ,

[263] Wyatt, S.P. & Cahn, J.H. 1983, APJ, 275, 225

[264] Young, J. S., Baldwin, J. E., Boysen, R. C., Haniff, C. A., Lawson, P. R., Mackay, C. D., Pearson, D., Rogers, J., St.-Jacques, D., Warner, P. J., Wilson, D. M. A., Wilson, R. W., 2000, MNRAS, 315, 635

[265] Young, K., 1995, APJ, 445, 872

[266] Zubko, V.G., 1998, MNRAS, 295, 109